

ROLE OF ARCTIC SEA ICE VARIABILITY IN CLIMATE MODELS

A  
THESIS

Presented to the Faculty  
of the University of Alaska Fairbanks

in Partial Fulfillment of the Requirements  
for the Degree of

MASTER OF SCIENCE

By

Dyre Oliver Dammann, B.S.

Fairbanks, Alaska

August 2011

### **Abstract**

Arctic sea ice plays an important role in climate by influencing surface heat fluxes and albedo, so must be accurately represented in climate models. This study finds that the fully coupled ice-ocean-atmosphere-land Community Climate System Model (CCSM3.0) underestimates day-to-day ice variability compared to observations and employs the Community Atmosphere Model (CAM3.0) to investigate the atmospheric sensitivity to sea ice variability. Three 100-ensemble experiments are forced with climatological, daily-varying, and smoothly-varying sea ice conditions from an anomalously low ice period (September 2006-February 2007). Daily ice variability has a large local impact on the atmosphere when ice undergoes rapid changes, leading to local cooling and subsequent circulation changes. The most notable example of a large-scale atmospheric response occurs over Northern Europe during fall where daily ice variability forces reductions in the number and strength of cyclones, leading to positive sea level pressure anomalies, surface warming, and reduced cloud cover.

## Table of Contents

<b>Signature Page.....</b>	<b>i</b>
<b>Title Page .....</b>	<b>ii</b>
<b>Abstract.....</b>	<b>iii</b>
<b>Table of Contents .....</b>	<b>iv</b>
<b>List of Figures.....</b>	<b>vi</b>
<b>List of Tables .....</b>	<b>x</b>
<b>List of Appendices.....</b>	<b>xi</b>
<b>1 Introduction .....</b>	<b>14</b>
<b>1.1 Introduction – Arctic Sea Ice Evolution .....</b>	<b>14</b>
<b>1.2 Introduction – Impact of Sea Ice on Atmosphere.....</b>	<b>17</b>
<b>1.3 Model Versus Observed Arctic Sea Ice .....</b>	<b>21</b>
1.3.1 Data Properties .....	21
1.3.2 Mean Ice Conditions .....	22
1.3.3 Standard Deviation .....	24
1.3.4 Day-to-day Change of Ice Concentration.....	27
<b>2 Model, Data and Methods.....</b>	<b>30</b>
<b>2.1 Model Description.....</b>	<b>30</b>
<b>2.2 Observations.....</b>	<b>31</b>
2.2.1 Data Used as Boundary Conditions in CTRL, DAILY and SMTH Experiments .....	32
<b>2.3 Methods .....</b>	<b>41</b>
2.3.1 Number of Ensembles .....	41
2.3.2 Storm Track Algorithm .....	42
2.3.3 Bandpassed Filtering .....	43

<b>3</b>	<b>Results and Discussion .....</b>	<b>44</b>
<b>3.1</b>	<b>Fall (September – October) Response.....</b>	<b>44</b>
<b>3.2</b>	<b>Winter (November – February) Response .....</b>	<b>55</b>
<b>3.3</b>	<b>Stormtrack Response in the Midlatitudes and the Arctic.....</b>	<b>59</b>
<b>3.4</b>	<b>Ensemble Analysis .....</b>	<b>62</b>
<b>4</b>	<b>Summary and Conclusions .....</b>	<b>65</b>
<b>5</b>	<b>References .....</b>	<b>68</b>

### List of Figures

Figure 1.1 Difference in Mean SIC in Model and Observations .....	23
Figure 1.2 Standard Deviation Difference of SIC Between Model and Observations.....	25
Figure 1.3 Ratio of Model/Observed Standard Deviation of SIC.....	26
Figure 1.4 Day-to-day SIC Change in Model and Observations .....	28
Figure 2.1 SIC Difference Between OLD SMTH and DAILY .....	34
Figure 2.2 SLP Response Difference Between Old and New SMTH .....	35
Figure 2.3 Difference in Mean SIC Between DAILY and SMTH .....	37
Figure 2.4 Sea Ice Concentration Comparison for Various Experiments.....	38
Figure 2.5 Distribution of Sea Ice Concentration in DAILY and SMTH.....	40
Figure 3.1 Sea Ice Concentration Forcing .....	48
Figure 3.2 Net Upward Surface Heat Flux Anomaly .....	49
Figure 3.3 Temperature Anomaly .....	50
Figure 3.4 Sea Level Pressure and 500 hPa Geopotential Height Anomalies .....	51
Figure 3.5 Precipitation Anomaly.....	52
Figure 3.6 Zonal Circulation at 200 hPa and v'T' 2-10 Day Bandpassed Anomalies .....	53
Figure 3.7 Storm Count .....	54
Figure 3.8 Sea Ice Concentration Forcing .....	56
Figure 3.9 SLP and Meridional Wind Anomaly .....	57
Figure 3.10 Temperature Anomaly.....	58
Figure 3.11 Midlatitude and Arctic Region .....	60
Figure 3.12 Seasonal Cycle of Storm Count.....	61
Figure 3.13 Ensemble Groups .....	63
Figure 3.14 Ensemble Spread .....	64

Figure A.1 SAT Ensemble Distribution in Midlatitudes and Arctic .....	76
Figure A.2 SAT Anomaly High and Low.....	77
Figure A.3 SAT Anomalies DAILY and SMTH.....	78
Figure B.1 Fluxes in High and Low SIC Areas in DAILY and SMTH .....	79
Figure B.2 Day-to-day Change in SIC DAILY – SMTH .....	81
Figure B.3 1% SIC Edge in Sep 06 and Feb 07.....	82
Figure B.4 Length of Time for Rapid Change in SIC .....	83
Figure B.5 Fall SIC Edge Evolution .....	84
Figure B.6 Fall SIC Evolution in Central Arctic .....	85
Figure B.7 Fall SIC Edge Evolution and Sensible Heat Flux Anomaly .....	87
Figure B.8 Fall SIC Central Evolution and Sensible Heat Flux Anomaly .....	88
Figure B.9 Winter SIC Edge Evolution .....	90
Figure B.10 Winter SIC Center Evolution.....	91
Figure B.11 Winter SIC Central Evolution and Sensible Heat Flux Anomaly ....	92
Figure B.12 Winter SIC Central Evolution and Sensible Heat Flux Anomaly ....	93
Figure C.1 Fall Sea Ice Concentration.....	95
Figure C.2 Fall Sensible Heat Flux Differences .....	97
Figure C.3 Fall Latent Heat Flux Differences .....	98
Figure C.4 Fall Longwave Radiation Differences .....	99
Figure C.5 Fall Shortwave Radiation Differences.....	100
Figure C.6 Fall Net Upward Heat Flux Differences .....	103
Figure C.7 Fall Temperature Differences .....	104
Figure C.8 Fall Sea Level Pressure Differences .....	105
Figure C.9 Fall 500 hPa Geopotential Height Differences .....	106
Figure C.10 Fall Precipitation Differences .....	107
Figure C.11 Fall Low-level Cloud Differences .....	108

Figure C.12 Fall Medium-level Cloud Differences .....	109
Figure C.13 Fall High-level Cloud Differences.....	111
Figure C.14 Fall Specific Humidity Differences .....	112
Figure C.15 Fall Poleward Heat Transport Differences .....	114
Figure C.16 Fall Poleward Momentum Transport Differences .....	115
Figure C.17 Fall Smoothed Storm Density Differences .....	116
Figure C.18 Fall Zonal Wind.....	117
Figure D.1 Winter Sea Ice Concentration.....	120
Figure D.2 Winter Sensible Heat Flux Differences .....	121
Figure D.3 Winter Latent Heat Flux Differences .....	122
Figure D.4 Winter Longwave Radiation Differences .....	123
Figure D.5 Winter Shortwave Radiation Differences.....	124
Figure D.6 Winter Net Upward Heat Flux Differences.....	125
Figure D.7 Winter Temperature Differences .....	126
Figure D.8 Winter Sea Level Pressure Differences .....	127
Figure D.9 Winter 500 hPa Geopotential Height Differences .....	129
Figure D.10 Winter Precipitation Differences .....	130
Figure D.11 Winter Low-level Cloud Differences .....	131
Figure D.12 Winter Medium-level Cloud Differences .....	133
Figure D.13 Winter High-level Cloud Differences .....	134
Figure D.14 Winter Specific Humidity Differences .....	135
Figure D.15 Winter Poleward Heat Transport Differences .....	137
Figure D.16 Winter Poleward Momentum Transport Differences .....	138
Figure D.17 Winter Smoothed Storm Density Differences .....	139
Figure D.18 Winter Zonal Wind.....	140
Figure E.1 Regions of Focus.....	141
Figure E.2 Storm Count NE Region .....	144
Figure E.3 Storm Count WCUS Region .....	146

Figure E.4 Storm Count NEA and BCS Region ..... 149



**List of Tables**

Table 2.1 Model Simulations .....	32
Table 2.2 SLP Regional Standard Deviation .....	41

## List of Appendices

<b>Appendix A</b>	<b>Analysis of SAT Ensemble Spread .....</b>	<b>75</b>
<b>Appendix B</b>	<b>Differences Between Experiment Forcings .....</b>	<b>79</b>
B.1	Forcing Impacts on Fluxes in the Arctic During Fall.....	82
B.2	Forcing Impacts on Fluxes in the Arctic During Winter .....	89
<b>Appendix C</b>	<b>Difference Between DAILY and SMTH Atmospheric</b>	
	<b>Response During Fall.....</b>	<b>94</b>
C.1	Surface Heat Fluxes .....	96
C.2	Atmospheric Response .....	101
C.3	Storm Track Response .....	113
<b>Appendix D</b>	<b>Difference Between DAILY and SMTH Atmospheric</b>	
	<b>Response During Winter .....</b>	<b>118</b>
D.1	Surface Flux Response .....	118
D.2	Atmospheric Response.....	119
D.3	Storm Track Response.....	136
<b>Appendix E</b>	<b>Synthesis of Atmospheric Response by Region .....</b>	<b>141</b>
E.1	Northern Europe Region (Fall) .....	142
E.2	West Coast US (Fall) .....	144
E.3	Gulf of Alaska and Northeast Pacific (Fall).....	147
E.4	Northeast Atlantic and Caspian-Black Sea (Fall) .....	148
E.5	East Siberian, Laptev and Kara Seas (Fall).....	149
E.6	Continental United States (Winter) .....	151

## **Acknowledgements**

First I would like to acknowledge and thank my advisor Professor Uma Bhatt who has contributed substantially to this work and supported me throughout my degree at UAF with endless encouragement and life wisdom. I further would like to thank my other committee members Professor Igor Polyakov and Professor Xiangdong Zhang for their constructive feedback on my research. I would like to thank all three for helping me achieve my future academic goals.

I would like to acknowledge the remaining co-authors on my paper Dr. Peter Langen that contributed greatly by modifying the model making this study possible and Jeremy Krieger who helped set up the model experiments.

A sincere thanks to Professor Greg Newby and the Arctic Region Supercomputing Center for providing me a research assistantship that made this all possible. A special thanks to Oralee Nudson, Don Bahls, Craig Stephenson, and the ARSC Help Desk for outstanding user support and debugging help and for patiently accepting my use of massive amounts of disk space.

I greatly appreciate the faculty and my fellow peers in or associated with the Department of Atmospheric Sciences for making this a great place to be. Especially, I would like to thank Peter Bieniek for substantial help with programming, debugging and scientific ideas.

This material is based upon work supported by the National Science Foundation under Grant No. 0904411. Any opinions, findings, and conclusions or recommendations expressed in this material are those of the authors and do not necessarily reflect the views of the National Science Foundation. This work was also funded through graduate research assistant fellowship and a grant of HPC resources from the Arctic Region Supercomputing Center as a part of the Department of Defense High Performance Computing Modernization Program.

This research uses data and a model provided by the Community Climate System Model project ([www.cesm.ucar.edu](http://www.cesm.ucar.edu)), supported by the Directorate for Geosciences of the National Science Foundation and the Office of Biological and Environmental Research of the U.S. Department of Energy. NOAA\_ERSST\_V3 data provided by the NOAA/OAR/ESRL PSD, Boulder, Colorado, USA, from their Web site at <http://www.esrl.noaa.gov/psd/>. Thanks to Dr. Josefino Comiso for providing daily sea ice data.

I want to express my gratitude to my wife Brittany Billingsley who has been extremely patient and supportive and had the great idea that we apply to the University of Alaska. A great thanks to my parents Heidi Dammann and Rein Dammann and my brother Mikkel Narvaq Dammann, who through much encouragement have helped me become who I am and given me the confidence to pursue whom I want to be. Finally, a special thanks to Jens Amundsen, a great family friend, who through a lot of time has greatly contributed in helping me reach my academic potential.

## **1 Introduction**

### **1.1 Introduction – Arctic Sea Ice Evolution**

Sea ice is an important part of the global climate system. Its dynamic processes are highly complex in the way it evolves and interacts with the surrounding atmosphere and ocean. The distinctly different characteristics of sea ice from the ocean water lead to large impacts of sea ice changes on atmosphere-ocean interaction. The albedo of ice is several times higher than that of the ocean underneath, which consequently influences the shortwave radiation budget. The ice also acts as an insulator between the atmosphere and ocean decreasing net upward sensible and latent heat fluxes. Sea ice is highly dynamical and is capable of changing concentration, thickness and other properties quickly. A better understanding of the evolution of sea ice and how sea ice changes impact the atmosphere is crucial for understanding our climate system, properly representing sea ice in climate models and making climate projections.

The Arctic sea ice extent has been measured by satellite since the 1970's with use of passive microwave radiometers. The first consecutive dataset with good polar coverage and quality started with the National Aeronautics and Space Administration's (NASA) Nimbus 7 satellite in 1978 (Cavalieri et al. 1999). The data collection process was only first dependable starting in 1982. Prior to the satellite record and starting in 1972, weekly observations were compiled into maps for the Arctic at the National Ice Center (NIC). Ships and polar expeditions have recorded sea ice conditions since the middle of the 19th century. With the study of marine sediments collected from the ocean floor it is possible to construct a picture of what the sea ice concentrations must have been like prior to the instrumental record. This patchy reconstruction has been constructed back to the early Holocene and has found similar sea ice extent as in the 20th century (de Vernal et al. 2008). These records indicate previous maximums, but it is difficult

to know whether the 2007 low was an all time minimum over the past millennium or longer.

The most significant variability in sea ice extent are annual fluctuations due to the warming and cooling of the poles. In the Arctic the overall maximum (minimum) sea ice extent and concentration occurs typically in March (September). However, interannual variations can be more than  $5^{\circ}$  in latitude in most longitudinal sectors (Walsh and Johnson 1979).

Since the modern observations began, yearly averaged sea ice concentrations have increased for the 20 years between 1955 and 1975 (Walsh and Johnson 1979). This trend continued for the Bering Sea and the Labrador Sea during the next one-and-a-half decade from 1979 to 1993, but sea ice decreased in most other areas of the Arctic. During the following decade from 1993 to 2007 sea ice concentration has decreased around nearly the entire Arctic (Deser and Teng 2008). The sea ice edge in the Bering Sea appears to be controlled by the flow associated with the Aleutian Low, hence, governed by the Pacific Decadal Oscillation (PDO), which had a positive phase during 1980's. The positive phase might explain the continued increased average sea ice in the Bering Sea in the 1980s (Francis and Hunter 2007).

The maximum sea ice extent has been relatively stable during the last decades and displayed about a 1.5% decrease per decade. However in 2005 and 2006 the maximum extent was observed to be 6% lower than average (Comiso 2006a). The sea ice during winter consists of perennial and first year sea ice. The first year sea ice is about a meter thick, but the perennial ice can be several meters. So even while winter sea ice extent has remained relatively stable for the duration of satellite records, the average thickness has decreased. The lack of extensive observational data makes it difficult to precisely determine ice volume, but collected submarine data suggest that the average thickness decreased by about 1.25 meters between 1980 and 2000 (Rothrock et al. 2008). A continued

decrease is indicated in a recent study (Kwok and Rothrock 2009) that showed the 1980 to 2008 decrease to be 1.75m.

There is large uncertainty in the rate of sea ice decline in global climate models. This uncertainty is due to the lack of detailed observations of ice thickness limiting the ability to evaluate 20<sup>th</sup> century simulated thickness. In the Coupled Model Intercomparison Project (CMIP3) models, the average sea ice thickness ranges from less than a meter to more than three meters. The predictions for the 21st century are in large part a function of the 20th century values. Therefore, the uncertainty in 20<sup>th</sup> century values lead to errors in projections (due to a doubling of CO<sub>2</sub>) and can be off by up to a meter (Bitz 2008).

The perennial sea ice has decreased by about 10% per decade (Comiso 2006b) whereas ice extent has decreased by a more modest 3% per decade (Bjorgo et al. 1997; Parkinson et al. 1999) since the beginning of satellite records. The decrease in perennial ice seems to have made the winter sea ice thinner and consequently more vulnerable to wind and thermal effects. Thinner sea ice may explain the sudden decrease of annual maximum sea ice extent in 2005 and 2006 (Comiso 2006a).

The observed changes in sea ice are in large part caused by forcing from the atmosphere above and the ocean water underneath. Temperature change in the lower atmosphere and in upper ocean play a dominant role in the retreat of the arctic sea ice from 1979 to 2007 (Deser and Teng 2008). Dynamical forcing is at least on the same order of importance for changes in sea ice extent as temperature forcing (Polyakov et al. 2003). Recent work further support this notion (Polyakov et al. 2010).

## **1.2 Introduction – Impact of Sea Ice on Atmosphere**

The influence of sea ice concentration (SIC) on the atmosphere has been investigated in fixed sea ice and sea surface temperature (SST) Global Climate Model (GCM) experiments. Screen and Simmonds (2010) found a large correspondence in surface air temperature (SAT), SIC, and surface flux trends and recent warming trends in the Arctic might be a result of increased ocean-to-atmosphere surface fluxes (net solar radiation at surface) due to a decreasing ice cover in the winter (summer). Bhatt et al. (2008) showed that a realistic reduction in sea ice concentration during summer (1995 conditions) in an atmospheric GCM causes an increase in surface fluxes of latent and sensible heat due to the increased area of open water. This decrease in ice concentration also causes an increase in SAT and a slight decrease in SLP. Sea ice changes can also impact midlatitudes causing storm tracks shifts, which lead to changes in precipitation patterns. Similar atmospheric anomalies were also found with only regional sea ice decrease limited to individual sections of the Arctic Ocean (Bhatt et al. 2008). Petoukhov and Semenov (2010) showed that decreasing sea ice only in the Barents and Kara seas can significantly change the atmospheric circulation and can cause extreme cold events when the local heating results in a strong anticyclonic anomaly over the Polar Ocean.

Alexander et al. (2004) used a GCM to examine winter arctic sea ice impacts for the 1982-1983 (maximum) and 1995-1996 (minimum) winters. The sea ice anomalies during winter are generally not as large as those in the summer but can have large atmospheric impacts, since the strong vertical temperature gradient between SST and SAT cause large surface flux anomalies. In proximity of ice anomalies, the GCM shows a shallow enhanced SAT up to 700 hPa and precipitation, and decreased SLP over a reduced sea ice area. The opposite atmospheric response is found over enhanced sea ice areas. If the sea ice edge anomaly is co-located with a storm track, this can cause an alteration of the storm



track course, as was found in the North Atlantic Basin. Change in storm tracks can change large-scale circulation patterns and inter-annual oscillations. The response to wintertime anomalies is twice as large for sea ice concentration as for sea ice extent.

The warming of the Arctic favors a sea ice decrease (Comiso 2003). But how important is the reduced sea ice at forcing SAT changes? Rigor et al. (2002) suggested that the positive state of the Arctic Oscillation during the 90's caused advection of ice away from the arctic shoreline and caused thinner ice to be produced in East Siberian and Laptev seas. The thinner sea ice has further contributed to more ice-free areas and hence a warming of the Arctic due to increased long wave surface fluxes.

Herman and Johnson (1978) pioneered sea ice impacts studies and found that sea ice extent anomalies are not only correlated with atmospheric pressure anomalies, but are also causing them. Using a GCM forced with SIC and SST, they analyzed an idealized sea ice extreme forced simulation based on a 17-year period of observed SIC versus a 6-year control based on climatological sea ice. They found a pressure response of 8 hPa over Barents Sea. The total poleward energy flux was up to 13% larger in the midlatitudes when sea ice was increased. They suggest that the ice margin is capable of influencing local synoptic structure as well as that on a hemispheric scale. The later statement is based on the Atlantic Ocean sea ice that changes the Icelandic low, which displayed a strong correlation with the Azores high in the subtropics.

Singarayer et al. (2006) investigated how much of the current temperature increase in the Arctic is caused by SIC changes. Future scenarios are examined from the year 2000 to 2099. The study used a moderate sea ice decrease (roughly the rate of observed 1980-2000 decrease for the 21st century) and found a total increase of 1.6K from 2000 to 2099 of annual average SAT. More rapid ice declines resulted in annual average SAT increases of up to 3.9K. This experiment

shows a warming of the entire Arctic versus only in Fram Strait in a 1980 to 2000 simulation. Seasonally the increased temperatures occurred in the winter when air-sea temperature gradients are high. Decreasing sea ice during summer shows only a small effect on an annually averaged Arctic temperature increase. This study therefore indicates that the albedo change has little effect on the Arctic SAT, but likely depends more on SST and ocean circulation. This experiment finds that the temperature change alters SLP and therefore changes the midlatitude North Atlantic and North Pacific storm tracks significantly.

Deser et al. (2010) investigated the difference between the atmospheric response to 1980 – 1999 and projected 2080 – 2099 sea ice concentrations. They found the largest flux and temperature response during winter although arctic sea ice decline is largest in summer and fall. They found that most of the arctic warming is due to arctic sea ice decline. Their results indicate that the atmospheric response to future sea ice loss is most likely to correlate with the net surface energy flux than with sea ice concentration itself. The temperature response seems to cause a decrease in static stability of the boundary layer of up to 50%. Snowfall in northern Canada and Siberia increased over a percent of a centimeter a day (November – December).

Balmaseda et al. (2010) demonstrated how the arctic sea ice has implications beyond the Arctic region. Change in sea ice can alter temperature and SLP, which can have implications for synoptic weather patterns as well as multi-year oscillations like the Arctic and the North Atlantic Oscillation. Long-range atmospheric transport can be significantly altered by changes in sea ice. The atmospheric response is highly nonlinear and is largely dependant on the background mean atmosphere-ocean state. Balmaseda et al. (2010) further argued that accurate sea ice predictions are necessary for a precise seasonal forecast of the extratropical summer and hence use daily sea ice variability. Observed realistic sea ice was also used by Strey et al. (2010) in Weather Reseach Forecast

(WRF) model (Skamarock et al. 2005) experiments with 40-kilometer horizontal grid size. The atmospheric response was generally consistent with GCM results mentioned above (Alexander et al. 2004; Bhatt et al. 2008; Deser et al. 2004; Higgins and Cassano 2009).

These studies show the importance of sea ice and what role it plays in the climate system. Fixed sea ice experiments in uncoupled GCM simulations allow investigations of the atmospheric response to sea ice. Through several studies different mechanisms of atmosphere-ice interactions have been illuminated. Long-term responses in temperatures are documented by Singarayer et al. (2006) showing temperature increase as a result of decreased arctic sea ice. The strong link between decreased sea ice and temperature increase is surface fluxes from the underlying ocean (Alexander et al. 2004). This study also points out the difference between representing the ice as concentration or extent. The effects of fluxes are dependant on SAT, which determines the vertical temperature gradient between the ocean surface with relatively stable SST and the atmosphere (Deser et al. 2010).

Several seasonal and regional studies show significant effects of ice from different ice scenarios. Remote effects of ice anomalies can occur through changes in diabatic heating anomalies, advection of temperature and vorticity, and displacement of stationary waves (Honda et al. 1999). Changes in sea ice can alter pressure patterns (Magnusdottir et al. 2004) and cyclone activity (Higgins and Cassano 2009) during Arctic winter. Although flux responses are lower during summer, SIC changes are larger and significant responses are seen in geopotential height, storm activity and precipitation (Bhatt et al. 2008).

Sea ice concentration can appear to change slowly over the seasons, which to some extent, it does. However a closer look indicates that rapid changes occur over relatively large areas on a daily basis. Understanding the atmospheric

response to daily ice variations has not been well explored and is a timely exercise as the demand for seasonal forecasts and long-term projections are growing.

### **1.3 Model Versus Observed Arctic Sea Ice**

Sea ice observations and AR4 (Fourth Assessment Report of the Intergovernmental Panel of Climate Change) fully coupled CCSM3.0 model simulations were analyzed to characterize and compare sea ice concentration. The purpose of this analysis is to answer the question: How well do state-of-the-art models capture day-to-day variations of the arctic sea ice concentration?

#### **1.3.1 Data Properties**

The observational sea ice concentrations for this study comes from the Special Sensor Microwave Imager (SSM/I) data modified using the bootstrap algorithm from 1982 to 2008 (Comiso and Nishio 2008). The data set has a 25-km resolution on a polar projected grid. A total of 1132 days are missing from a consecutive 27-year daily data and linear interpolation is used to fill in data gaps. The model data cover a 27-year period (1973 – 1999) from a fully coupled CCSM3.0 (Collins et al. 2006b) 20th century control simulation (b30.004) with T85 resolution ( $\sim 1.4^\circ \times \sim 1.4^\circ$ ). Note that 20th century simulations do not correspond to exact years in the observed record since they are coupled ocean-atmosphere simulations, and therefore unconstrained. This fact means that ocean SST for a given model month will not match observations for that month. These simulations are useful for comparing statistical properties like means and variability between model and observations over similar radiatively forced time period.

The higher resolution observational data was interpolated to the model T85 grid to allow a comparison at the same resolution. The mean, the standard

deviation, and the root-mean-square of the day-to-day change of sea ice concentration are investigated to compare differences between the model and observations.

### **1.3.2 Mean Ice Conditions**

Comparing monthly mean sea ice concentration (SIC) for two climatologically extreme months (March and September) indicates that model southern ice edge is too extensive compared to observations (Figure 1.1) in agreement with (Holland et al. 2006). The model overestimates the central Arctic SIC in March and underestimates it in September.

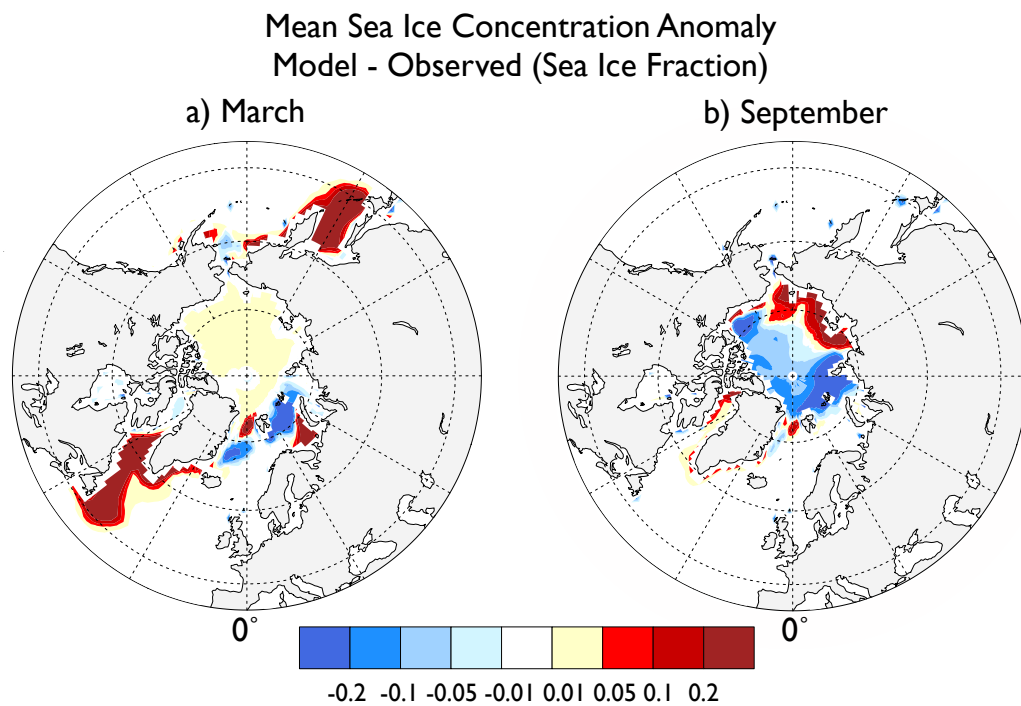


**Figure 1.1 Difference in Mean SIC in Model and Observations**

Difference of sea ice concentrations expressed as a fraction between 0 and 1 corresponding to 0% and 100%, respectively. March (left) and September (right) 26-year mean sea ice concentration (model – observed) (units: sea ice fraction).

### 1.3.3 Standard Deviation

The monthly variability of sea ice is generally underestimated in the model. Monthly standard deviations (using the standard formula) of arctic sea ice are found by calculating root mean square of 27 monthly anomalies. The differences in standard deviation between the model and observations express the climatological differences between model and observed SIC variability and are shown in Figure 1.2.

The monthly sea ice variability in the central Arctic is underestimated in the model during January but overestimated in July. Figure 1.3 displays the ratio of standard deviation sea ice in the model over observations, which is consistent with Figure 1.2. Monthly variance around the edges can be larger in the model than observations where model sea ice is more extensive than observations. In the central Arctic the model has a lower variability in the winter (by up to 4 times less) than the observations and a higher variability in the summer. Daily standard deviations averaged over a month (not shown) are very similar to the monthly standard deviation shown in Figure 1.2 and 1.3.

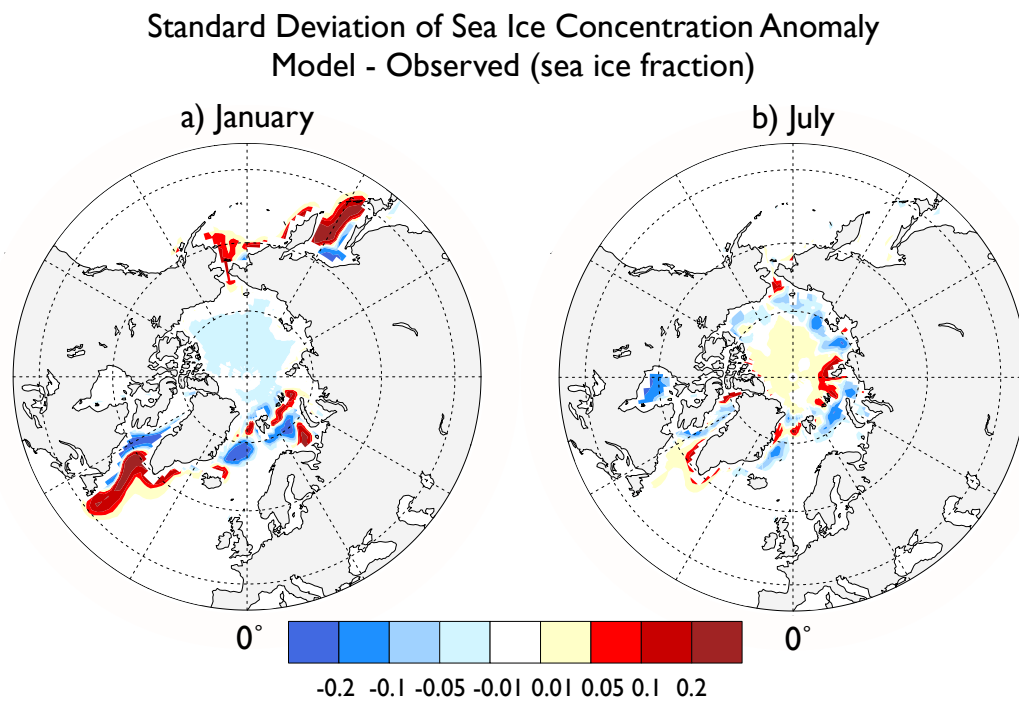


**Figure 1.2 Standard Deviation Difference of SIC Between Model and Observations**

Difference of January (left) and July (right) monthly standard deviation of sea ice concentration of model minus observed (units: sea ice fraction)



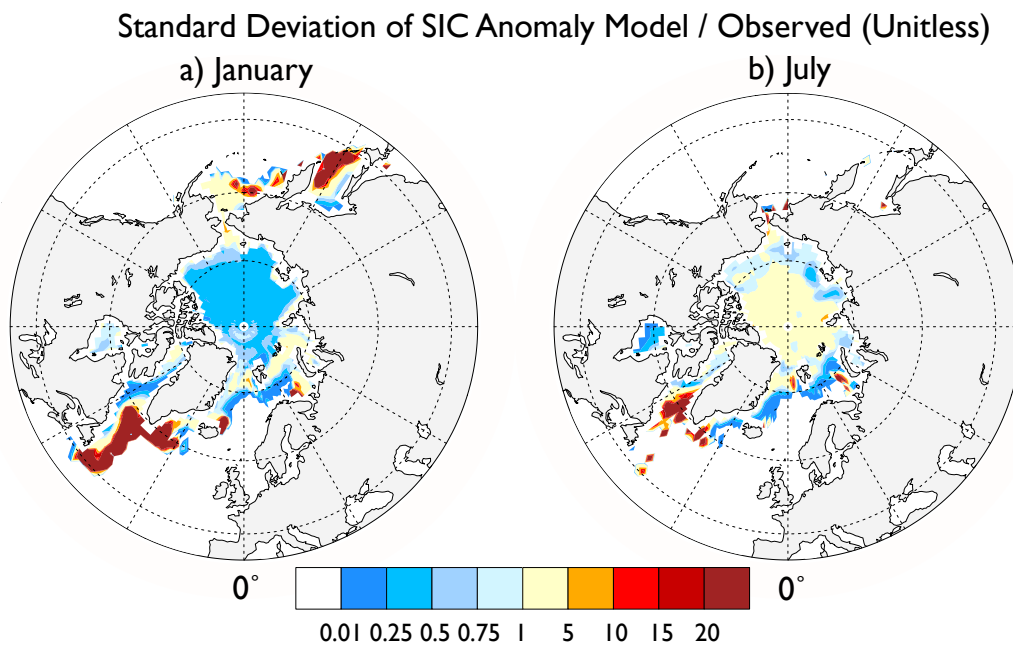


**Figure 1.3 Ratio of Model/Observed Standard Deviation of SIC**

January (left) and July (right) ratio of model/observed standard deviation of sea ice concentration (unitless).

### 1.3.4 Day-to-day Change of Ice Concentration

One of the most striking features of observed daily sea ice is its horizontal movement from wind forcing and the opening and closing of leads (e.g. see more at Cryosphere Today <http://arctic.atmos.uiuc.edu/cryosphere/>). To quantify this day-to-day variability, the difference between sea ice concentration ( $c$ ) on day  $i$  and on  $i-1$  is computed to find sea ice concentration tendency. This quantity is used to evaluate how daily changes are represented in the model. Equation 1.1

$$\frac{\partial c}{\partial t} = \frac{1}{m-1} \sum_{d=2}^m \sqrt{\frac{\sum_{y=1}^n (c(d, y) - c((d-1), y))^2}{n}} \quad (1.1)$$

describes the tendency taking the root mean square of 27 years of daily differences for one particular date. One-day tendencies are averaged over a time period ( $c$  is SIC,  $m$  and  $n$  is number of days and years respectively used in the calculation). The results are displayed in Figure 1.4 and show generally higher variability in observations for all seasons. Exceptions exist where the ice extent is greater in model than observed and around the North Pole where satellite data were not available in the early part of the record and have been replaced with 100% ice concentration. The model consistently underestimates daily variations along the ice edge during summer and fall (middle and lower rows Figure 1.4).

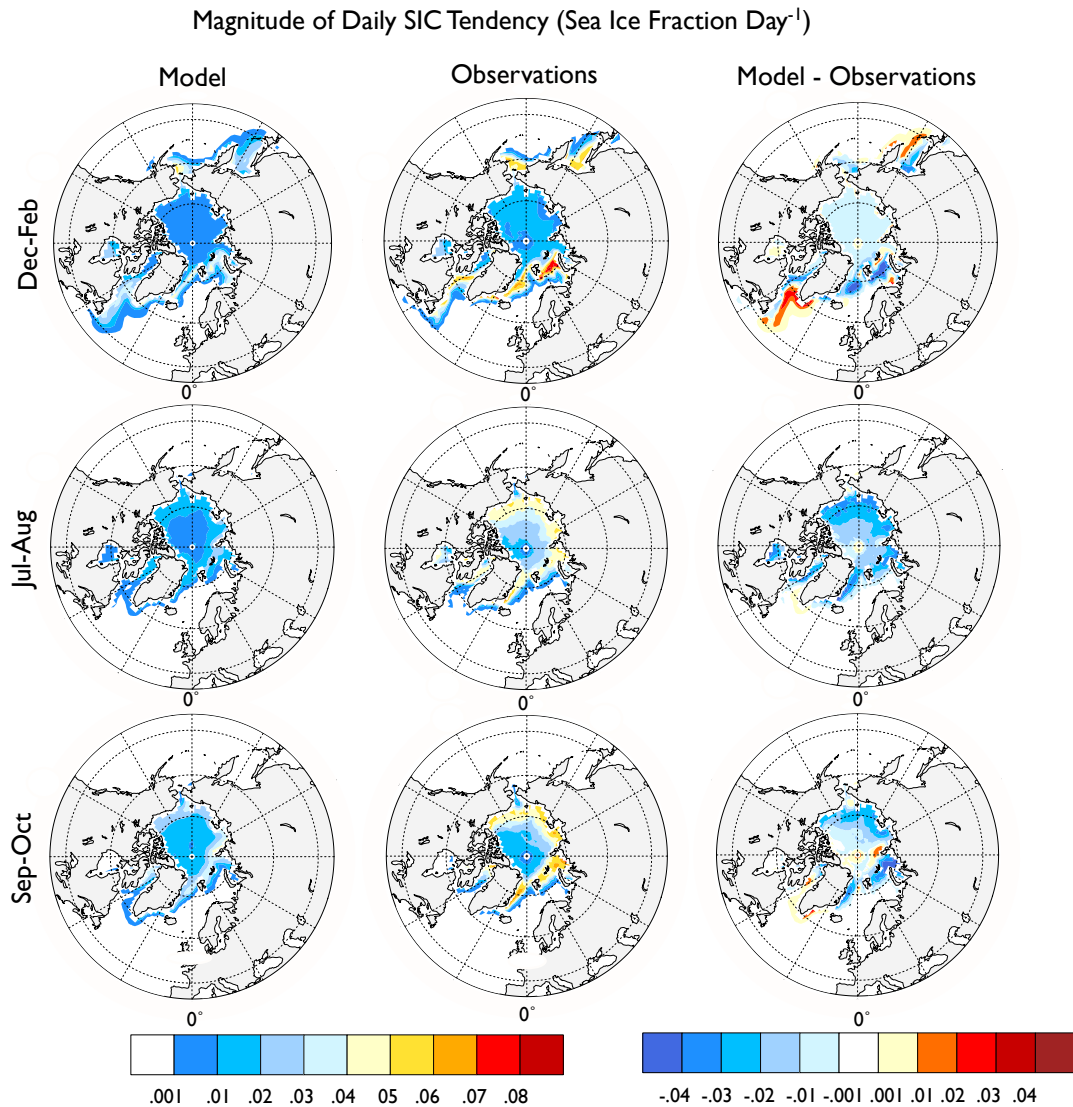


**Figure 1.4 Day-to-day SIC Change in Model and Observations**

Difference in SIC between two consecutive dates root-mean-squared over 27 years of the same day interval. Daily tendency values are averaged from December to February (DJF) (top), July to August (JA) (middle), and September to October (SO) (bottom). Left column displays model SIC tendency, middle column shows SIC tendency from observations, and the right shows the difference of model-observations SIC tendency (units: sea ice fraction day<sup>-1</sup>).

SIC variability is underestimated in models both on a climatological and a day-to-day time scale, which leads to questions regarding the feedback of these biases on the atmosphere. The focus of this thesis is to investigate the following questions:

- Does higher temporal and spatial variability of sea ice forcing lead to a different atmospheric response than a more smoothed forcing?
- What consequences do the above results have for future fixed sea ice GCM studies as well as coupled model integrations?

The organization of the thesis is as follows. Section 2 describes the methods and model experimental set up employed to investigate these questions. Section 3 documents the model results and discussion. Finally, Section 4 provides a summary and conclusions. Appendices A-E provide substantial material that was drawn upon for the analysis presented in the main part of the thesis. Evaluation of ensembles and the relationship between heat fluxes and sea ice concentration is documented in Appendices A and B. The majority of variables considered studying the atmospheric response during fall and winter are included in Appendices C-D in the form of plots and analysis to provide detailed documentation of how conclusions were drawn. Appendix E offers a regional synthesis of the atmospheric response.

## **2 Model, Data and Methods**

### **2.1 Model Description**

This study employs the Community Atmosphere Model 3 (CAM3.0) (Collins et al. 2006a). This is one of the components of the Community Climate System Model 3.0 (CCSM3.0) (Collins et al. 2006b). The CCSM model is a widely used global climate model developed at the National Center for Atmospheric Research (NCAR) in collaboration with other national laboratories and university partners. Version 3.0 was released June 2004 and was used for the 4<sup>th</sup> assessment report by the Intergovernmental Panel of Climate Change (IPCC) released 2007. The model consists of five individual components modeling the atmosphere (CAM3) (Collins et al. 2006a), ocean (POP) (Smith and Gent 2002), landsurface (CLM3) (Dickinson et al. 2006), and sea ice (CSIM5) (Briegleb et al. 2004), which are held together by the flux coupler (CPL6) (Kauffman et al. 2002).

When running CAM3 only the CAM and the Community Land Model (CLM) components are interactive. The Parallel Ocean Program (POP) and the Community Ice Model (CSIM) are replaced by data models where SST and SIC values are specified as boundary conditions.

CAM is a global atmospheric general circulation model, with 26 vertical levels and is based upon the Eulerian spectral dynamical core with triangular truncation at 31, 42, and 85 wave numbers, horizontal resolutions of approximately 3.75", 2.8", and 1.4", respectively (Collins et al. 2006b). The Community Land Model (CLM3) horizontal resolutions are similar to that of CAM3.

The data ocean component of the CAM3 was modified to read in daily values of sea ice fraction and sea surface temperature. The standard model reads in monthly ice and SST then interpolates to obtain daily values. The modified code employed here reads new two-dimensional sea ice and temperature fields

each day of the model integration at 00 hrs, and these values are then used to force the model for the next 24 hours. Apart from the changed frequency of the input boundary conditions, the model treats and uses the fields in the same manner as the standard distribution of the code.

Three simulations using the modified version of CAM were integrated to investigate the atmospheric response to climatological SIC, smoothed SIC, and daily varying SIC from observations.

## **2.2 Observations**

Observational SST and sea ice concentrations were used to force the climate model. The sea ice concentration data set used in this study is derived from passive-microwave satellite sensors (Comiso et al. 2003). These measurements are the most consistent source of arctic sea ice data. The full data set is reconstructed from radiances collected from multiple satellite programs during several decades. The first satellite carrying a passive microwave scanner was the NASA Nimbus 5, which was launched in December 1972 carrying a single-channel Electrically Scanning Microwave Radiometer (ESMR). From 1978 the SeaSat and the Nimbus 7 carried Scanning Multichannel Microwave Radiometer (SMMR). Starting 1987, the Defense Meteorological Satellite Program (DMSP) collected data using the special sensor microwave/imager (SSM/I) (Comiso et al. 2003; Cavalieri et al. 1999). From 2002 the Advanced Microwave Scanning Radiometers AMSR-E and AMSR sensors collect the most accurate data to date (Comiso et al. 2003). Based on the radiances from these separate observational methods a long-term consistent ice concentration dataset was created using three algorithms: The enhanced NASA Team (NT2) algorithm (Markus and Cavalieri 2000), the Bootstrap Basic Algorithm (BBA), and the AMSR Bootstrap Algorithm (ABA) (Comiso et al. 2003). This study utilizes SIC data from 1982 to 2008.

All simulations were forced with the climatological annual cycle of sea ice for Antarctica provided by the Hadley Centre (HadISSL\_1.1\_ICE) and climatological SSTs. The sea surface temperature data set comes from the National Oceanic and Atmospheric Administration (NOAA) Extended Reconstructed Sea Surface Temperature V3b (Smith et al. 2008) (<http://www.esrl.noaa.gov/psd/>). This dataset is constructed using the International Comprehensive Ocean-Atmosphere Data Set (ICOADS) release 2.4 SST data and improved statistical methods to construct a continuous data set from sparse data.

**Table 2.1 Model Simulations**

<b>Integration</b>	<b>Sea Ice Boundary Conditions in the Arctic</b>
<i>Control (CTRL)</i> (105 years)	Monthly mean ice conditions smoothed to daily values using averaged 1982-2007 ice concentrations.
<i>Daily06-07 (DAILY)</i> (100 ensembles)	Daily varying ice conditions over the period July 1, 2006 to November 30, 2007.
<i>Monthly06-07 (SMTH)</i> (100 ensembles)	Smoothed daily ice conditions over the period July 1, 2006 to November 30, 2007.

### **2.2.1 Data Used as Boundary Conditions in CTRL, DAILY and SMTH Experiments**

For the 100-year control simulation (CTRL) CAM was forced with averaged SIC and SST (1982 – 2007) and the annual cycle of forcings was repeated for 105 years. The analysis used the last 100 years of the simulation initialized on July 1.

The first experiment (DAILY) is forced with observed daily SIC in the Arctic for 17 months from July 2006 to November 2007. SST and southern

hemisphere SIC are specified as climatological values. This experiment (DAILY) is comprised of 100 members, each initialized on July 1<sup>st</sup> from different years of the control simulation.

A smooth version of the daily data for northern hemisphere is used to represent SIC in models (Figure 2.4). The initial forcing conditions use monthly averages smoothly interpolated to daily values using a cubic spline (OLD SMTH). This is the standard method used in GCMs (McCaa et al. 2004, Section 2.5.2). It turns out that for sea ice concentration the monthly means of daily and splined values may not match and can have large differences (Figure 2.1a). Modified forcing values were constructed based on an algorithm ensuring the monthly average in each grid point differed by less than  $\pm 0.5\%$  (Figure 2.3). Using the new smoothed forcing the difference in atmospheric response between daily and smoothed is largely due to differences in sea ice forcing variability and not in difference in overall monthly average sea ice concentration. Running the model with the old forcing conditions (DAILY – OLD SMTH, Figure 2.2a), where monthly mean sea ice differs, results in a larger atmospheric response than in DAILY – SMTH (Figure 2.2b).



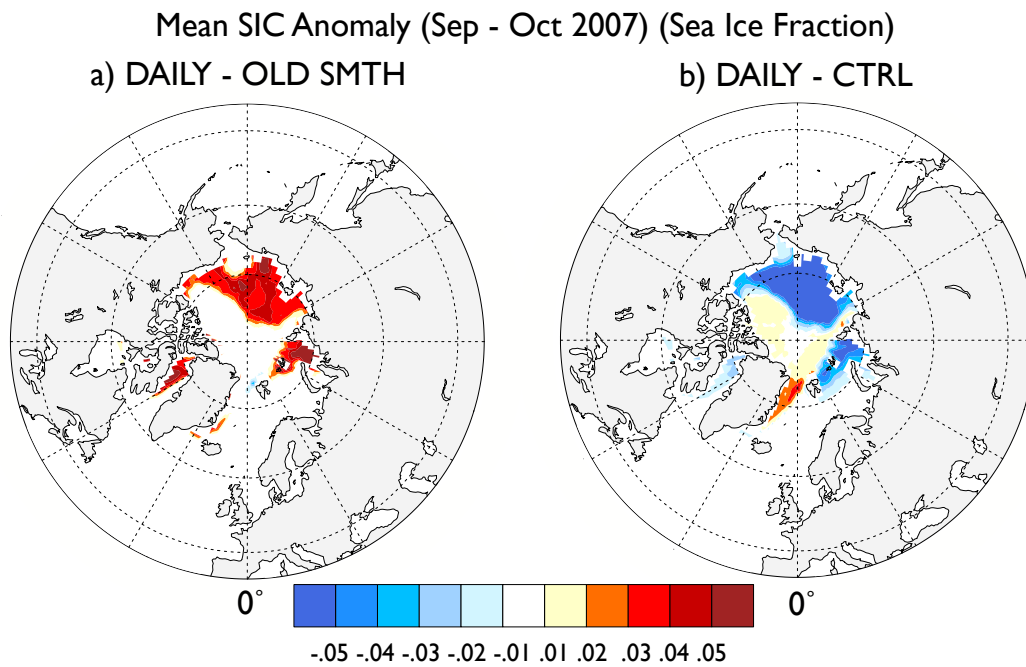


**Figure 2.1 SIC Difference Between OLD SMTH and DAILY**

a) DAILY – OLD SMTH sea ice concentration averaged over Sep – Oct 2007.  
b) DAILY – CTRL averaged over Sep – Oct 2007 (Climatology is 1982 – 2008)  
(units: sea ice fraction).

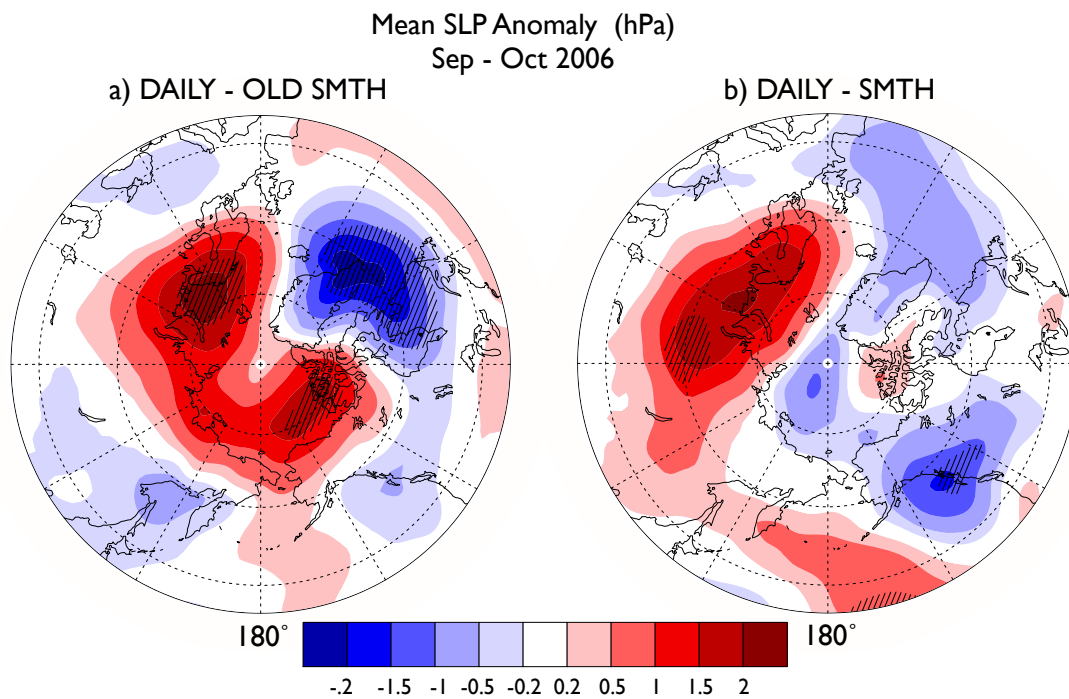


**Figure 2.2 SLP Response Difference Between Old and New SMTH**

Ensemble average (50 ensembles) (Sep – Oct 2006) sea level pressure anomaly (hPa) for a) DAILY – OLD SMTH, b) DAILY – SMTH. Crosshatching represents significance at the 95% or greater level based on Student’s t-test. A larger response is seen using OLD SMTH.

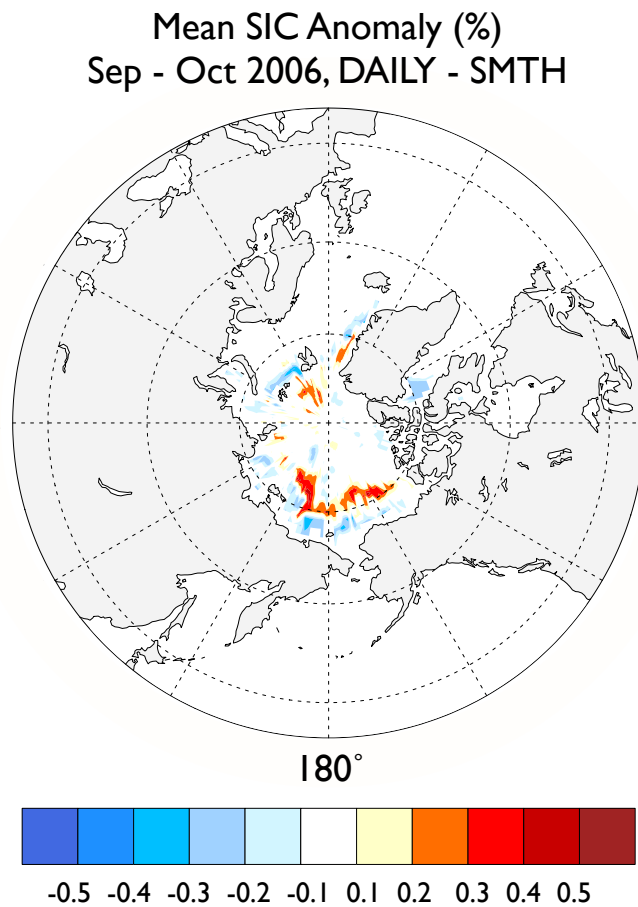
The first step in creating the monthly smooth forcing was calculating a 30-day running average of daily sea ice concentration. This means that each value is the average starting with 15 days before to 15 days after it. This creates a smooth forcing set but still does not ensure monthly averages within 0.5% of daily values.

The second step applies the following algorithm to each grid point on a month basis: Find difference between monthly average daily values and monthly average of smooth values. This difference is multiplied by the number of days in the month and divided by a larger number so we can distribute the amounts added or subtracted unevenly to ensure that values added to the middle of the month are larger by a factor of 4 in order to minimize jumps between the months. If the new daily value for SMTH is higher than 1, then it is set to 1 and if it is below 0, then it is set to 0. Since the correction for below-zero and above-one occurred frequently the algorithm needed to be repeated several times for certain grid points.

All of the days in a month (even the first and last day) must be altered in a few grid points to ensure all points differ less than  $\pm 0.5\%$ . This can cause the data to be less smooth. Areas where all days in a month must be altered are highly non-smooth points and does not seem to affect the SMTH forcing.

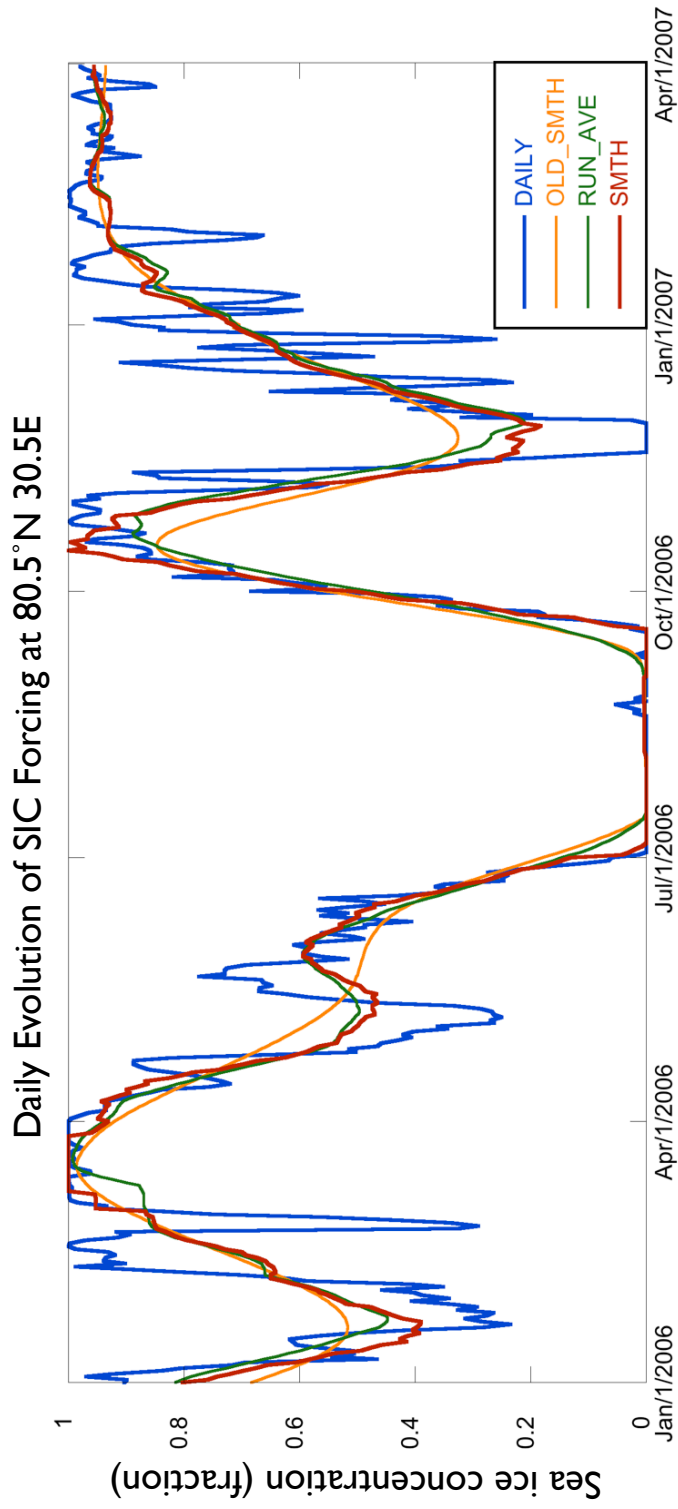
The SMTH experiment is forced with the smoothed version of the daily ice concentrations and follows the experimental design for DAILY: SST and southern hemisphere SIC were fixed to an annual cycle of climatological values. This experiment is an ensemble of 100 members, initiated using July 1 initial conditions from the control simulation.

Figure 2.4 shows several time series at a sample grid point of OLD SMTH, DAILY, running average and SMTH forcings.



**Figure 2.3 Difference in Mean SIC Between DAILY and SMTH**

DAILY – SMTH monthly mean SIC (Sep – Oct 2006). Figure shows regions that differ with between -0.5% and 0.5% in monthly means (units: sea ice % concentration).



**Figure 2.4 Sea Ice Concentration Comparison for Various Experiments**  
 SIC forcing evolution of an example grid point (80.5N and 30.5E). DAILY (blue), 30-day running average (green), SMTH (a 30-day running average adjusted for the monthly mean to match the monthly mean of daily values) (red), and OLD SMTH (created using cubic splined values) (orange) (units: sea ice concentration (fraction)).

The two experiments have a similar average SIC forcing in each grid point, but there are notable differences of SIC distribution.

The December 2006 forcings for the two experiments display these differences when counting the SIC values occurring between each percent value: [0], <0,1], <1,2] ,..., <99,100] for every grid point that during the month contained positive SIC at least once. These differences are quantified in the December 2006 distribution of sea ice concentration category count (Figure 2.5).

There are more occurrences of the highest (99-100%) and lowest (0%) SIC values in the daily sea ice forcing since the other forcing is smoothed (see insets Figure 2.5). Note that the total number of counts over all percent intervals is not the same for the two experiments. This is caused by the way the smoothed forcing is created using values outside the particular month which can cause sea ice to occur in the smoothed forcing even when there are no occurrences of ice in the daily observed forcing. On any given day, roughly 80 more points contains sea ice in SMTH than in DAILY.

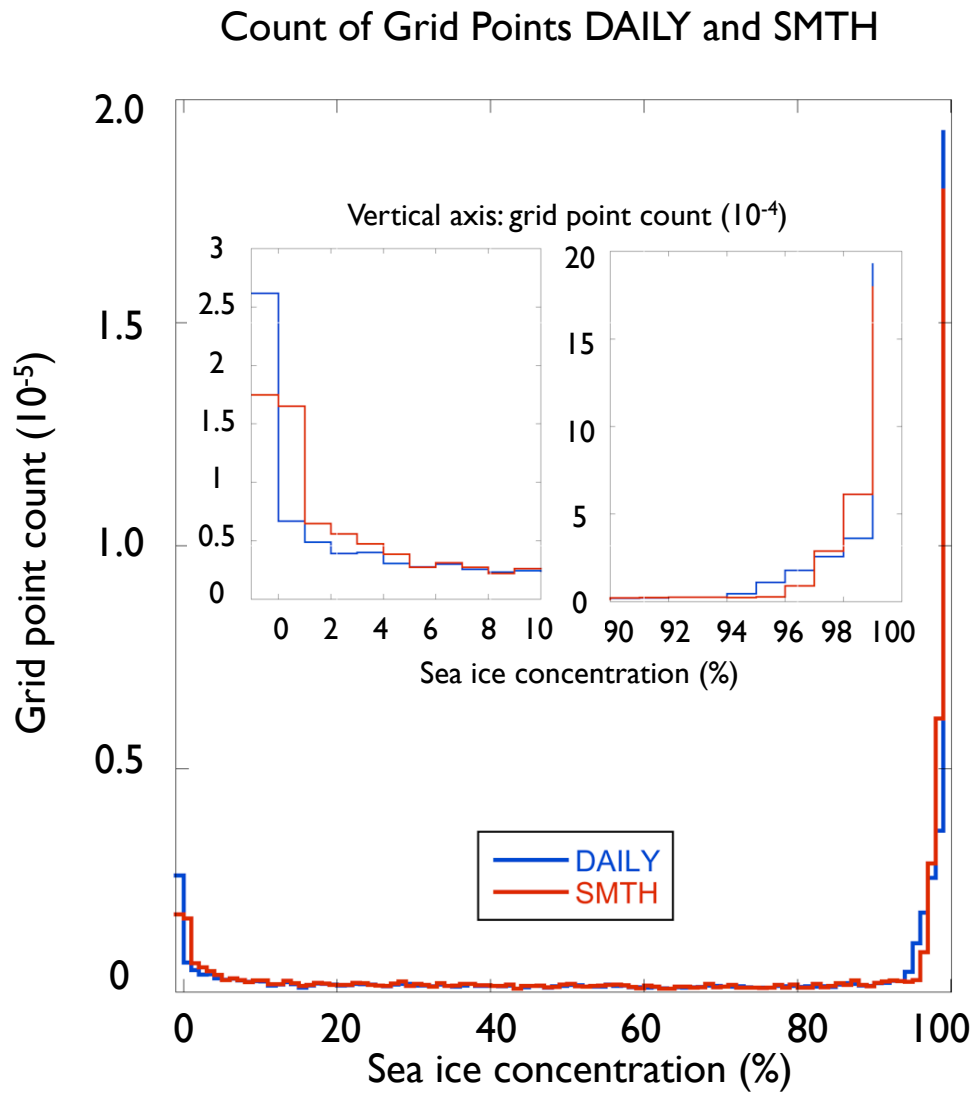


**Figure 2.5 Distribution of Sea Ice Concentration in DAILY and SMTH**

December 2006 ice forcing displayed as number of grid cells containing SIC in the 100 percentage intervals four times daily. SIC = 0 is counted separately in the grid points that at least one time during the month contains sea ice. Insets display blown-up depiction of the low (left) and the high (right) ends of the scale.

## 2.3 Methods

### 2.3.1 Number of Ensembles

The significance of atmospheric response in the experiments is evaluated using Student's t-test. The number of ensembles needed to achieve a robust significance is dependant on the ensemble average of the field as well as the standard deviation of a given variable. Simulations of variables with higher intrinsic variability require more ensemble members. Equation 2.1 is used to determine the number of ensembles required by the Student's t-test for a significant shift in the mean to achieve a level of 95% significance (Alexander et al. 2004; Sardeshmukh et al. 2000).  $N$  is the minimum number of ensembles,  $x'$  is the response, and  $\sigma$  is the standard deviation.

$$N > \frac{8}{\frac{x'}{\sigma}} \quad (2.1)$$

The following standard deviations of SLP (Table 2.2) occur in the first 50 ensembles of the control simulation for two latitude regions (30 – 70N and 70 – 90N) during August 2007 and November 2007.

**Table 2.2 SLP Regional Standard Deviation**

Standard deviation of SLP (hPa) in two regions: 30-70°N and 70-90°N.

	<b>August 2007</b>	<b>November 2007</b>
<b>30 – 70°N</b>	2.2	4.2
<b>70 – 90°N</b>	5.6	7.0



The largest response in SLP occurring in DAILY – SMTH is about 2 hPa. Equation 2.1 indicates that with a standard deviation of 6 hPa, 72 ensembles are required to reach 95% significance. Therefore 100 ensembles are used instead of the original 50.

### **2.3.2 Storm Track Algorithm**

To analyze the atmospheric response to varied SIC forcing this study uses a storm track algorithm (Zhang et al. 2004) to analyze change in cyclones. The method is based on a previous algorithm (Serreze 1995) and has been modified by Zhang et al. (2004).

The algorithm uses SLP to track storms. A storm is recorded and tracked if it follows a few criteria. 1) In a grid cell, the SLP is lower than in all the eight surrounding grid points. 2) The pressure gradient from the grid point to the eight surrounding points is at least 0.15 hPa per 100 km on average. 3) The gradient from the surrounding four closest grid points to all their surrounding grid points must point outwards. 4) If two possible cyclones are closer than 1200 km they are considered to be the same cyclone. 5) A low center has to persist for 12 hours (three time steps) or more to be counted. For the cyclone to be tracked, it cannot have moved more than 600 km during one time step (6 hour).

This storm track code is designed to read in NCEP reanalysis data from binary files (Zhang et al. 2004). The code used in this study was altered to read in NetCDF files of SLP on a T85 CAM3 output grid.

### **2.3.3 Bandpassed Filtering**

Bandpassed filtering (2 to 10 days) is used as an additional diagnostic to investigate cyclone activity in the three simulations using six hourly data. Filtering is based on 30-day running averages (leaving out first half of July 06 and last half of November 07) and applying bandpassed filtering weights. Poleward heat ( $v'T'$  at 850 hPa) and momentum ( $u'v'$  at 200 hPa) transport were calculated and analyzed. High values indicates high storm activity in both these variables.

### **3 Results and Discussion**

In this section, the following question is answered: Is there a difference between the atmospheric response to daily as compared to smoothly varying sea ice concentration? If so, then how do the differences arise? To this end, sea ice forcing is first quantified, followed by the atmospheric response for two seasons, fall (September-October) and winter (November-February). The seasonal divisions were constructed based on similarities of sea ice forcing as well as atmospheric response. Finally, there is a discussion of regional storm track response and of the ensemble spread.

#### **3.1 Fall (September – October) Response**

During fall 2006, there were large negative sea ice anomalies in the Siberian sector of the Arctic. As the seasonal cooling proceeded, there were rapid expansions of sea ice concentration from near 0% to 100% in less than a week, which occurred primarily in the Laptev, Kara and East Siberian Seas. These rapid SIC changes lead to large differences between the DAILY and SMTH forcing, with more days with SIC values close to 100% in DAILY than SMTH. Figure 3.1 displays the sea ice evolution in two sample grid points in the Arctic that are representative for surrounding areas. Rapid change and large differences between DAILY and SMTH are found in the Siberian sector but are not evident in the Atlantic sector of the Arctic (Figure 3.1). See Appendix B for additional details on the differences between sea ice conditions between DAILY and SMTH.

More days with near 100% SIC in DAILY lead to reduced heat fluxes out of the ocean when compared to SMTH. Figure 3.2 displays net surface heat (sum of latent, sensible and longwave) flux anomaly out of the Arctic Ocean between the two experiments (DAILY – SMTH). DAILY has reduced ocean-to-atmosphere fluxes over the Kara, Laptev, and East Siberian Sea when compared

to SMTH. These reduced fluxes are co-located over the area where there was rapid equatorward ice expansion in the Siberian seas. The large flux anomalies (DAILY – SMTH) over ocean grid points are found in the far North Atlantic and the midlatitude Northern Hemispheric oceans. These non-arctic heat flux anomalies occur mainly due to circulation shifts and changes in cyclone activity between experiments, and will be confirmed by subsequent analysis.

The DAILY-SMTH temperature response during fall displays significant cooling of more than 0.5K over the Kara, Laptev, and parts of the East Siberian seas in DAILY (Figure 3.3). This cooling is co-located with reduced fluxes out of the Arctic Ocean in DAILY compared to SMTH. The anomalously cool temperatures extend southward into Siberia and downstream eastward leading to reduced temperatures over Alaska. The DAILY-SMTH temperature anomalies do not compare favorably with the pattern of differences in monthly mean SIC between DAILY and SMTH (Figure 2.3), suggesting these small differences in monthly mean (less than 0.5% are not the cause of the different atmospheric temperature responses.

The DAILY – SMTH SLP anomaly displays a significant high-pressure anomaly over Northern Europe with a central magnitude of roughly 1.5 hPa (Figure 3.4a) and a weaker (~1 hPa) low just west of Spain over the Atlantic Ocean. The 500 hPa DAILY – SMTH geopotential height anomaly displays significant positive values over Northern Europe with a central magnitude of about 12 m (Figure 3.4b) and a weaker (~8 m) low west of Spain. The 500 hPa geopotential height atmospheric response is colocated with the SLP anomaly indicating an equivalent barotropic structure in the atmospheric response. Theoretical work has shown that the anomalous equivalent barotropic structure is associated with an anomalous eddy circulation that leads to changes in storm tracks (Peng and Whitaker 1999). The subsequent analysis primarily investigates

whether the anomalous SLP high over Northern Europe is associated with reduced cyclone activity.

The DAILY – SMTH precipitation anomaly displays reduced precipitation (up to  $0.4 \text{ mm day}^{-1}$ ) over Northern Europe in DAILY and is consistent with fewer or weaker storms (Figure 3.5). A notable southward shift in precipitation occurs over the Pacific Northwest and is consistent with a strengthening of the Pacific jet (Figure 3.6a). Note: this feature does not attain 95% or greater significance based on a t-test. Positive precipitation anomalies of up to  $0.2 \text{ mm day}^{-1}$  are evident just west of Spain in Figure 3.5. The increased (reduced) precipitation anomalies are co-located and consistent with the negative (positive) SLP and 500 hPa height anomalies. Figure 3.6a displays 200 hPa average fall zonal wind (u) for SMTH with contours and anomalies of DAILY – SMTH with shading. A southward shift in the polar jet in DAILY is apparent in most parts of the jet and is consistent with the negative arctic surface air temperature anomalies (Figure 3.3). The anomalously cool Arctic leads to a stronger equator-to-pole temperature gradient shifting regions of strongest temperature gradient southward and hence the polar jet also equatorward. The increased temperature gradient in DAILY is consistent with a higher poleward heat transport. DAILY  $v'T$  shows  $2.6 \text{ K m s}^{-1}$  higher heat transport than SMTH vertically averaged between 1000 – 500 hPa and zonally averaged at  $70^\circ\text{N}$ . Over the North Atlantic, the 200 hPa jet streak is reduced and retracted (Figure 3.6a). Storms often form in the downwind poleward region of the jet streak and the reduced jet streak in the North Atlantic is unfavorable for storm development over Northern Europe.

Storm activity in DAILY and SMTH is investigated through analyzing variability in poleward heat transport at 850 hPa on synoptic timescales of 2 – 10 days. Figure 3.6b displays DAILY – SMTH bandpassed (2-10 days) 850 hPa  $v'T'$  anomalies. The DAILY – SMTH  $v'T'$  at 850 hPa displays significant

negative anomalies (up to  $0.3 \text{ K m s}^{-1}$ ) over Northern Europe and is consistent with reduced storm activity in DAILY. There are also weakly significant positive 850 hPa bandpassed heat transport anomalies across northeastern North America that are consistent with a stronger 200 hPa jet (Figure 3.6a).

Individual storms are tracked and counted based on six-hourly SLP method of Zhang et al. (2004) to further substantiate the storm track response to the different sea ice forcings. Figure 3.7 displays an ensemble average frequency distribution of storm count over the Northern European positive SLP anomaly (55-75N, 0-60E) for DAILY (blue) and SMTH (red). Storms are categorized based on their central pressure. The SMTH simulation has a larger storm count for central pressures of less than 995 hPa while DAILY has a larger storm count for central pressures of greater than 995 hPa. The storm counts support the notion that there are fewer (4%) and weaker storms in DAILY than SMTH over Northern Europe. See Appendix C for additional plots (e.g. cloud amounts and individual heat fluxes) characterizing the atmospheric response during fall to DAILY versus SMTH sea ice forcing.

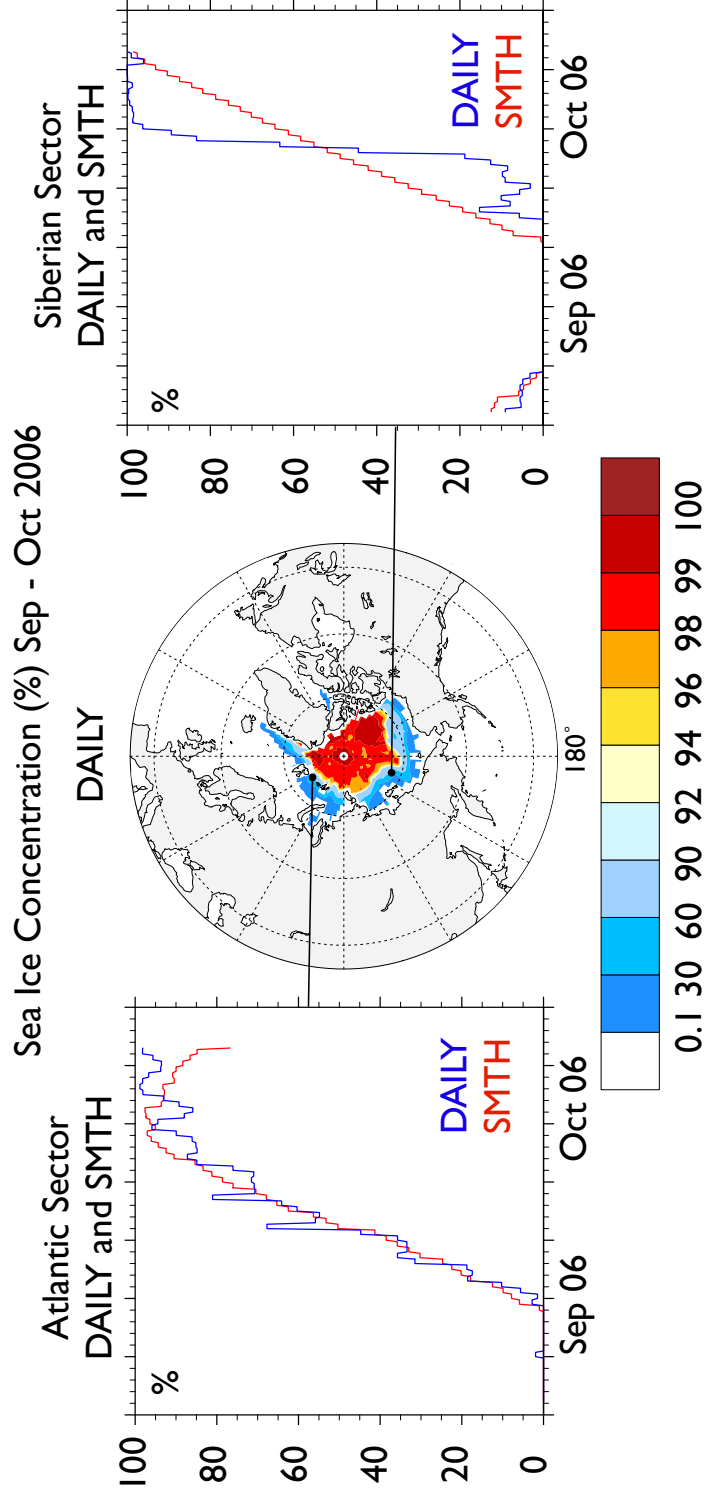


**Figure 3.1 Sea Ice Concentration Forcing**  
 September and October 2006 average SIC (%) for DAILY (Middle) Note non-linear scale in middle panel. Time series plots of DAILY (blue) and SMTH (red) show SIC changing from September 1<sup>st</sup> to October 31<sup>st</sup> in two locations, the North Atlantic (left panel) and the Siberian Seas (right panel). Rapid changing SIC is seen in the Siberian sector of the sea ice leading to different atmospheric responses in DAILY and SMTH experiments.

Net Upward Surface Heat Flux Anomaly ( $\text{W m}^{-2}$ )  
(Latent, Sensible, & Longwave)  
DAILY - SMTH (Sep-Oct)

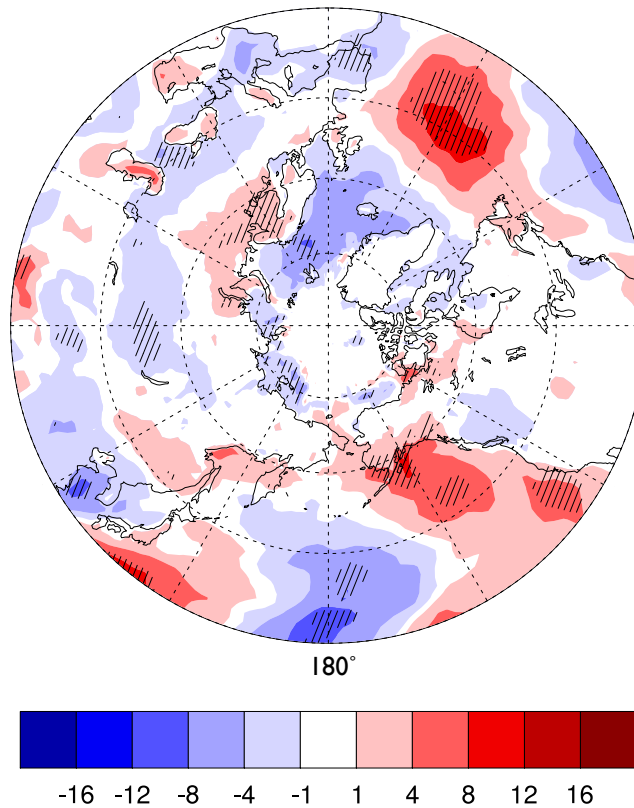


**Figure 3.2 Net Upward Surface Heat Flux Anomaly**

Ensemble average (Sep – Oct) total upward surface heat flux anomaly ( $\text{W m}^{-2}$ ) DAILY-SMTH. Crosshatching signifies statistical significance at the 95% or greater level based on Student's t-test.



Surface Air Temperature Anomaly (K)  
DAILY - SMTH (Sep-Oct)

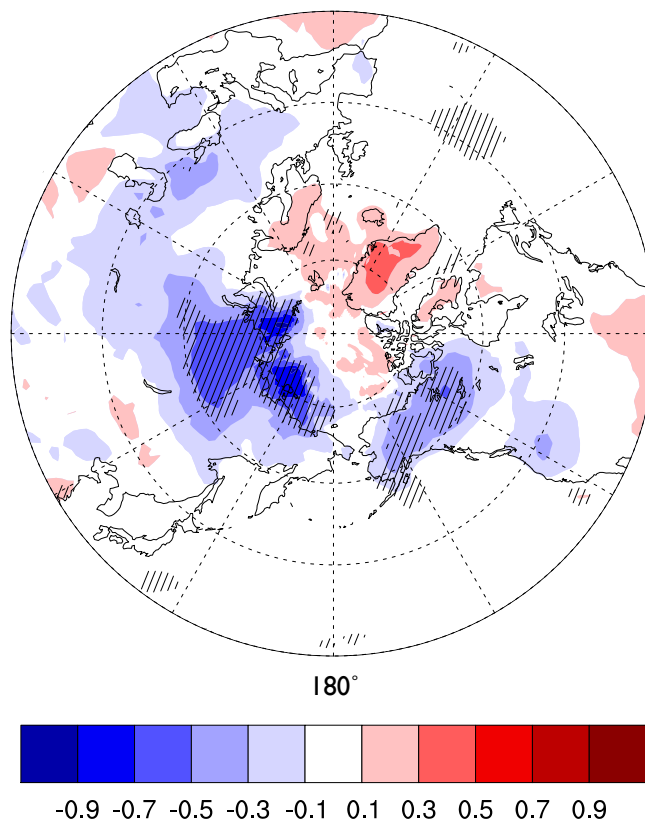


**Figure 3.3 Temperature Anomaly**

Ensemble average (Sep – Oct) temperature anomaly (K) DAILY-SMTH. Crosshatching signifies statistical significance at the 95% or greater level based on Student's t-test.

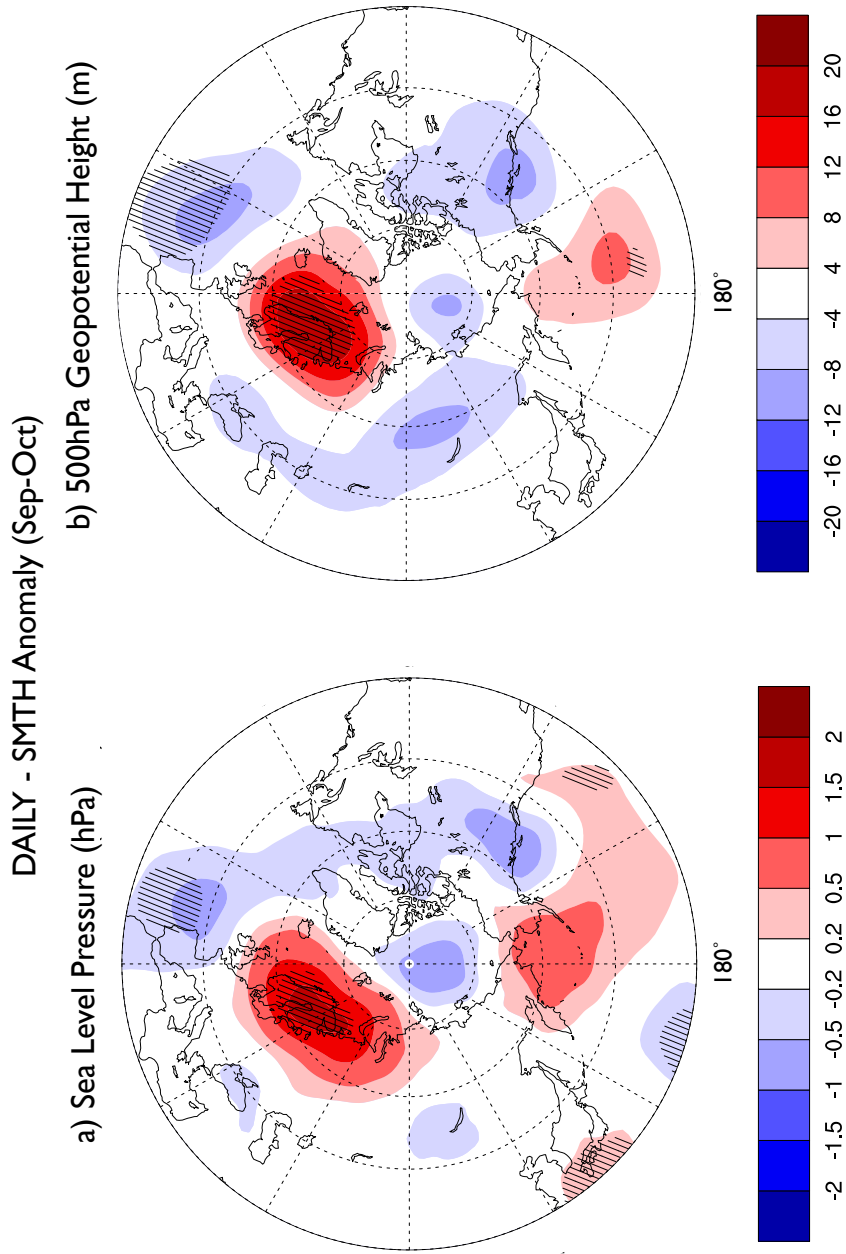


**Figure 3.4 Sea Level Pressure and 500 hPa Geopotential Height Anomalies**  
 a) Ensemble average (Sep – Oct) sea level pressure anomaly (hPa) DAILY-SMTH. b) Ensemble average (Sep – Oct 2006) 500 hPa geopotential height anomaly (m) DAILY-SMTH (right). Crosshatching signifies statistical significance at the 95% or greater level based on Student’s t-test.

Precipitation Anomaly ( $\text{mm day}^{-1}$ )  
DAILY - SMTH (Sep-Oct)  
Contours: Mean SMTH

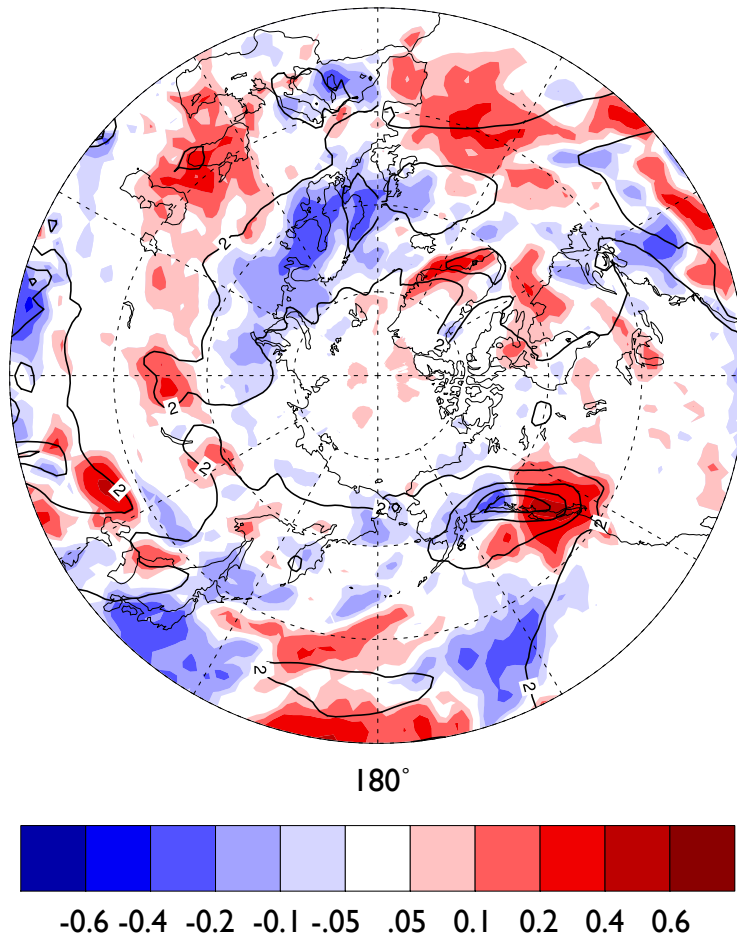


**Figure 3.5 Precipitation Anomaly**

Ensemble average (Sep – Oct 2006) total precipitation anomaly ( $\text{mm day}^{-1}$ ) DAILY-SMTH shown by shaded colors. Contours display climatological precipitation from the SMTH simulation. For significance see Figure C.10c.

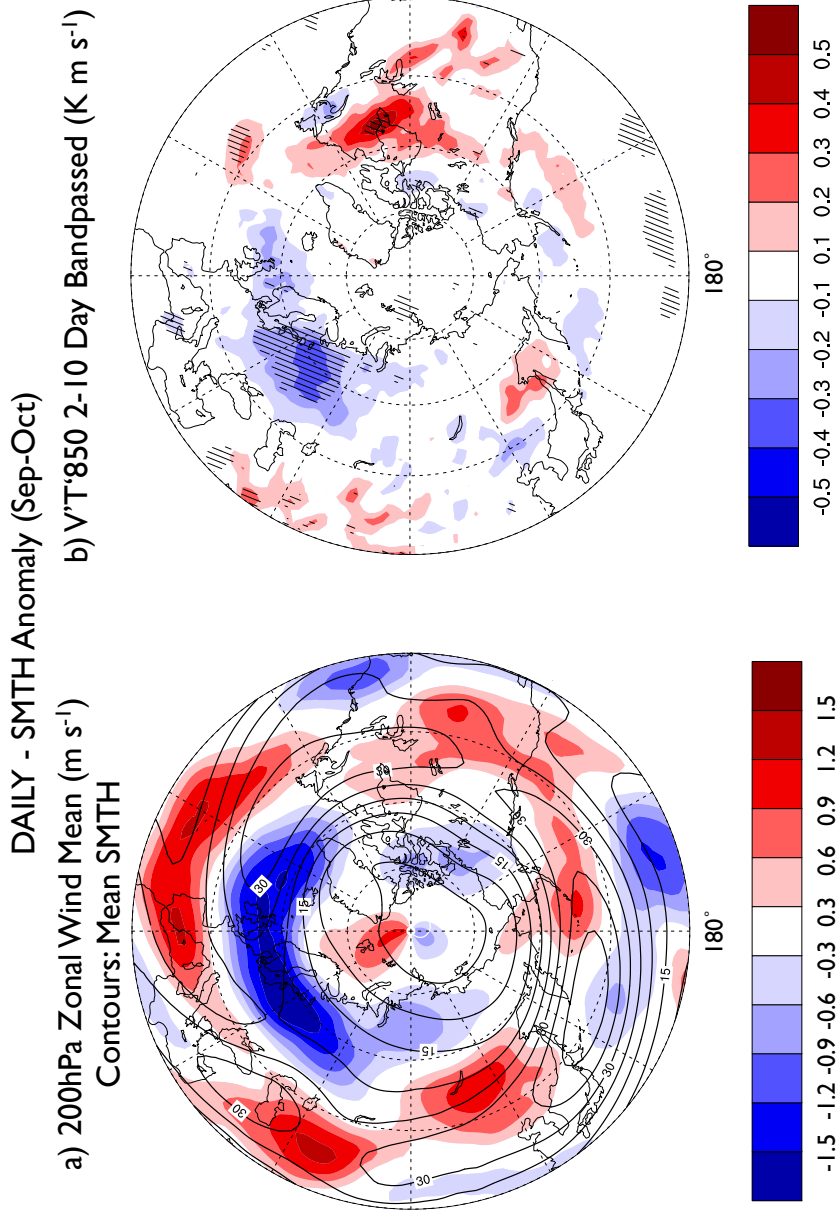


**Figure 3.6 Zonal Wind at 200 hPa and  $v'T'$  2-10 Day Bandpassed Anomaly**  
 a) Ensemble mean (Sep – Oct 2006) zonal wind speed 200 hPa ( $m s^{-1}$ ). Shading indicates DAILY-SMTH and contours represent climatological 200 hPa zonal wind from SMTH. Positive and negative anomaly in the North Atlantic and negative anomaly in the North Pacific are significant at the 95% or greater level based on Student's t-test. b) Ensemble average (Sep – Oct 2006)  $v'T'$  850 hPa ( $K m s^{-1}$ ) DAILY-SMTH. Crosshatching signifies statistical significance at the 95% or greater level based on Student's t-test.

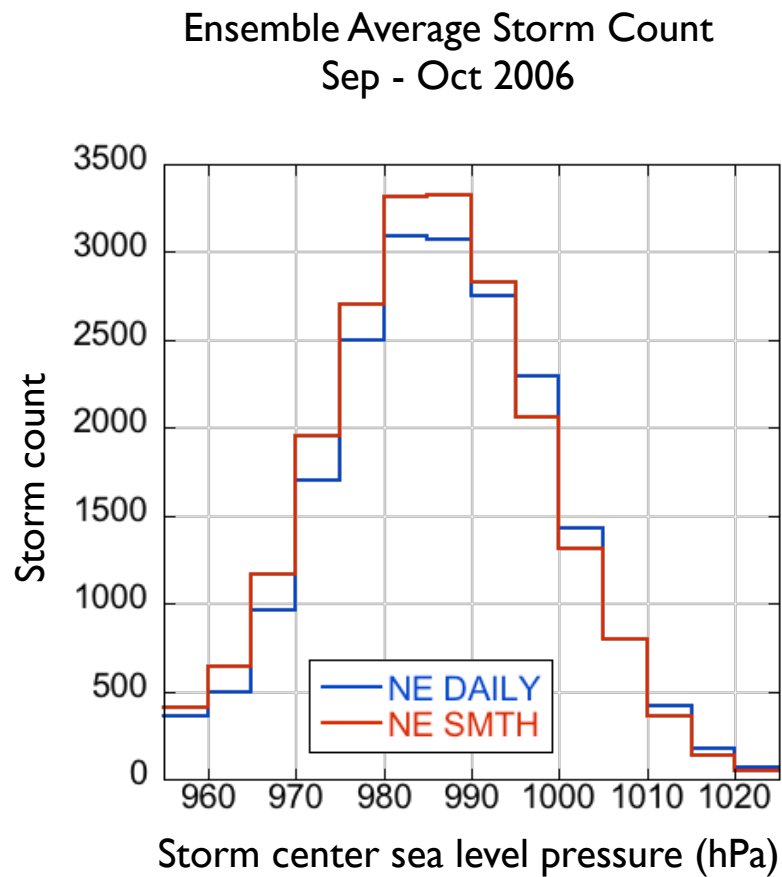


**Figure 3.7 Storm Count**

Sep – Oct 2006 storm center pressure (hPa) and ensemble average number of storm centers in the Northern Europe region (55-75N, 0-60E).

### 3.2 Winter (November – February) Response

Sea ice in various sectors of the Arctic Ocean evolves differently over the course of winter from November to February. The evolution of daily sea ice in the Atlantic and Pacific domains of the marginal ice zone are displayed in Figure 3.8. In the Pacific sector the sea ice rapidly expands equatorward during winter, which leads to large differences between DAILY and SMTH sea ice concentrations. This subsequently results in negative total heat flux anomalies in DAILY – SMTH (Figure D.6c). In the Atlantic sector the daily sea ice edge is quite dynamic and is characterized by a slower equatorward expansion as compared to the Pacific Sector (Figure B.3 and 3.8, left panel). See Appendix B for more details on sea ice evolution during winter.

The DAILY – SMTH SLP anomaly displays a significant positive center over southern Alaska and western Canada (Figure 3.9a). This strong ridge that is characterized by an anomalous anticyclonic circulation leads to increased flow of cold arctic air into the western US (Figure 3.9b) and deepens the trough resulting in anomalously cool temperatures over the West Coast that extend eastward from the general westerly flow contributing to reduced surface air temperatures over the continental US in DAILY (Figure 3.10c). Comparing the surface air temperature anomalies for DAILY-CNTRL (Figure 3.10a) and SMTH-CTRL (Figure 3.10b) reveals generally similar patterns in the Arctic but an opposite temperature response over the continental US. It is noteworthy that these two different sea ice boundary conditions leads to strikingly different temperature anomalies over the continental US (Figure 3.10c). This is relevant in light of recent studies that suggest that reduced sea ice in the Arctic may be one possible explanation for recent cold and stormy east coast US winters (Overland et al. 2010; Strey et al. 2010). See Appendix D for further information on the atmospheric response during winter.

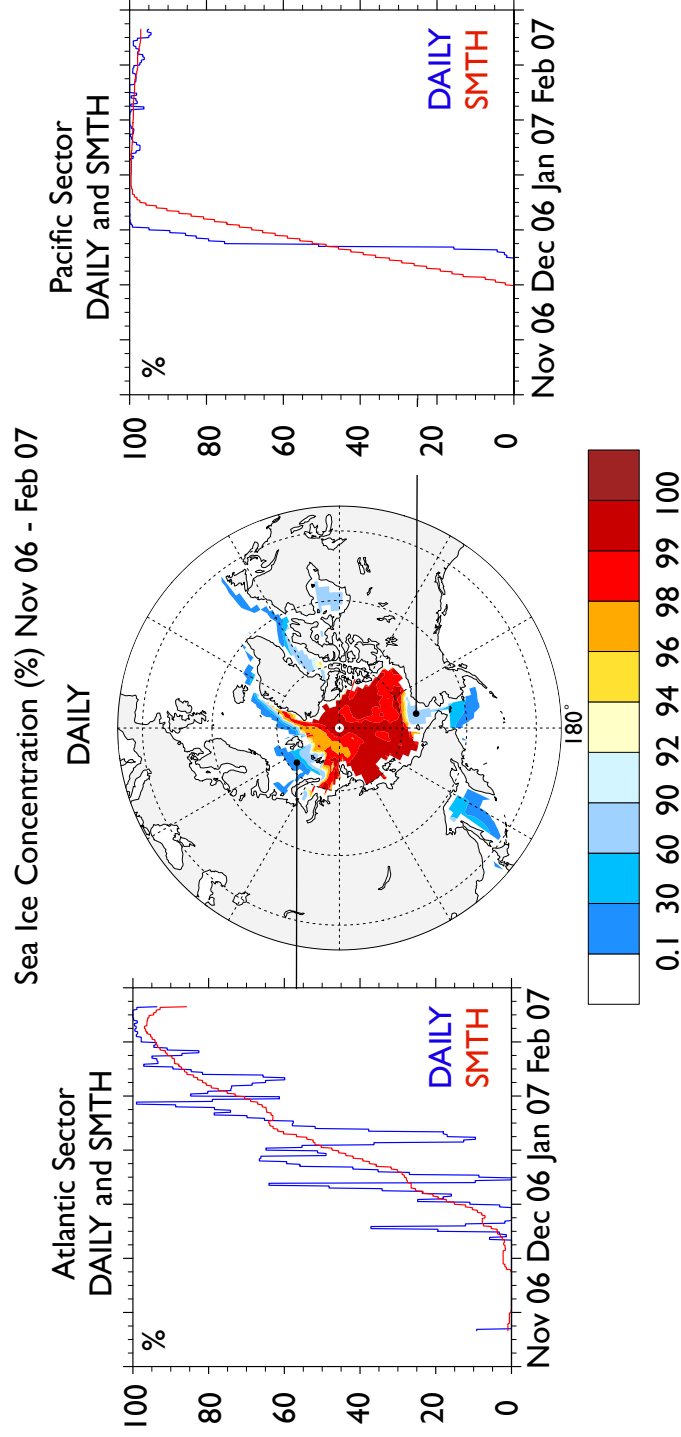


**Figure 3.8 Sea Ice Concentration Forcing**

November – February average SIC (%) DAILY (Middle). Note non-linear scale in middle panel. Time series plots of DAILY (blue) and SMTH (red) show SIC changing from November 2006 to February 2007 in two locations, the North Atlantic (left panel) and the Pacific (right panel).

DAILY - SMTH Anomaly (Nov 06 - Feb 07)

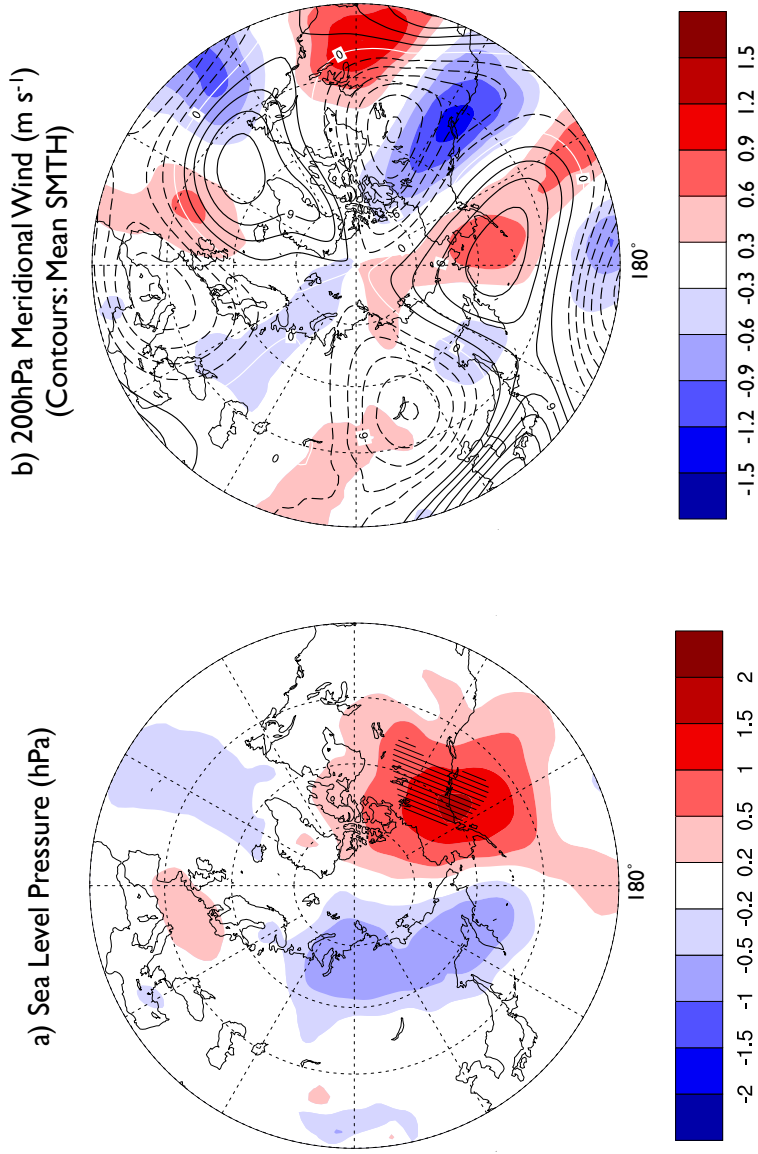


**Figure 3.9 SLP and Meridional Wind Anomaly**

a) Ensemble average (Nov 06 – Feb 07) sea level pressure anomaly (hPa) DAILY-SMTH. Crosshatching signifies statistical significance at the 95% or greater level based on Student's t-test. b) Ensemble average (Nov 06 – Feb 07) 200 hPa meridional wind ( $\text{m s}^{-1}$ ): Shading indicates DAILY-SMTH and contours represent climatological 200 hPa zonal wind from SMTH (contour interval is  $3 \text{ m s}^{-1}$ ). Anomaly over Bering Sea, West Coast US, Midwest US and western North Atlantic are significant at the 95% or greater level based on Student's t-test.



Surface Air Temperature Anomaly (K) (Nov 06 - Feb 07)

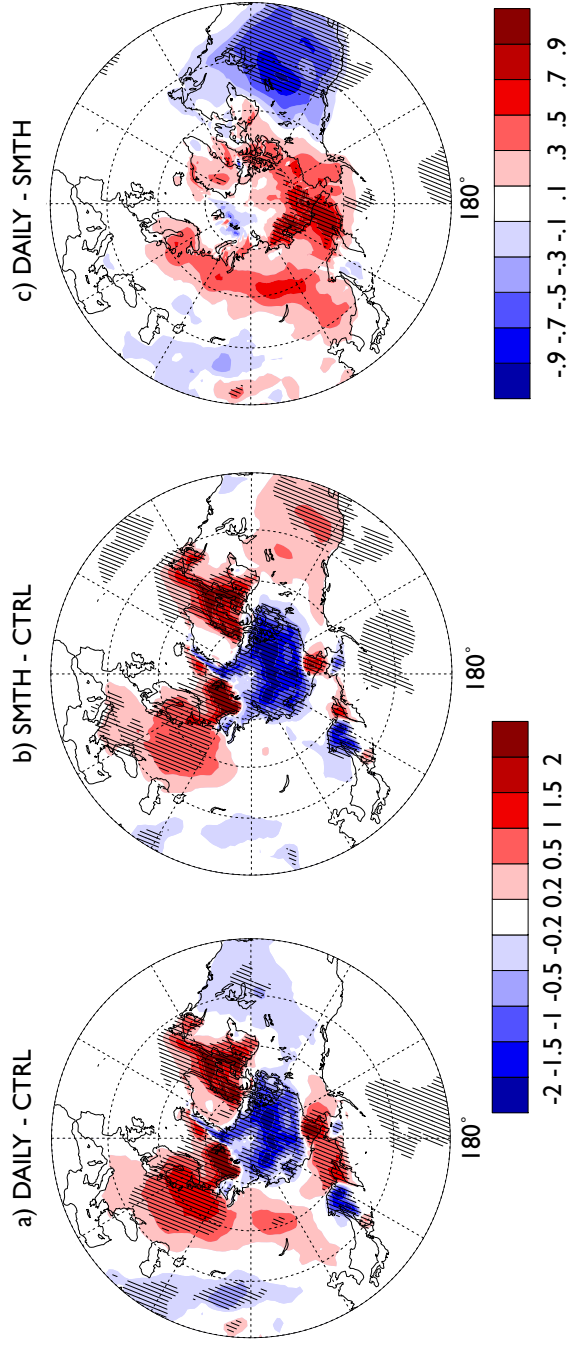


**Figure 3.10 Temperature Anomaly**

Ensemble average (Nov – Feb) temperature anomaly (K) a) DAILY-CTRL, b) SMTH-CTRL, c) DAILY - SMTH. Crosshatching signifies statistical significance at the 95% or greater level based on Student’s t-test.

### **3.3 Stormtrack Response in the Midlatitudes and the Arctic**

The relatively small sea ice forcing differences between DAILY and SMTH results in significantly different atmospheric responses in the Arctic as well as the midlatitudes. The response can most easily be summarized by counting the ensemble average annual cycle of storm counts in the Arctic and midlatitudes (domain definition in Figure 3.11) for both experiments (Figure 3.12). From March –October DAILY displays higher storm counts than SMTH in the Arctic (Figure 3.12a) and in all months except June-July in the midlatitudes (Figure 3.12b). These storm count differences are relatively small average (1-2%) over the midlatitudes and the Arctic but can be up to 40% over particular regions. What this analysis shows is that apparently small differences in the nature of the sea ice forcing leads to shifts in the atmospheric general circulation from the Arctic to the midlatitudes. Note the general shape of the seasonal cycle of the model storm counts compares favorably with observations (Black NCEP line). NCEP displays a much higher storm count but is likely not that high due to the simple scaling used to compare the different model and NCEP grids.

## Midlatitude and Arctic Domains

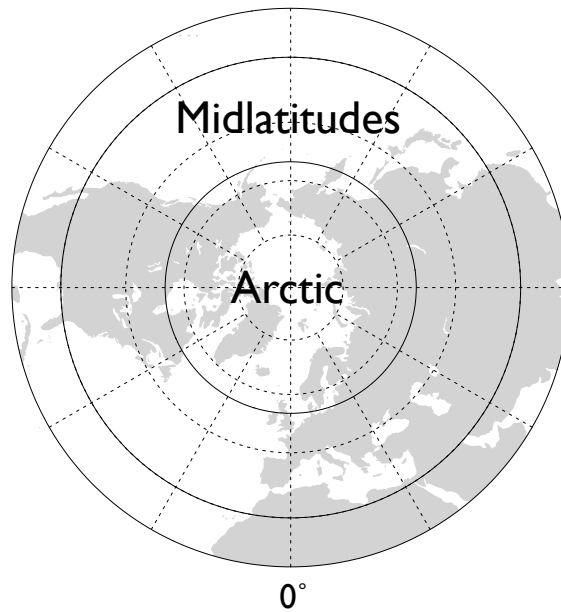


**Figure 3.11 Midlatitude and Arctic Region**

The Arctic (55-90N) and midlatitudes (30-55N) regions are defined for the storm count analysis.

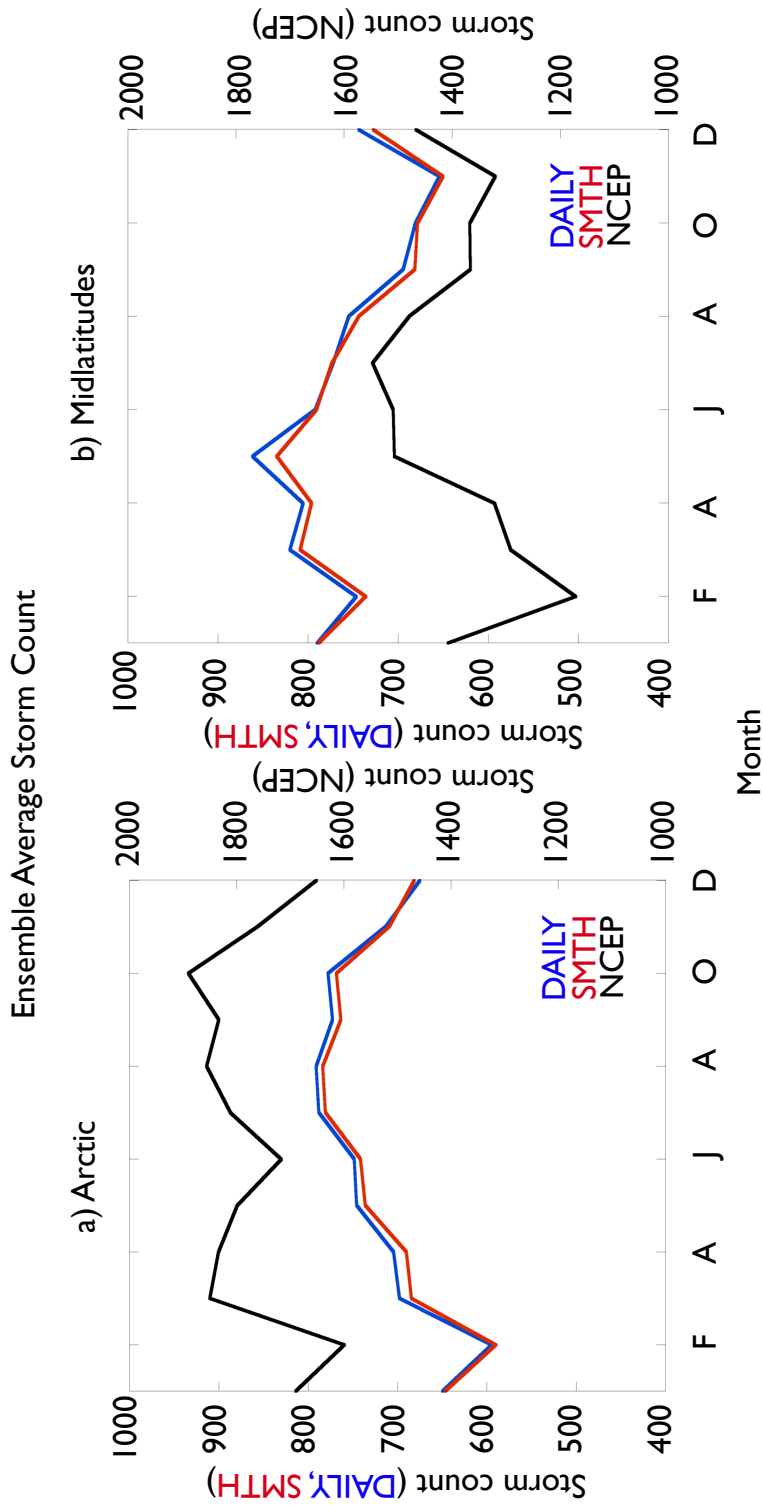


**Figure 3.12 Seasonal Cycle of Storm Count**

Figure shows ensemble average storm count for DAILY (blue) and SMTH (red) in each month for the Arctic (left) and midlatitudes (right). 1948 – 2009 average storm count from NCEP reanalysis is multiplied with 2.67 (scaling to account for smaller grid size in model) (black).

### 3.4 Ensemble Analysis

Most analysis of atmospheric response to DAILY and SMTH in this study uses ensemble averages. Due to high model atmospheric variability in the Arctic, here follows an evaluation of the ensembles.

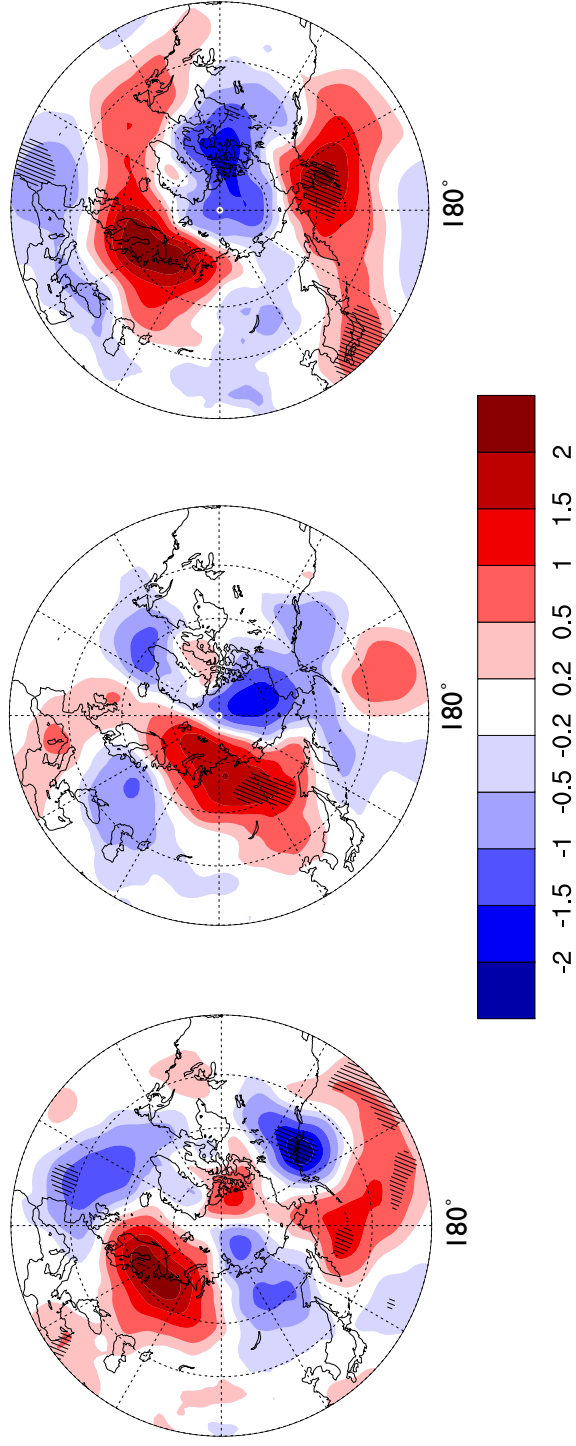
Figure 3.13 displays ensemble averages of fall SLP. Three sets of 30 ensembles of a total of 90 ensembles from our 100-ensemble experiments are averaged. Large differences in atmospheric response occur between ensemble sets. Opposite features are evident in DAILY – SMTH anomalies between the three panels.

Figure 3.14 displays SLP for each ensemble member DAILY – SMTH over a small spatial average (68-72N, 30-35E) near the center of the high-pressure anomaly over Northern Europe during fall. The figure reveals a large ensemble spread with ensemble members commonly deviating up to 10 hPa from the ensemble mean (~1.5 hPa).

The large ensemble spread points out the importance of employing large ensembles when running climate models with focus on the Arctic regions.

Sea Level Pressure Anomaly (hPa)  
DAILY - SMTH (Nov 06 - Feb 07)

a) Ensemble Average 1-30 b) Ensemble Average 31-60 c) Ensemble Average 61-90



**Figure 3.13 Ensemble Groups**

Figure shows ensemble average sea level pressure (hPa) of three groups of thirty ensembles DAILY - SMTH (Sep - Oct 2006): a) ensembles 1 - 30, b) ensembles 31 - 60, c) ensembles 61 - 90. Crosshatching signifies statistical significance at the 95% or greater level based on Student's t-test.

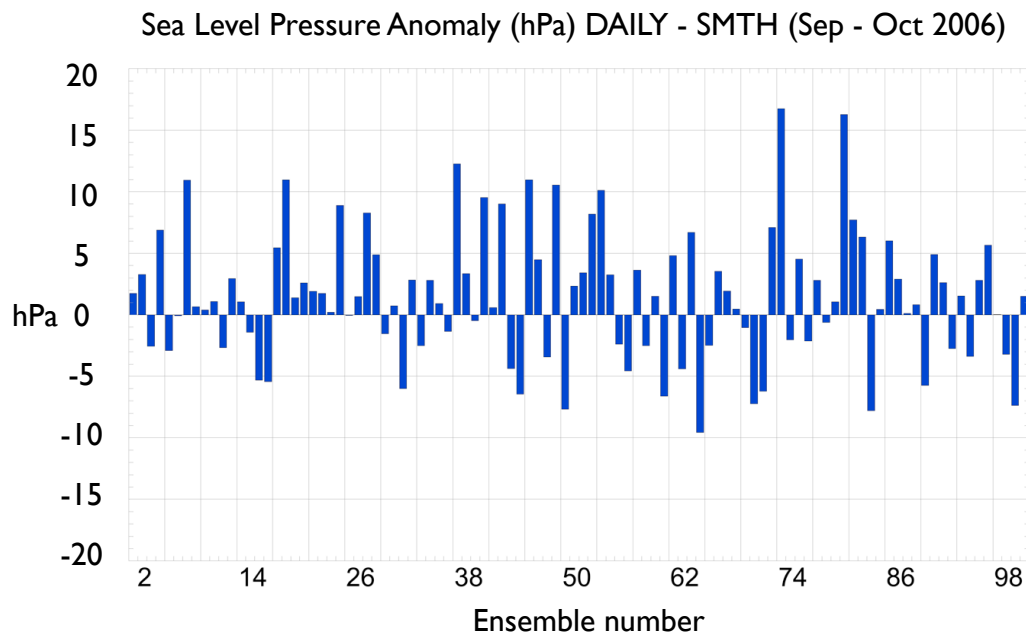


**Figure 3.14 Ensemble Spread**

Sea level pressure anomaly (hPa) DAILY – SMTH spatial average (68-72N, 30-35E) for ensemble member 1 – 100 (Sep - Oct).

#### 4 Summary and Conclusions

The purpose of this study was to evaluate how well the day-to-day variability in arctic sea ice is captured in global climate models and to examine the atmospheric response to different temporal scales of sea ice variability. This study employs a global atmospheric circulation model – the NCAR Community Atmosphere Model (CAM3) – to investigate the atmospheric impact of forcing the model with observed daily (DAILY) sea ice concentration (SIC) and with smoothly varying forcing (SMTH - resembling current global atmospheric model forcings).

This work documents that ice modeled by the Community Sea Ice Model (CSIM5) does not capture the variability in arctic sea ice in fully coupled CCSM3.0 20<sup>th</sup> century simulations. Annual variability as well as day-to-day variability is underestimated in the model by upwards of 50% over the central Arctic Ocean.

This study examines the method of temporal interpolation of monthly data to create daily SIC values through cubic splines which is the method used by the majority of global climate models. This method leads to a difference in SIC between DAILY and SMTH and is not capable of preserving accurate monthly mean SIC. Differences in means are found up to over 4% in large areas. This has important consequences for how realistic fixed sea ice concentration GCM experiments should be conducted.

The seasonal sea ice evolution has been examined and the largest differences between DAILY and SMTH occur in regions and seasons with rapid change in total SIC. Large differences between DAILY and SMTH sea ice is the case for the equatorward ice edge and especially in Kara, Laptev, East Siberian and Chukchi seas. In these regions, DAILY sea ice concentration typically expands from near 0% to near 100% in less than two weeks. The forcing in



SMTH is based on a 30-day running average and is incapable of representing such high variability leading to common occurring SIC differences of over 40% between DAILY and SMTH.

Atmospheric parameters for two seasons, fall 2006 and winter 2006-07 are extensively documented and seven regions with many statistically significant differences are investigated further in Appendix E. Fall was investigated due to the rapid change in SIC and the large anomalies during this season. Winter was chosen for analysis due to large sea ice extent and strong temperature gradients between the ocean and atmosphere resulting in relatively large fluxes from openings in the sea ice. Six of these large regional responses occur during fall and may originate from the differences in SIC evolution, surface fluxes and temperature over the Kara, Laptev and East Siberian seas. The most pronounced difference during fall is a remote response to sea ice that occurs over Northern Europe. In DAILY, a high-pressure anomaly of over 1.5 hPa occurs associated with a decrease and weakening of storm tracks, decrease in poleward heat transport, clouds, and precipitation. During winter the most pronounced feature is an anomalous high over Alaska in DAILY, leading to decreased westerlies from the Pacific Ocean and more arctic air advection from the north onto the West Coast of the US leading to a general cooling of the continental US.

Several regions far from the sea ice, experience large differences between DAILY and SMTH due to a change in the general circulation and storminess. An increase in SLP is closely linked to reduced cyclone activity. DAILY sea ice forcing is capable of rapid change and quickly reaches high SIC values as sea ice extends equatorward. Rapidly extending sea ice in DAILY allows the insulating effect between ocean and atmosphere to prevail longer than in SMTH and reduces heat fluxes out of the ocean leading to a cooler Arctic in DAILY. A regional cooling is expected to lead to an increase in regional baroclinic stability, which is unfavorable for the development of extratropical

cyclones. An increase in regional baroclinic stability and hence a reduction in storms might explain the reduced SLP over Northern Europe during fall. However, more storms are seen in DAILY for all seasons in both the Arctic and the midlatitudes on average. This is likely due to the increase in poleward heat transport, a consequence of the general cooling of the Arctic in DAILY. More study is needed to completely understand the mechanistic link between the differences in SIC variability and the atmospheric anomalies seen in these experiments.

As seen, regions with a rapid change in SIC are important to consider when estimating the biases arising from using smooth SIC forcing. It is important to point out that the most significant regions in this respect – the Kara, Laptev and East Siberian seas – only recently became ice free in the summer. If the sea ice continues to decrease during summer in the Arctic Ocean, using observed daily ice forcing likely becomes more important for accurate seasonal atmospheric predictions.

## 5 References

Alexander, M. A., U. S. Bhatt, J. E. Walsh, M. S. Timlin, J. S. Miller, and J. D. Scott, 2004: The atmospheric response to realistic arctic sea ice anomalies in an AGCM during winter. *J Climate*, 17, 890-905.

Balmaseda, M. A., L. Ferranti, F. Molteni, and T. N. Palmer, 2010: Impact of 2007 and 2008 Arctic ice anomalies on the atmospheric circulation: Implications for long-range predictions. *Q J Roy Meteor Soc*, 136, 1655-1664.

Bhatt, U. S., and Coauthors, 2008: The Atmospheric Response to Realistic Reduced Summer Arctic Sea Ice Anomalies. *Arctic Sea Ice Decline: Observations, Projections, Mechanisms, and Implications*, Geophysical Monograph, , E. T. DeWeaver, C. M. Bitz, and L.-B. Tremblay, Eds., American Geophysical Union, 91-110.

Bitz, C. M., 2008: Some Aspects of Uncertainty in Predicting Sea Ice Thinning Arctic Sea Ice Decline : Observations, Projections, Mechanisms, and Implications, *Geophysical Monograph*,, E. T. DeWeaver, C. M. Bitz, and L.-B. Tremblay, Eds., American Geophysical Union, 63-76.

Bjorgo, E., O. M. Johannessen, and M. W. Miles, 1997: Analysis of merged SMMR-SSMI time series of Arctic and Antarctic sea ice parameters 1978-1995. *Geophys Res Lett*, 24, 413-416.

Briegleb, B. P., C. M. Bitz, E. C. Hunke, W. H. Lipscomb, M. M. Holland, J. L. Schramm, and R. E. Moritz (2004), Scientific description of the sea ice component in the Community Climate System Model, version three, NCAR Tech. Note, NCAAR/TN-463+STR, Nat. Cent. for Atmos. Res., Boulder, Colo.

Cavalieri, D. J., C. L. Parkinson, P. Gloersen, J. C. Comiso, and H. J. Zwally, 1999: Deriving long-term time series of sea ice cover from satellite passive-microwave multisensor data sets. *J Geophys Res-Oceans*, 104, 15803-15814.

Collins, W. D., and Coauthors, 2006a: The formulation and atmospheric simulation of the Community Atmosphere Model version 3 (CAM3). *J Climate*, 19, 2144-2161.

Collins, W. D., and Coauthors, 2006b: The Community Climate System Model version 3 (CCSM3). *J Climate*, 19, 2122-2143.

Comiso, J. C., 2003: Warming trends in the Arctic from clear sky satellite observations. *J Climate*, 16, 3498-3510.

Comiso, J. C., 2006a: Abrupt decline in the Arctic winter sea ice cover. *Geophys Res Lett*, 33, L18504, doi 10.1029/2006gl027341.

Comiso, J. C., 2006b: Arctic warming signals from satellite observations, *Weather*, 61, 70-76.

Comiso, J. C., and F. Nishio, 2008: Trends in the sea ice cover using enhanced and compatible AMSR-E, SSM/I, and SMMR data. *J Geophys Res-Oceans*, 113, C02s07, doi 10.1029/2007jc004257.

Comiso, J. C., D. J. Cavalieri, and T. Markus, 2003: Sea ice concentration, ice temperature, and snow depth using AMSR-E data. *Ieee T Geosci Remote*, 41, 243-252.

de Vernal, A., C. Hillaire-Marchel, S. Soliganac, T. Randi, and A. Rochon, 2008: Reconstructing sea-ice conditions in the Arctic and subarctic prior to human observations. In Arctic Sea ice decline: observations, projections, mechanisms, and implications. AGU Monograph, E. T. DeWeaver, C. M. Bitz, and L.-B. Tremblay, Eds., American Geophysical Union, 27-45.

Deser, C., and H. Teng, 2008: Evolution of Arctic sea ice concentration trends and the role of atmospheric circulation forcing, 1979-2007. *Geophys Res Lett*, 35, L02504, doi 10.1029/2007gl032023.

Deser, C., G. Magnusdottir, R. Saravanan, and A. Phillips, 2004: The effects of North Atlantic SST and sea ice anomalies on the winter circulation in CCM3. Part II: Direct and indirect components of the response. *J Climate*, 17, 877-889.

Deser, C., R. Tomas, M. Alexander, and D. Lawrence, 2010: The seasonal atmospheric response to projected arctic sea ice loss in the late twenty-first century. *J Climate*, 23, 333-351.

Dickinson, R. E., and Coauthors, 2006: The Community Land Model and its climate statistics as a component of the Community Climate System Model. *J Climate*, 19, 2302-2324.

Francis, J. A., and E. Hunter, 2007: Drivers of declining sea ice in the Arctic winter: A tale of two seas. *Geophys Res Lett*, 34, L17503  
Doi 10.1029/2007gl030995.

Herman, G. F., and W. T. Johnson, 1978: The sensitivity of the general circulation to arctic sea ice boundaries: A numerical experiment. *Mon. Wea. Rev.*, 106, 1649–1664.

Higgins, M. E., and J. J. Cassano, 2009: Impacts of reduced sea ice on winter Arctic atmospheric circulation, precipitation, and temperature. *J Geophys Res-Atmos*, 114, D16107, doi 10.1029/2009jd011884.

Holland, M. M., C. M. Bitz, E. C. Hunke, W. H. Lipscomb, and J. L. Schramm, 2006: Influence of the sea ice thickness distribution on polar climate in CCSM3. *J Climate*, 19, 2398-2414.

Honda, M., K. Yamazaki, H. Nakamura, and K. Takeuchi, 1999: Dynamic and thermodynamic characteristics of atmospheric response to anomalous sea-ice extent in the Sea of Okhotsk. *J Climate*, 12, 3347-3358.

Kauffman, B.G. and W.G. Large. 2002. The CCSM coupler, version 5.0, combined user's guide, source code reference, and scientific description. National Center for Atmospheric Research: Boulder, CO. 47 pp.

Kwok, R., and D. A. Rothrock, 2009: Decline in Arctic sea ice thickness from submarine and ICESat records: 1958-2008. *Geophys Res Lett*, 36, doi 10.1029/2009GL039035.

Magnusdottir, G., C. Deser, and R. Saravanan, 2004: The effects of North Atlantic SST and sea ice anomalies on the winter circulation in CCM3. Part I: Main features and storm track characteristics of the response. *J Climate*, 17, 857-876.

Markus, T., and D. J. Cavalieri, 2000: An enhancement of the NASA Team sea ice algorithm. *Ieee T Geosci Remote*, 38, 1387-1398.

McCaa, J., M. Rothstein, B. Eaton, J. Rosinski, E. Kluzek, and M. Vertenstein, cited 2004: User's guide to the NCAR Community Atmosphere Model (CAM 3.0). [Available4132 *JOURNAL OF CLIMATE* VOLUME 23 online at <http://www.cesm.ucar.edu/models/atm-cam/docs/usersguide/>.]

Overland, J. E., Wood, K. R., Wang, M. (2010) Hot Arctic-Cold Continents: Hemispheric Impacts of Arctic Change. Abstract #GC12B-03 presented at 2010 Fall Meeting, AGU, San Francisco, Calif., 13-17 Dec

Parkinson, C. L., D. J. Cavalieri, P. Gloersen, H. J. Zwally, and J. C. Comiso, 1999: Arctic sea ice extents, areas, and trends, 1978-1996. *J Geophys Res-Oceans*, 104, 20837-20856.

Peng, S. L., and J. S. Whitaker, 1999: Mechanisms determining the atmospheric response to midlatitude SST anomalies. *J Climate*, 12, 1393-1408.

Petoukhov, V., and V. A. Semenov, 2010: A link between reduced Barents-Kara sea ice and cold winter extremes over northern continents. *J Geophys Res-Atmos*, 115, D21111, doi 10.1029/2009jd013568.

Polyakov, I. V., and Coauthors, 2003: Long-term ice variability in Arctic marginal seas. *J Climate*, 16, 2078-2085.

Polyakov, I. V., V. A. Alexeev, U. S. Bhatt, E. I. Polyakova, and X. D. Zhang, 2010: North Atlantic warming: patterns of long-term trend and multidecadal variability. *Clim Dynam*, 34, 439-457.

Rigor, I. G., J. M. Wallace, and R. L. Colony, 2002: Response of sea ice to the Arctic oscillation. *J Climate*, 15, 2648-2663.

Rothrock, D. A., D. B. Percival, and M. Wensnahan, 2008: The decline in arctic sea-ice thickness: Separating the spatial, annual, and interannual variability in a quarter century of submarine data. *J Geophys Res-Oceans*, 113, C05003, doi 10.1029/2007jc004252.

Sardeshmukh, P. D., G. P. Compo, and C. Penland, 2000: Changes of probability associated with El Nino. *J Climate*, 13, 4268-4286.

Screen, J. A., and I. Simmonds, 2010: Increasing fall-winter energy loss from the Arctic Ocean and its role in Arctic temperature amplification. *Geophys Res Lett*, 37, L16707, doi 10.1029/2010gl044136.

Serreze, M. C., 1995: Climatological aspects of cyclone development and decay in the Arctic. *Atmos Ocean*, 33, 1-23.

Singarayer, J. S., J. L. Bamber, and P. J. Valdes, 2006: Twenty-first-century climate impacts from a declining Arctic sea ice cover. *J Climate*, 19, 1109-1125.

Skamarock, W. C., and Coauthors, 2005: A Description of the Advanced Research WRF Version 2. Defense Technical Information Center.



Smith, R. D., and P. R. Gent, cited 2002: Reference manual for the Parallel Ocean Program (POP), ocean component of the Community Climate System Model (CCSM2.0 and 3.0). Tech. Rep. LA-UR-02-2484, Los Alamos National Laboratory. [Available online at <http://www.cesm.ucar.edu/models/ccsm3.0/pop/>.]

Smith, T. M., R. W. Reynolds, T. C. Peterson, and J. Lawrimore, 2008: Improvements to NOAA's historical merged land-ocean surface temperature analysis (1880-2006). *J Climate*, 21, 2283-2296.

Strey, S. T., W. L. Chapman, and J. E. Walsh, 2010: The 2007 sea ice minimum: Impacts on the Northern Hemisphere atmosphere in late autumn and early winter. *J Geophys Res-Atmos*, 115, D23103, doi 10.1029/2009jd013294.

Walsh, J. E., and C. M. Johnson, 1979: An analysis of Arctic sea ice fluctuations, 1953-1977. *J Phys Oceanogr*, 9, 580-591.

Zhang, X. D., J. E. Walsh, J. Zhang, U. S. Bhatt, and M. Ikeda, 2004: Climatology and interannual variability of arctic cyclone activity: 1948-2002. *J Climate*, 17, 2300-2317.

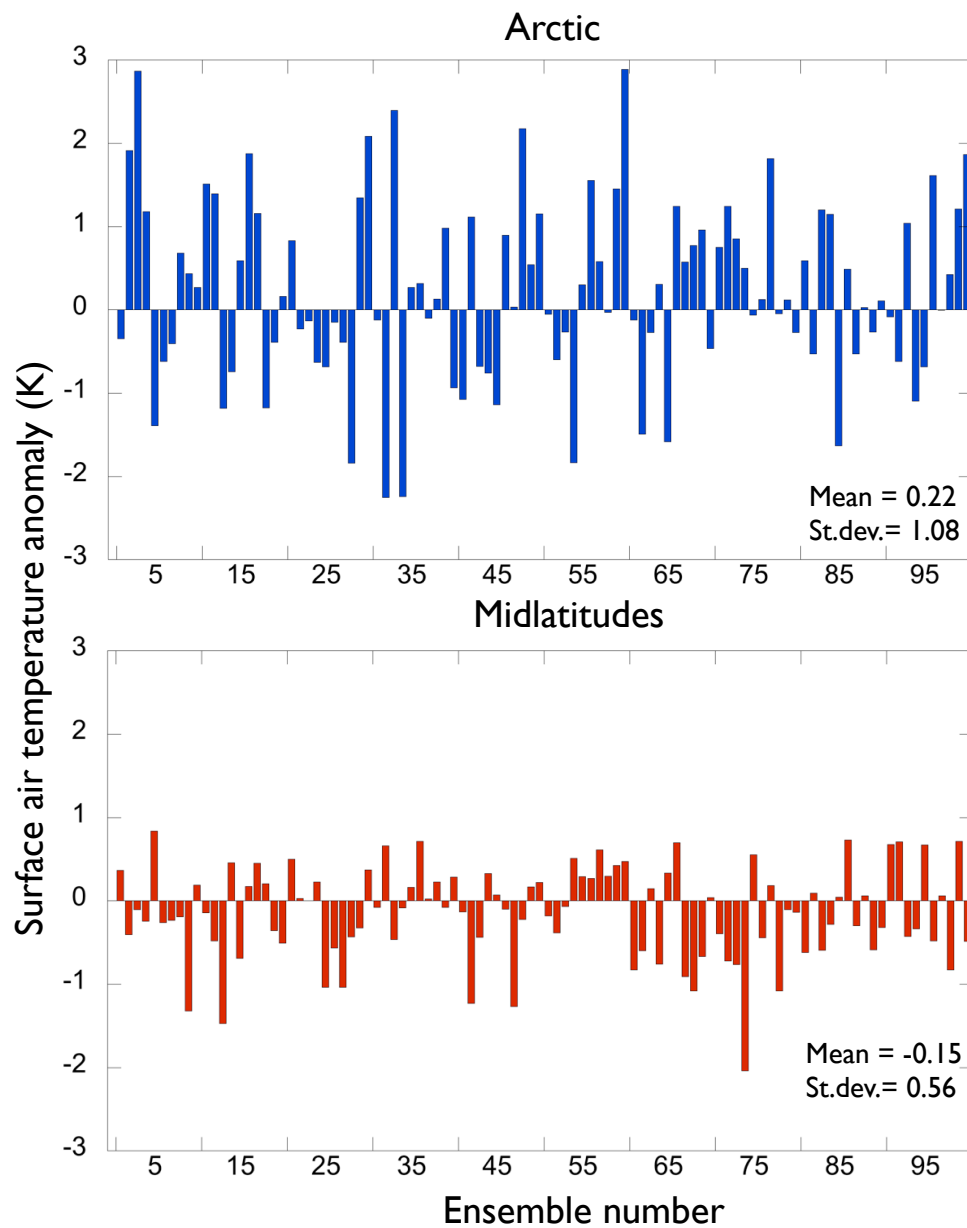
## Appendix A Analysis of SAT Ensemble Spread

Figure A.1 displays the ensemble spread of average midlatitude and arctic SAT anomalies calculated as DAILY-CNTRL. There is a larger ensemble spread in the Arctic, which is consistent with the higher climate variability in the Arctic in observations as well as the model than in the midlatitudes. The ensemble average SAT anomaly for the Arctic is 0.2K while for the midlatitudes is -0.2K. The standard deviations between ensemble members anomaly for the Arctic is 1.1K and for the midlatitudes is 0.6K. Note that for analysis purposes two Northern Hemisphere regions are defined as follows: midlatitudes span from 30N to 55N and Arctic from 55N to 90N.

Figure A.2 displays the spatial ensemble average (Sep 06 – Feb 07) of SAT anomalies (DAILY-CTRL) (Figure A.2a), for 10 ensembles with lowest SAT in the midlatitudes (Figure A.2b), and the 10 ensembles with highest temperatures in the Arctic (Figure A.2c). The general spatial patterns do not change significantly in the Arctic when the ensembles are subsampled, however, they do for the far field responses in the lower latitudes. The cool continental US feature is evident in all subsamples.

Figure A.3 displays the ensemble average SAT in DAILY and SMTH and indicate similar spatial patterns between DAILY and SMTH, except most notably over the continental US. The large spread between individual simulations highlights the need for a sufficient number of ensemble members.

## Ensemble Distribution of SAT Anomalies



**Figure A.1 SAT Ensemble Distribution in Midlatitudes and Arctic**

SAT anomaly (K) December 2006 for all ensembles using daily SIC in model (DAILY - CTRL). Top: Arctic ( $55 - 90^{\circ}\text{N}$ ) and bottom: midlatitudes ( $30 - 55^{\circ}\text{N}$ ).

### SAT Anomaly (K) (Sep 06 - Feb 07)

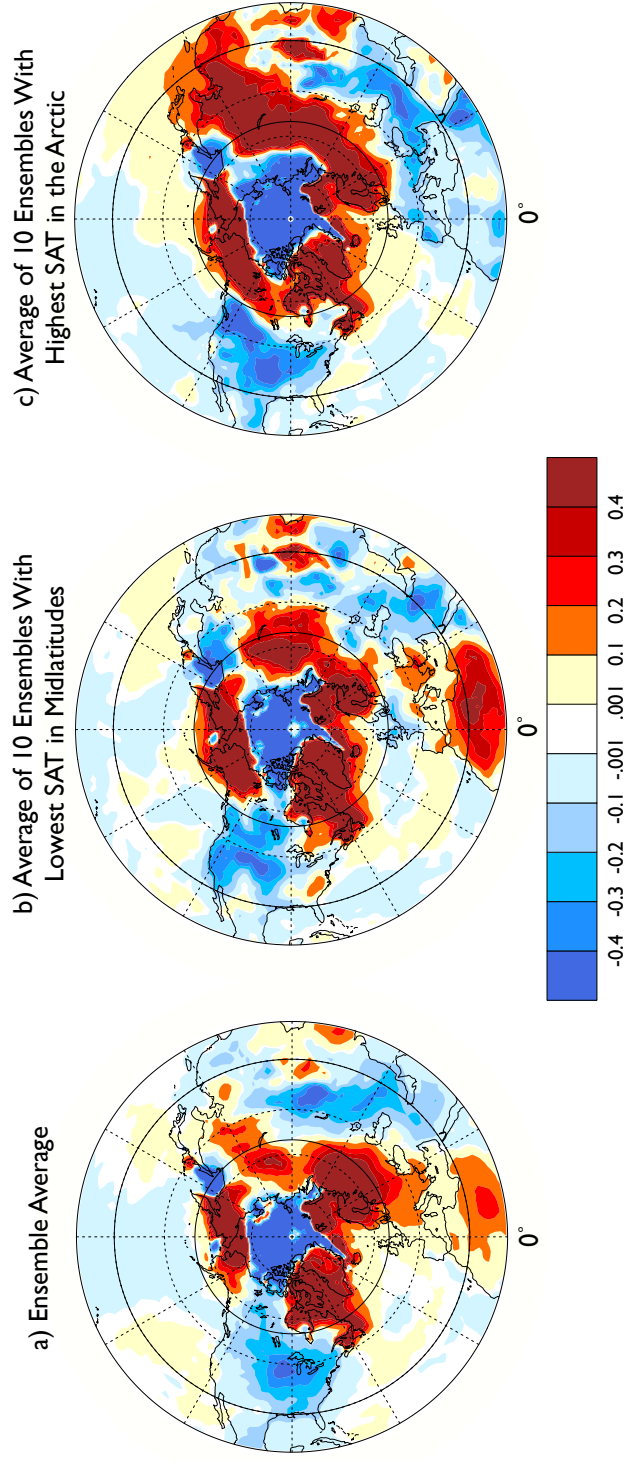


**Figure A.2 SAT Anomaly High and Low**  
DAILY – CTRL: Sep 06 – Feb 07: a) ensemble average SAT anomaly, b) 10 ensembles with the lowest SAT, and c) 10 ensembles with highest SAT in the Arctic (right).

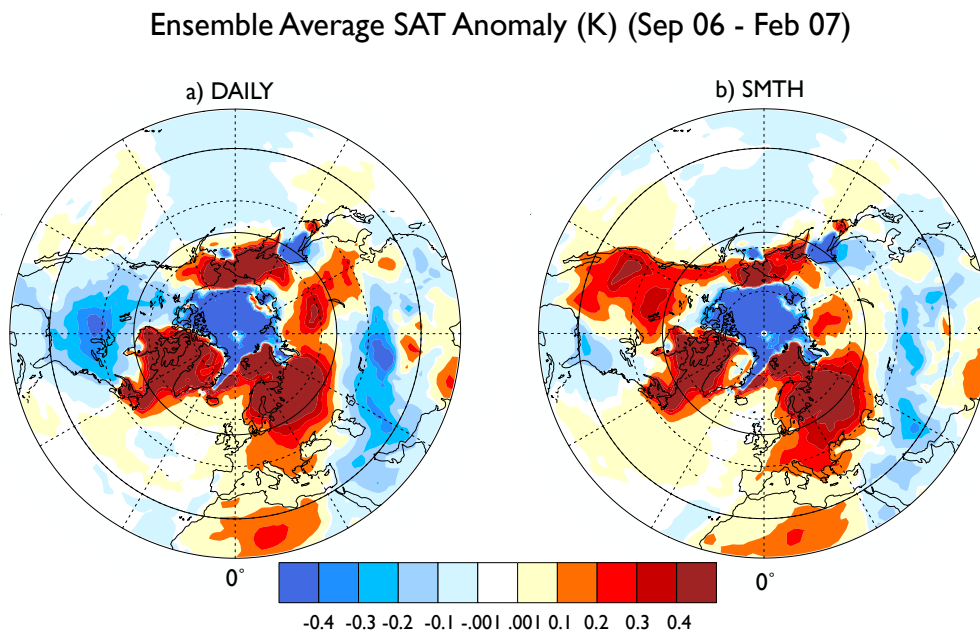


**Figure A.3 SAT Anomalies DAILY and SMTH**

Sep 06 – Feb 07: a) ensemble average SAT anomaly DAILY-CTRL. b) SMTH-CTRL.

## Appendix B Differences Between Experiment Forcings

The differences in the sea ice are largest in the low and high percentiles (Figure 2.5). Sensible and latent heat fluxes in the two experiments are investigated when sea ice is between 0 and 10 percent and also between 94 and 100 percent (Figure B.1).

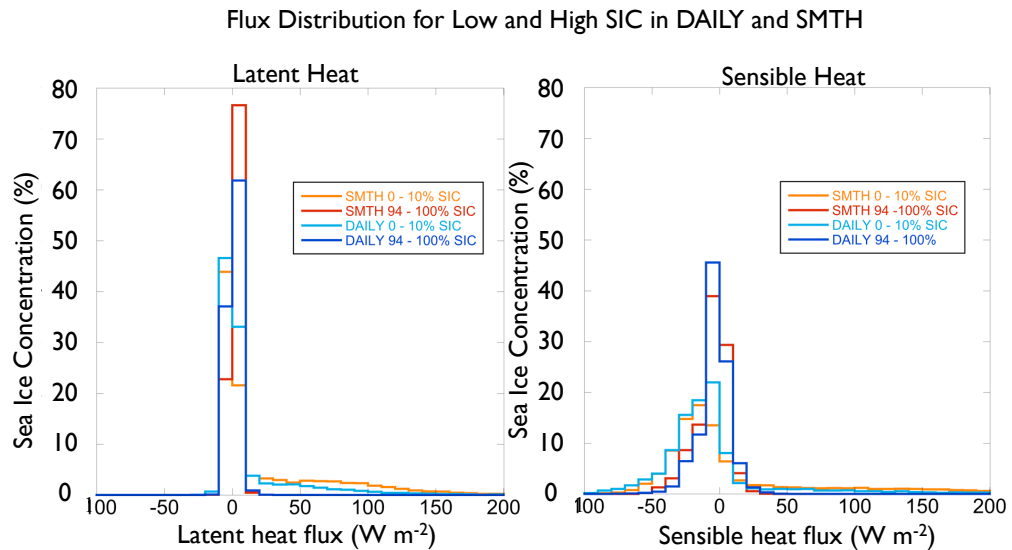


**Figure B.1 Fluxes in High and Low SIC Areas in DAILY and SMTH**

December (one ensemble member) percent of grid points north of 70N with ice that contain SIC from 94-100 % (dark color) and 0-10% (light color) for DAILY (blue) and SMTH (red/yellow) and the latent (left) and sensible (right) heat out of the sea/ice surface.

The different flux bins show that SMTH has larger outgoing sensible and latent heat fluxes in the high SIC percentiles. SMTH is created based on a running average causing the SIC to often not reach 100% and therefore leads to relatively large differences in fluxes compared to DAILY. SAT and moisture can differ greatly over an almost completely ice covered ocean in SMTH versus a completely ice covered ocean in DAILY (Figure B.1).

Figure B.2 shows that SIC tend to vary more at the edges than the central ice. This is calculated using Equation 1.1. There is a large amount of variability in both the Pacific and the Atlantic sectors along the ice edge.

Figure B.3 displays higher than 1% average SIC during September and February. The figure indicates that the movement of the equatorward ice edge from September to February is greater in the Pacific than the Atlantic sectors implying a difference in nature of variability between sectors of the ice. This feature of the seasonal cycles is consistent with differences noted between DAILY and SMTH responses.

Since SMTH forcing is based on a thirty day running average it is expected that the two forcings will differ the most in regions with most abrupt changes where SMTH cannot keep up with the daily change.

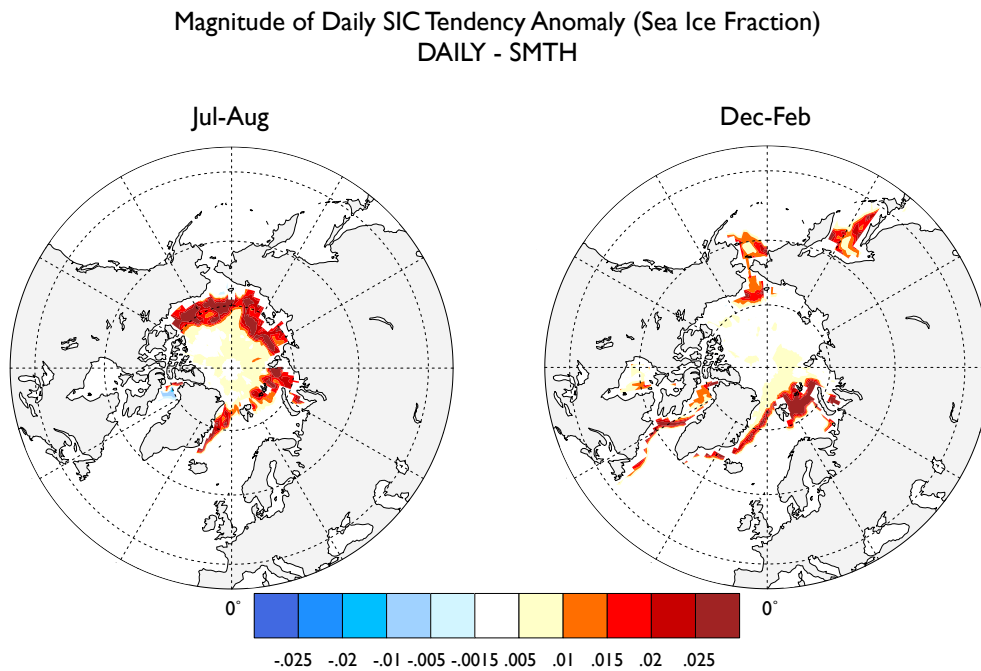


**Figure B.2 Day-to-day Change in SIC DAILY – SMTH**

Root mean square of day-to-day change in sea ice concentration anomaly (DAILY – SMTH) for a) July-August 2006 and b) December 2006 – February 2007.



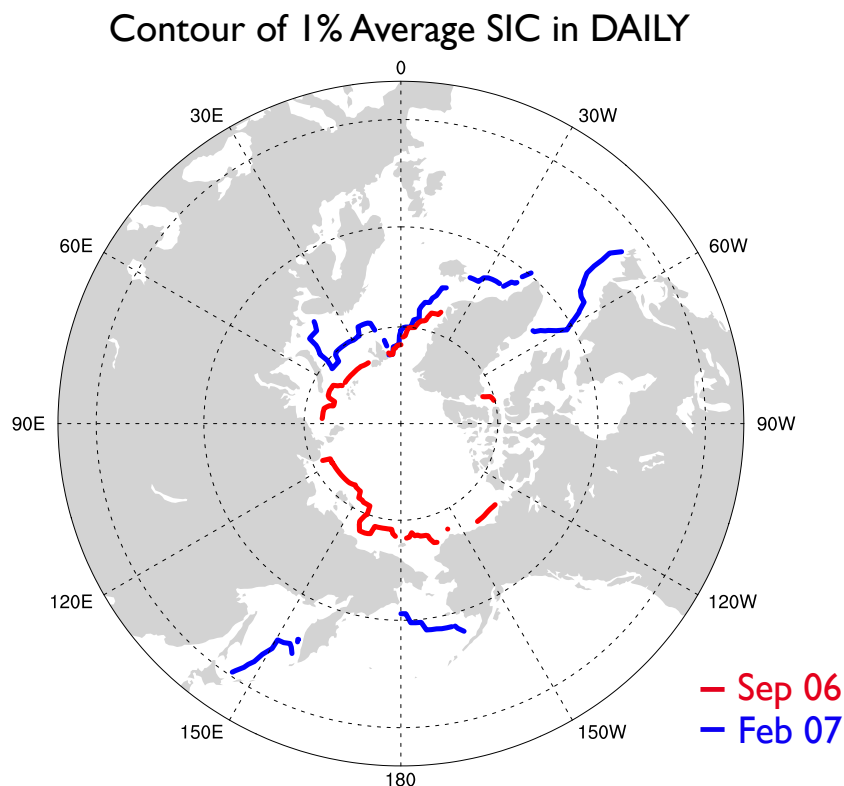


**Figure B.3 1% SIC Edge in Sep 06 and Feb 07**

The 1% average sea ice concentration September 2006 (red) and February 2007 (blue). Ice extends equatorward faster in the Pacific sector than in the northeast Atlantic.

### **B.1 Forcing Impacts on Fluxes in the Arctic During Fall**

Further analysis of sea ice evolution in several regions finds the largest SIC forcing difference between SMTH and DAILY occurs where SIC in DAILY changes rapidly (Figure B.4). Rapid change in SIC occurs mostly around the sea ice equatorward ice edge. This is where the largest expected flux differences between SMTH and DAILY are (Figure B.7). Differences are also larger in seasons with significant change in total ice concentration. The magnitude of the difference between DAILY and SMTH forcing is also dependent on the region. Several locations have been investigated and the ice along the Siberian coast (Kara, Laptev and East Siberian seas) is found to have more abrupt changes in ice concentration during fall 2006 (Figure B.5).

The equatorward ice edge in the Atlantic sector evolves slower and also seems to retract at times during fall (Figure B.5). The slow movement makes SMTH able to follow closer to DAILY leading to a smaller difference between the two experimental forcings.

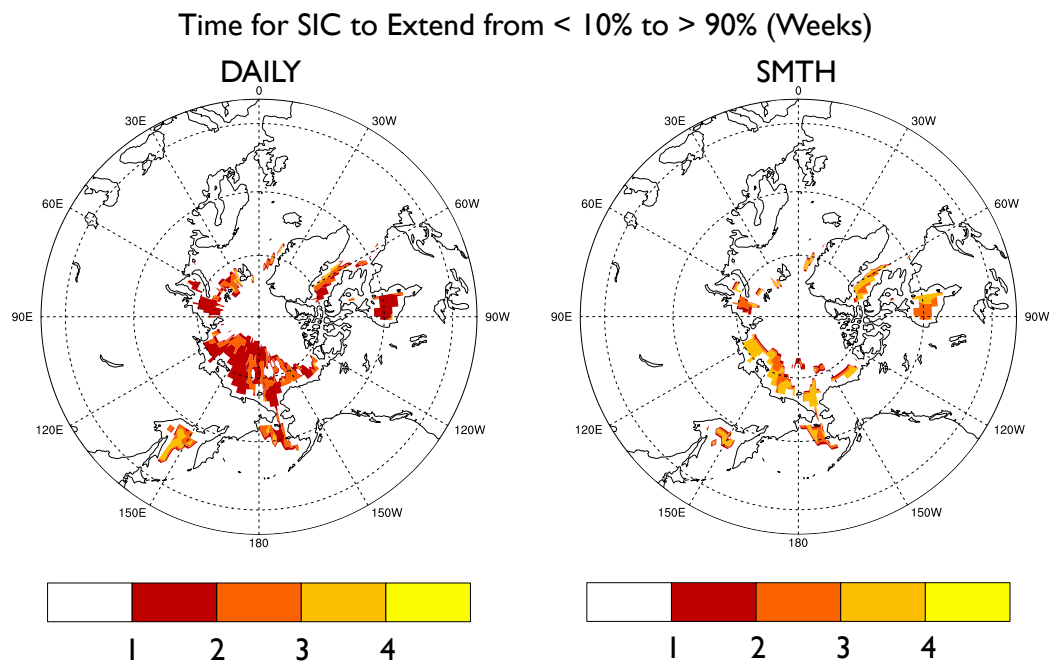


**Figure B.4 Length of Time for Rapid Change in SIC**

Evolution of SIC from less than 10% to greater than 90% during September 2006 and February 2007. DAILY (left) and SMTH (right).

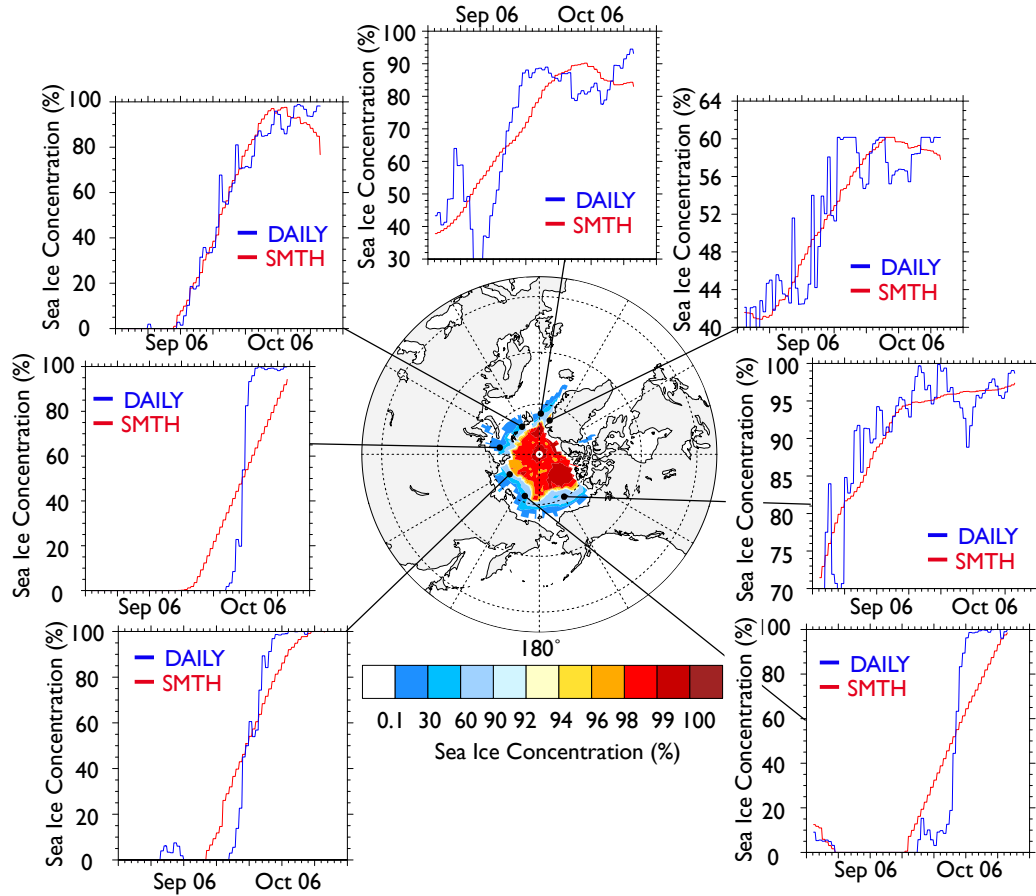


**Figure B.5 Fall SIC Edge Evolution**

September, October average SIC (%) DAILY (Middle). Time series plots of DAILY (blue) and SMTH (red) show SIC changing from September 1<sup>st</sup> to October 31<sup>st</sup> in specific locations. Rapidly changing SIC is seen in the Siberian sector leading ice forcings to differ substantially.

The analysis has thus far focused on differences in daily ice evolution between DAILY and SMTH. Figure B.6 shows that SMTH captures the average ice variation in the high Arctic.

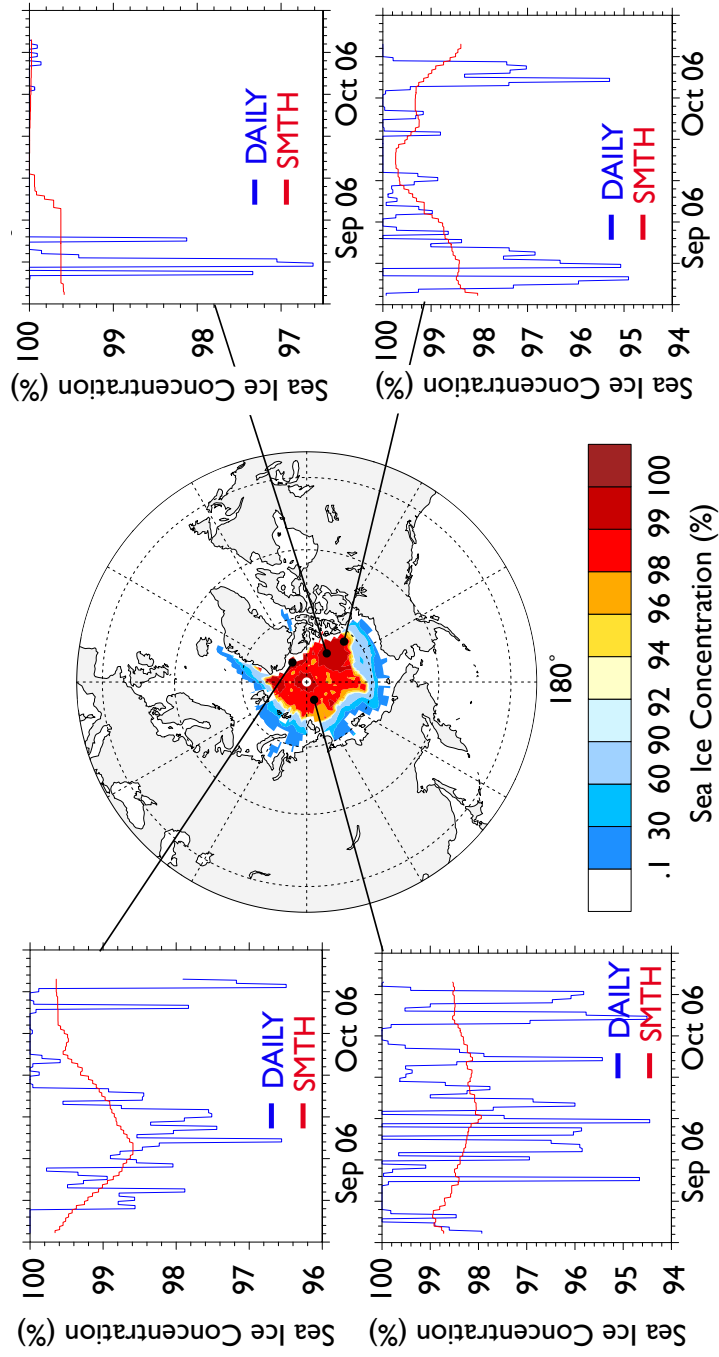


**Figure B.6 Fall SIC Evolution in Central Arctic**  
 September, October average SIC (%) DAILY (Middle panel). Time series plots of DAILY (blue) and SMTH (red) show SIC changing from September 1<sup>st</sup> to October 31<sup>st</sup> in specific locations.

Near the sea ice edge where rapid changes in sea ice concentration occur (Figure B.7) the evolution of the SMTH ice forcing impacts the fluxes out of the ocean. Differences of over 30% occur between DAILY and SMTH but more importantly (since the averages are the same), DAILY will reach higher ice concentrations (upper nineties in percent) faster. This leads to a higher total insulating effect of the ice and subsequently lower sensible heat fluxes out of the ocean in DAILY than in SMTH (Figure B.7).

Over the central Arctic there are regions of both weak positive and negative flux anomalies in DAILY compared to SMTH occur (Figure B.8). Four points has been investigated where the two top graphs show ice evolution in regions with negative flux anomalies and the two bottom graphs show ice evolution in regions with positive flux anomalies.

It appears that the fluxes are largely dependant on two factors: The amount of time where the ice has 100% ice and how many and large openings occurring in the DAILY ice. In the two top plots (Figure B.8) 100% ice is partially maintained in DAILY with small openings in the ice. SMTH will usually have less than 100% ice and have in these cases higher fluxes out of the ocean. In the bottom plots (Figure B.8) larger openings occur with less 100% ice favoring larger fluxes out of the ocean in DAILY than SMTH.

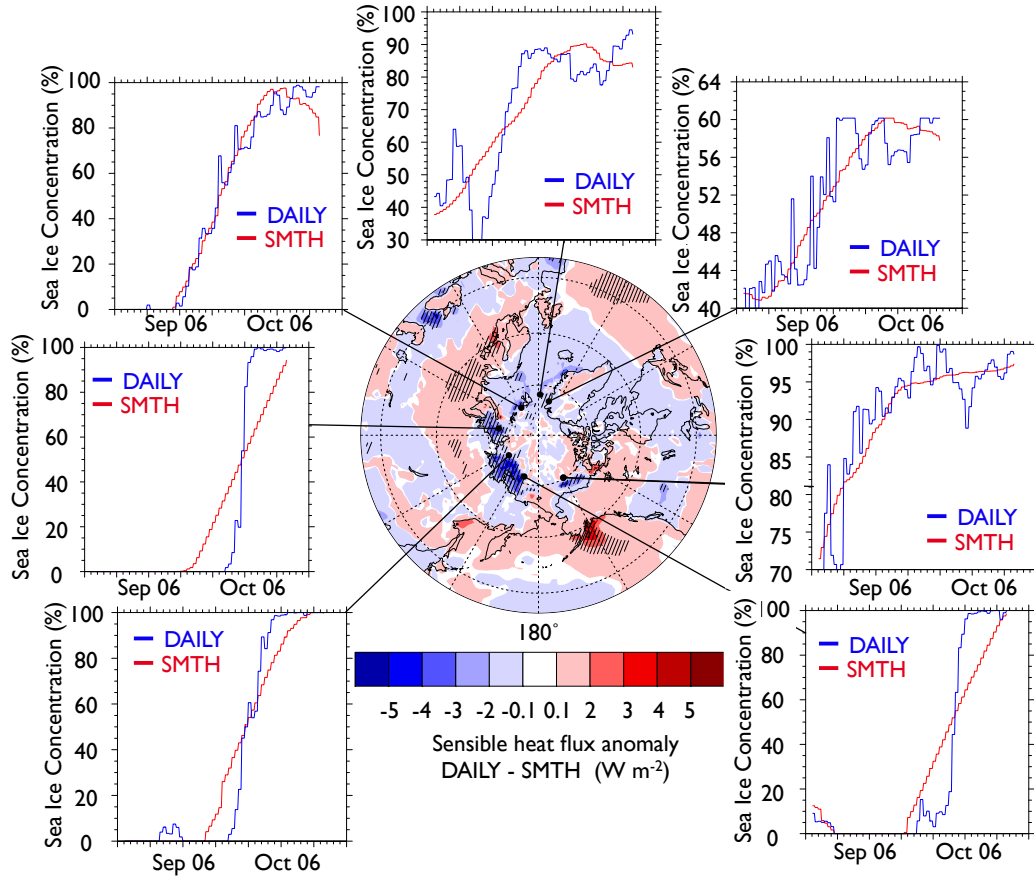


**Figure B.7 Fall SIC Edge Evolution and Sensible Heat Flux Anomaly**  
 September, October ensemble average sensible heat flux ( $\text{W m}^{-2}$ ) DAILY – SMTH (middle). Time series plots of DAILY (blue) and SMTH (red) show SIC changing from September 1<sup>st</sup> to October 31<sup>st</sup> in specific locations.

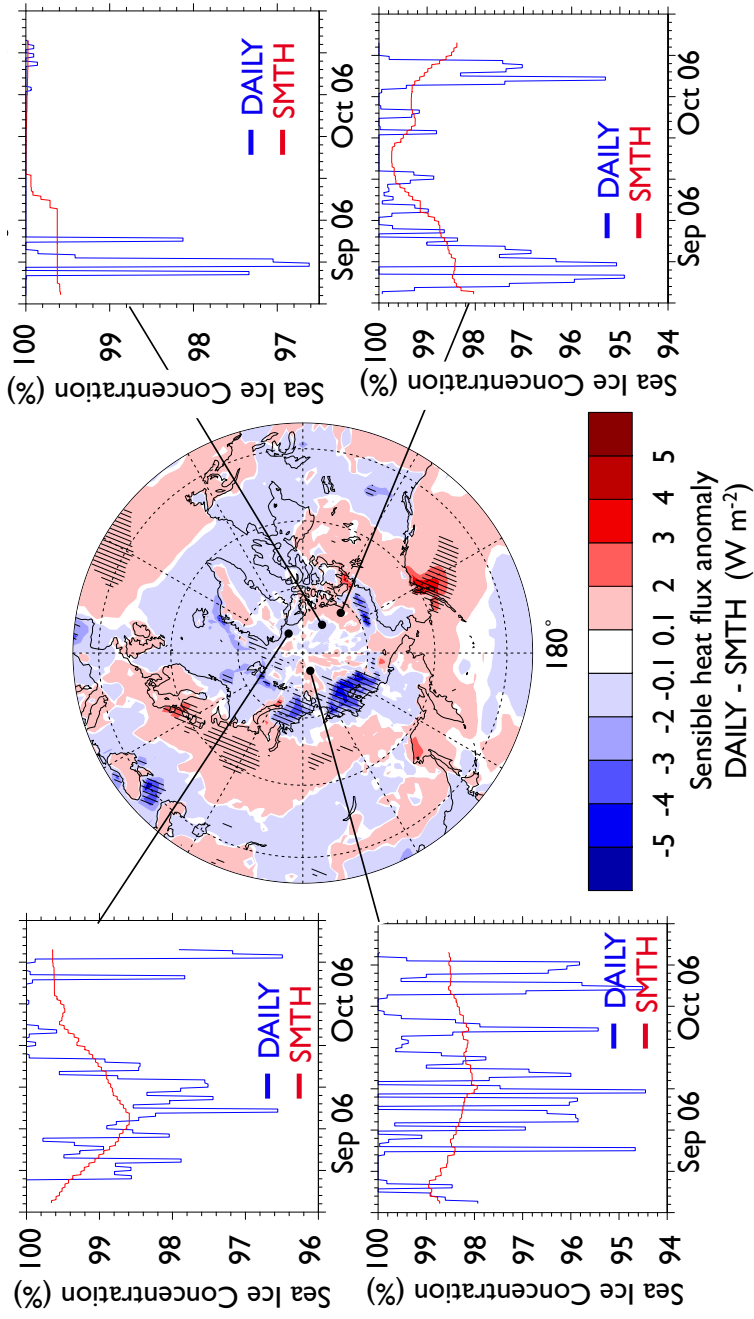


**Figure B.8 Fall SIC Central Evolution and Sensible Heat Flux Anomaly**  
 September, October ensemble average sensible heat flux ( $\text{W m}^{-2}$ ) DAILY - SMTH (middle). Time series plots of DAILY (blue) and SMTH (red) show SIC changing from September 1<sup>st</sup> to October 31<sup>st</sup> in specific locations.

## **B.2 Forcing Impacts on Fluxes in the Arctic During Winter**

Analyzing six points in the outer edge of the sea ice during winter does not reveal as pronounced differences between the Atlantic and Pacific sectors as for fall. The Pacific sector is where the most rapid changes in sea ice concentration occur and this shows an impact on the way daily ice is not well represented in SMTH (Figure B.9). In winter more than fall, ice evolution is slower and consists of both retraction and extension of equatorward ice edge during one season (see Beaufort and Barents seas in Figure B.9). This has an implication on the accuracy of ice representation in SMTH. Slower ice evolution is favorable for a good representation of SMTH.

During winter, the central arctic sea ice appears to have higher variability than during fall. SMTH is representing well the envelope of daily ice variability during winter (Figure B.10). The equatorward ice edge displays both higher and lower fluxes in DAILY compared to SMTH so does not have as consistent response compared to fall (Figure B.11). Also, the ice edge is farther south and is more interactive with wind stress passing over these areas. In winter, the regions have to be studied more closely to understand the differences. North in the Barents Sea frequent extension and retraction of sea ice occurs in DAILY causing more sensible heat to escape and leading to large positive anomalies in the region (DAILY – SMTH). In Baffin Bay there are weak negative anomalies of sensible heat flux. Negative anomalies usually occurs when ice concentrations are close to 100% since SMTH usually doesn't reach the 100% level and more heat will escape with this ice forcing. In the Chukchi Sea, the same scenario occurs as during fall in the Pacific region where SIC in SMTH cannot keep up with SIC in DAILY causing more heat loss from SMTH. In the Bering Sea, sea ice forms late and disappears quickly. This rapid increase and following decrease of sea ice is



not represented well in SMTH and causes more heat loss in SMTH than DAILY (Figure B.11).

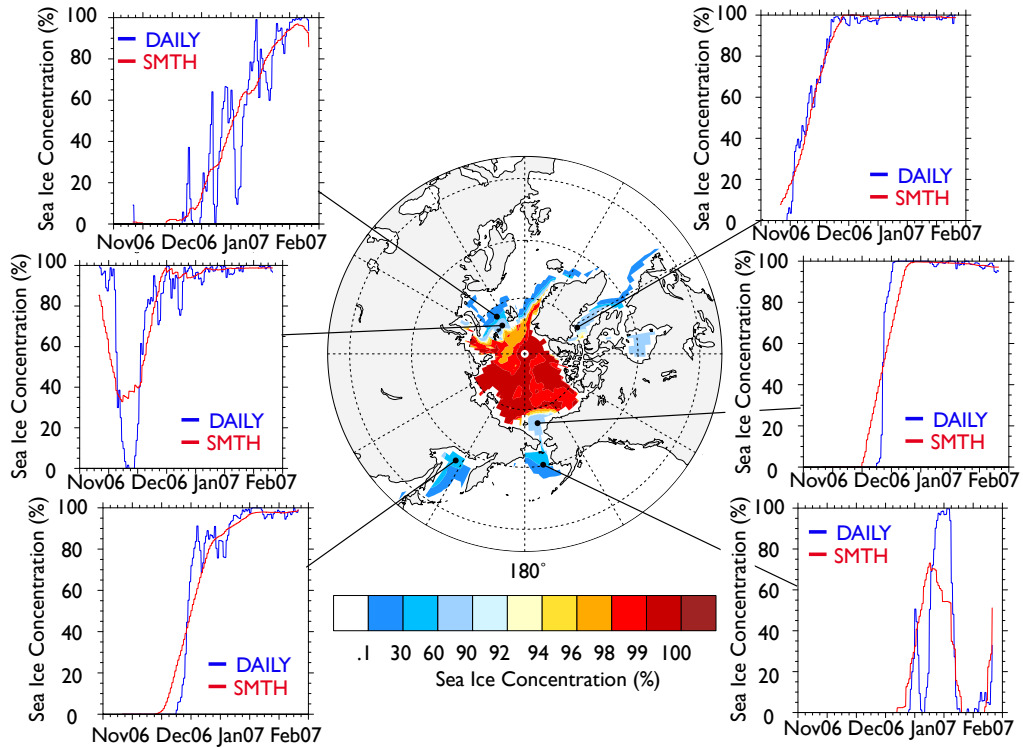


**Figure B.9 Winter SIC Edge Evolution**

November – February average SIC (%) DAILY (Middle). Time series plots of DAILY (blue) and SMTH (red) show SIC changing from September 1<sup>st</sup> to October 31<sup>st</sup> in specific locations.

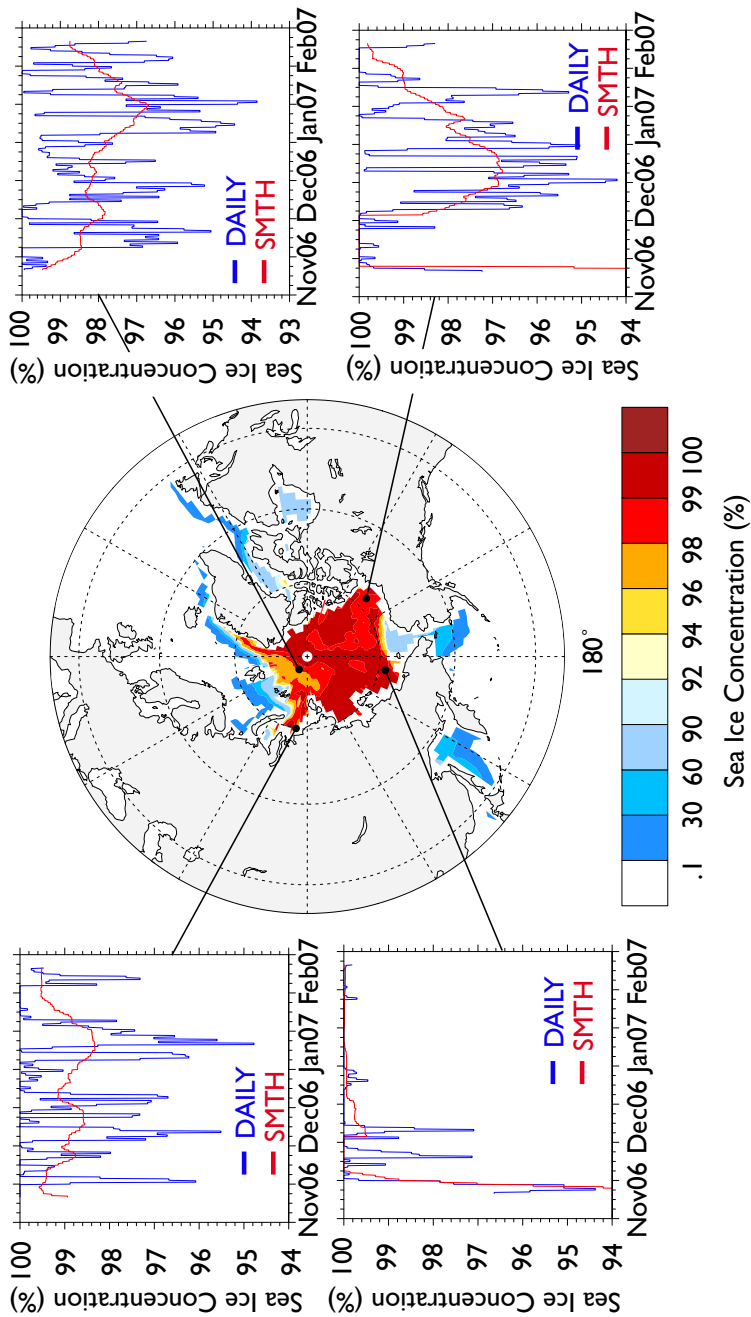


**Figure B.10 Winter SIC Center Evolution**  
 November – February average SIC (%) DAILY (Middle). Time series plots of DAILY (blue) and SMTH (red) show SIC changing from September 1<sup>st</sup> to October 31<sup>st</sup> in specific locations.

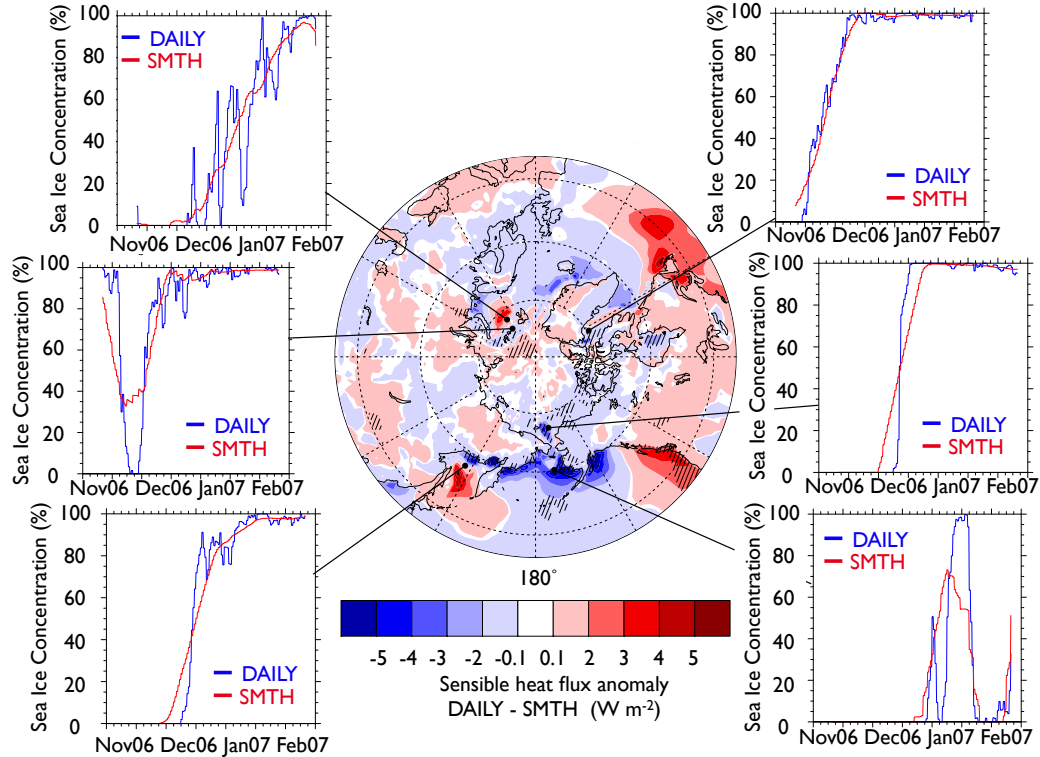


**Figure B.11 Winter SIC Central Evolution and Sensible Heat Flux Anomaly**

November – February ensemble average sensible heat flux anomaly ( $\text{W m}^{-2}$ ) DAILY – SMTH (Middle). Time series plots of DAILY (blue) and SMTH (red) show SIC changing from September 1<sup>st</sup> to October 31<sup>st</sup> in specific locations.

In Figure B.12 the two plots on the bottom show ice evolution in grid points with negative sensible heat flux anomaly and the two on top are of positive sensible heat flux anomaly (DAILY – SMTH). The main cause of differences between fluxes over the central Arctic between DAILY and SMTH is unclear during winter.

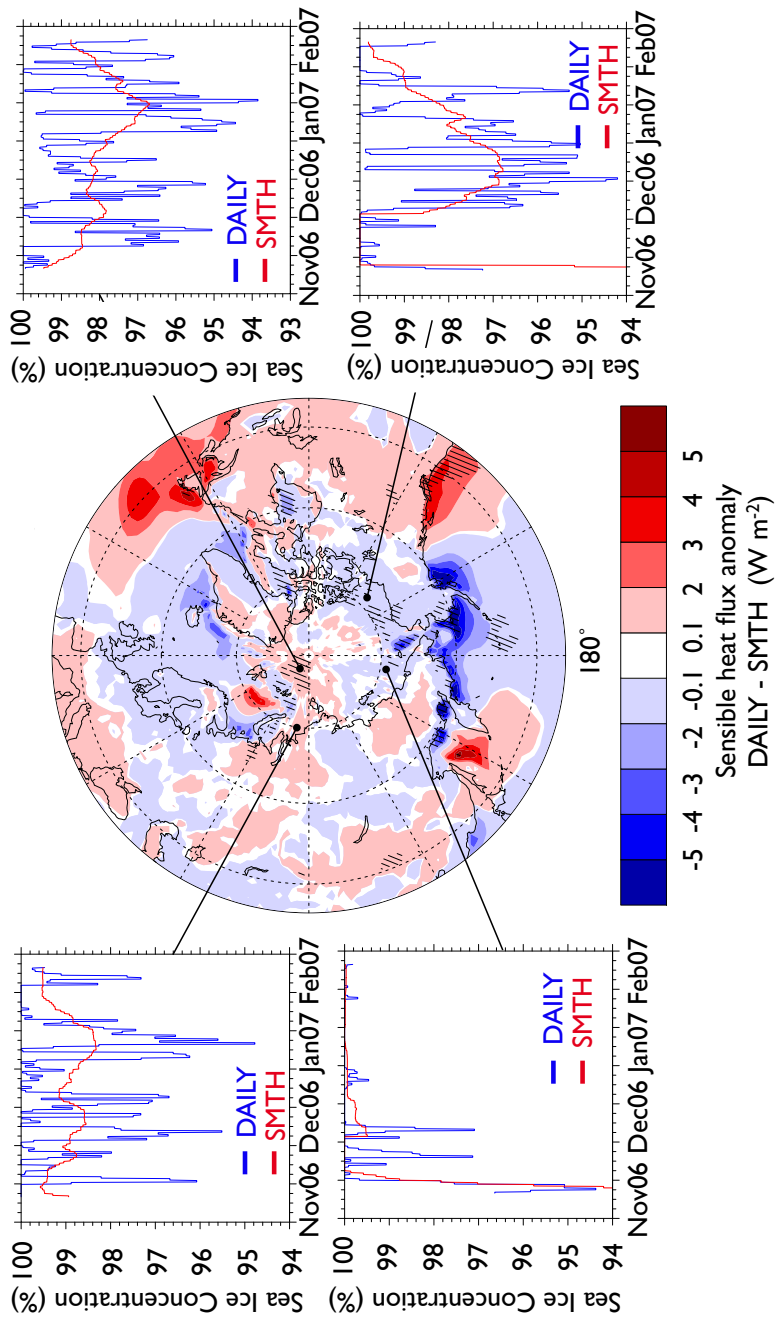


**Figure B.12 Winter SIC Central Evolution and Sensible Heat Flux Anomaly**  
 November – February ensemble average sensible heat flux anomaly ( $W\ m^{-2}$ ) DAILY – SMTH (Middle). Time series of DAILY (blue) and SMTH (red) plots show SIC changing from September 1<sup>st</sup> to October 31<sup>st</sup> in specific locations.

### **Appendix C    Difference Between DAILY and SMTH Atmospheric Response During Fall**

This section documents the atmospheric response to the two experiments. Notable differences are found between DAILY and SMTH. We present the analysis for two seasons, fall (Sep - Oct 2006) and winter (Nov – Feb 2006-07). These seasonal averages were chosen based on the similarity of the SIC forcing and atmospheric response.

While the primary focus of this study is on the difference, DAILY – SMTH, the atmospheric response to 2006-07 is included for interest since 2006 was an anomalously low sea ice year (see Figure C.1 and Figure D.1 displaying forcing SIC during fall and winter). The first two plots of the selected atmospheric variables (a - DAILY – CTRL and b - SMTH – CTRL) describe atmospheric conditions as a result of the 2006-07 ice conditions. The third plot (c - DAILY – SMTH) documents conditions as a result of DAILY forcing conditions.

Features present in both DAILY–CTRL and SMTH–CTRL experiments (panel a and b) are described with regard to the two left panels, and differences refer to DAILY–SMTH (panel c). The discussion focuses on anomalies that reach significance at the 95% or greater level based on Student’s t-test.

Figure C.1 displays the sea ice forcing conditions used in the experiments. The climatological (1982-2008 average) fall SIC (CTRL) (Figure C.1b) extends farther southward all around the Arctic compared to DAILY (Figure C.1a). The 2006-07 fall anomaly (Figure C.1c) displays negative anomalies at the ice edge and positive anomalies poleward of the ice edge.

Mean Sea Ice Concentration (%) (Sep - Oct 06)

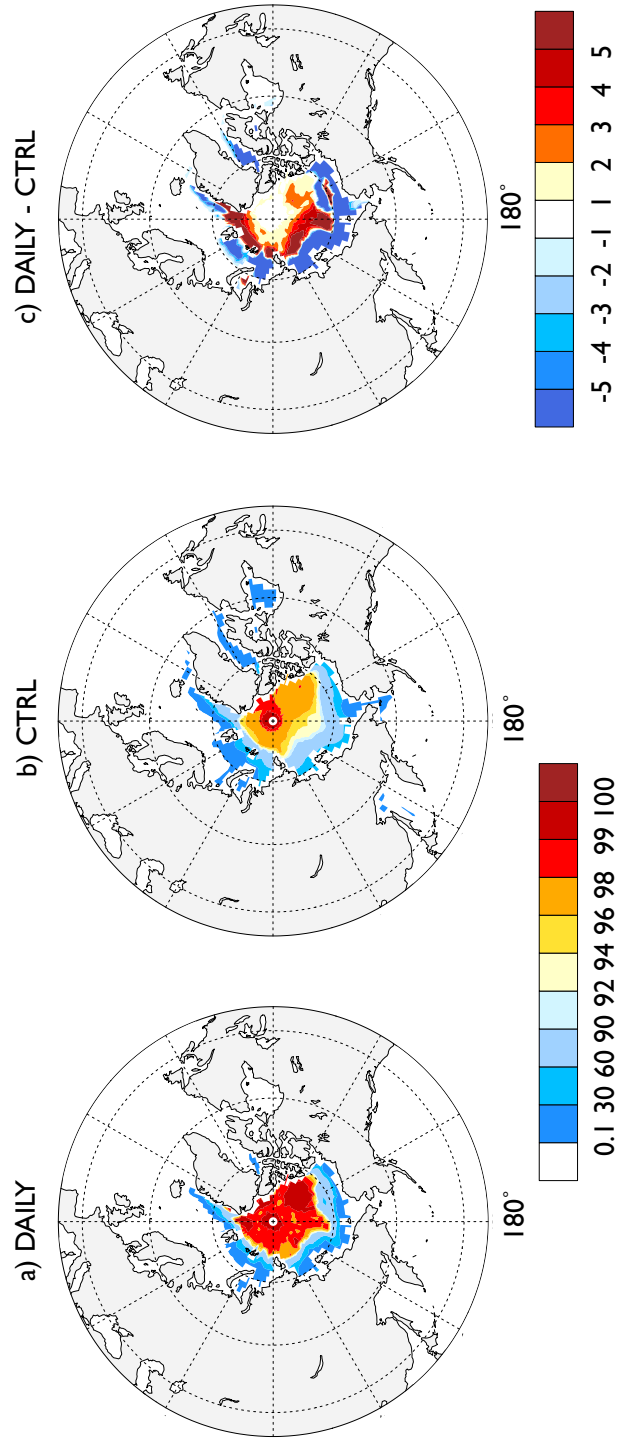


**Figure C.1 Fall Sea Ice Concentration**  
 Average sea ice concentration (%) (Sep - Oct) a) DAILY, b) CONTROL, c) DAILY-CTRL. Note scale is non-linear in left panels

### **C.1 Surface Heat Fluxes**

Sensible heat flux anomalies (DAILY-CTRL and SMTH-CTRL) are positive (from ocean to atmosphere) over a narrow region on the equatorward side of the ice edge during 2006 (Figure C.2a and b). The central basin as well as the ocean in the high latitude Pacific and Atlantic sectors has lower heat flux out of the ocean during 2006 than CTRL. In the East Siberian, Laptev and Kara seas, DAILY displays a lower flux out of the ocean than SMTH (Figure C.2c). Positive heat flux anomalies in the northeastern Europe, Gulf of Alaska and in the North Atlantic indicate more heat flux from the ocean to the atmosphere in DAILY than SMTH in these regions.

Latent heat flux anomaly patterns (Figure C.3a and b) compare favorably with sensible heat flux and also display positive anomalies south of the equatorward 2006 ice edge. There is also reduced latent heat loss in the central basin. Figure C.3c indicates lower fluxes out of the East Siberian, Laptev and Kara seas in DAILY and that the largest differences between DAILY and SMTH are in the midlatitude North Atlantic and North Pacific.

Fall longwave radiation anomalies are consistent with latent and sensible heat with increased longwave loss from the Arctic Ocean in areas of negative sea ice anomalies (Figure C.4a and b). Figure C.4c (DAILY – SMTH) displays a small positive anomaly of longwave radiation along the Northern Eurasian coast, in the Bering Sea and in the central North Atlantic Ocean.

### Sensible Heat Flux Anomaly ( $W m^{-2}$ ) (Sep - Oct 2006)

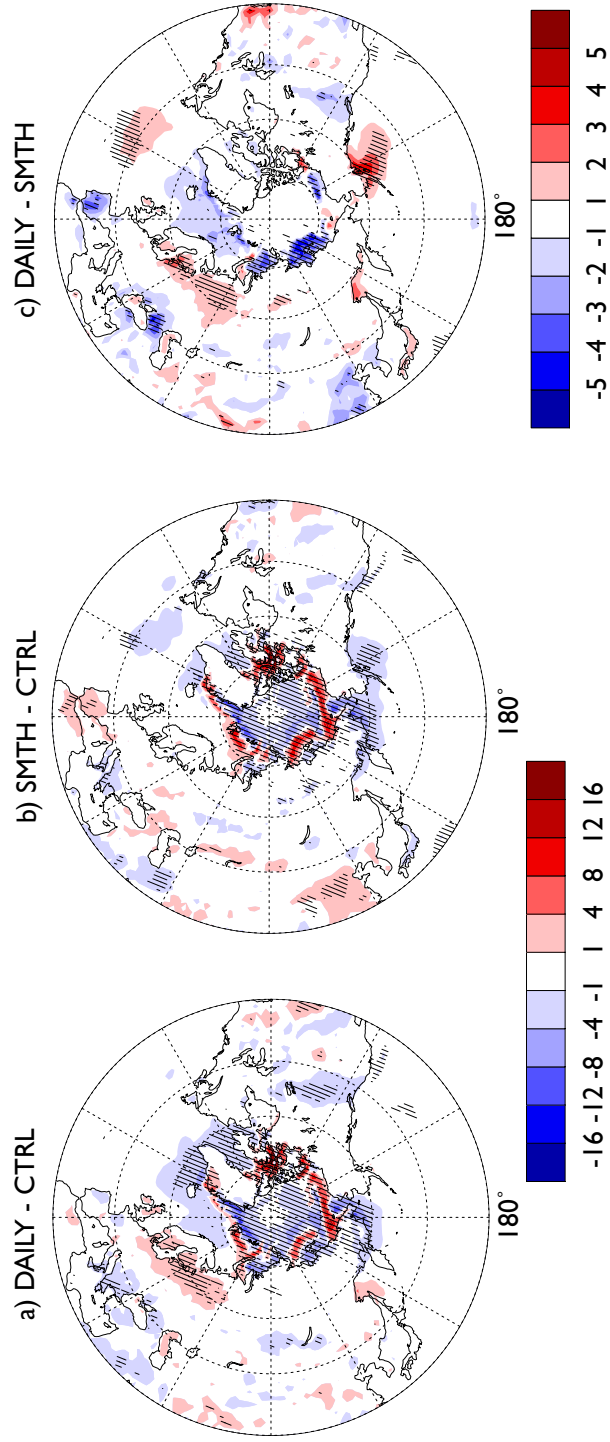


**Figure C.2 Fall Sensible Heat Flux Differences**  
Ensemble average (Sep - Oct) sensible heat flux anomaly ( $W m^{-2}$ ) a) DAILY-CONTROL, b) SMTH-CONTROL, c) DAILY-SMTH. Crosshatching signifies statistical significance at the 95% or greater level based on Student's t-test.



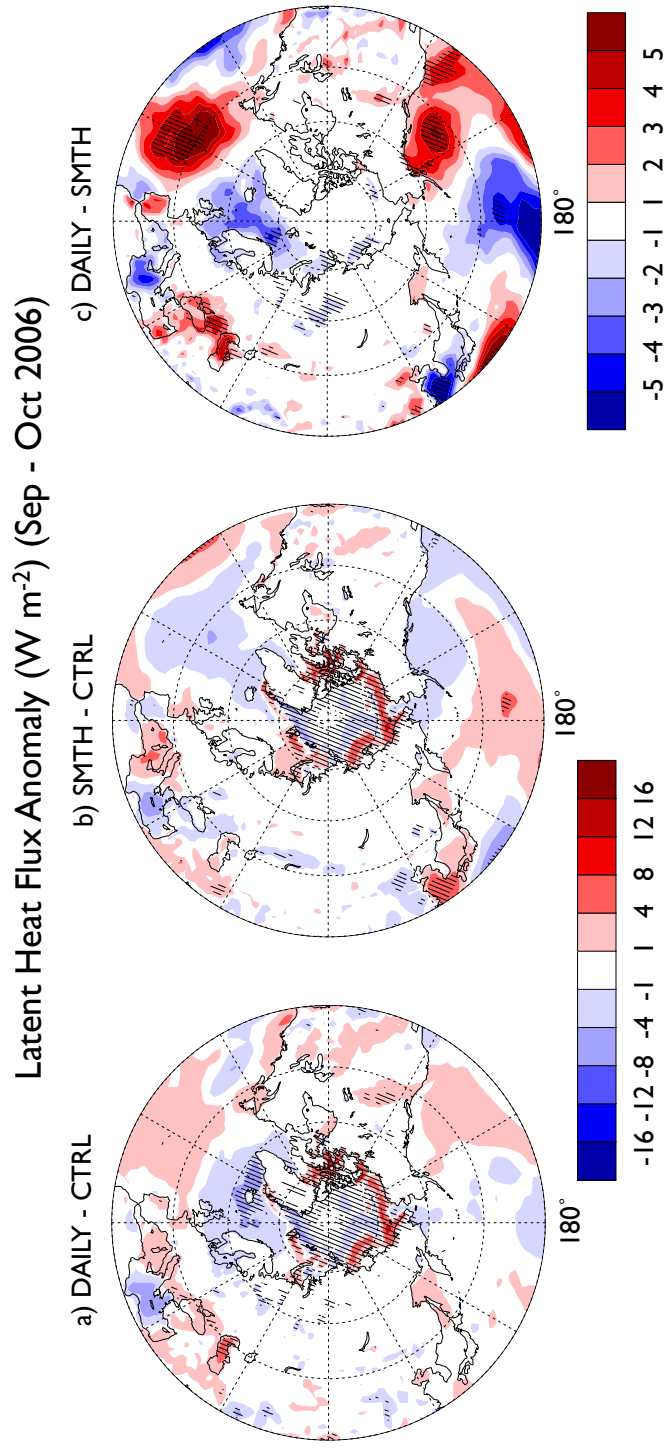


**Figure C.3 Fall Latent Heat Flux Differences**  
 Ensemble average (Sep - Oct) latent heat flux anomaly ( $W m^{-2}$ ) a) DAILY-CONTROL, b) SMTH-CONTROL, c) DAILY-SMTH. Crosshatching signifies statistical significance at the 95% or greater level based on Student's t-test.

### Longwave Radiation Anomaly ( $W m^{-2}$ ) (Sep - Oct 2006)

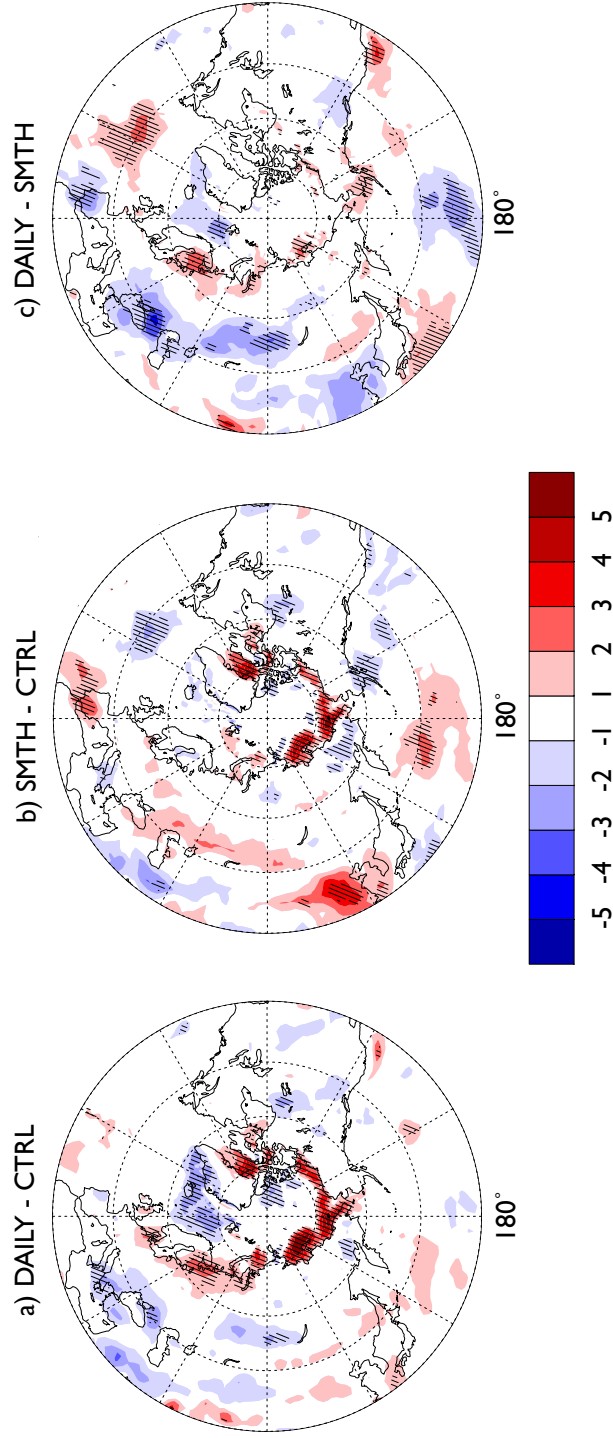


**Figure C-4 Fall Longwave Radiation Differences**  
Ensemble average (Sep - Oct) long wave radiation anomaly ( $W m^{-2}$ ) a) DAILY-CONTROL, b) SMTH-CONTROL, c) DAILY-SMTH. Crosshatching signifies statistical significance at the 95% or greater level based on Student's t-test.

### Shortwave Radiation Anomaly ( $W m^{-2}$ ) (Sep - Oct 2006)

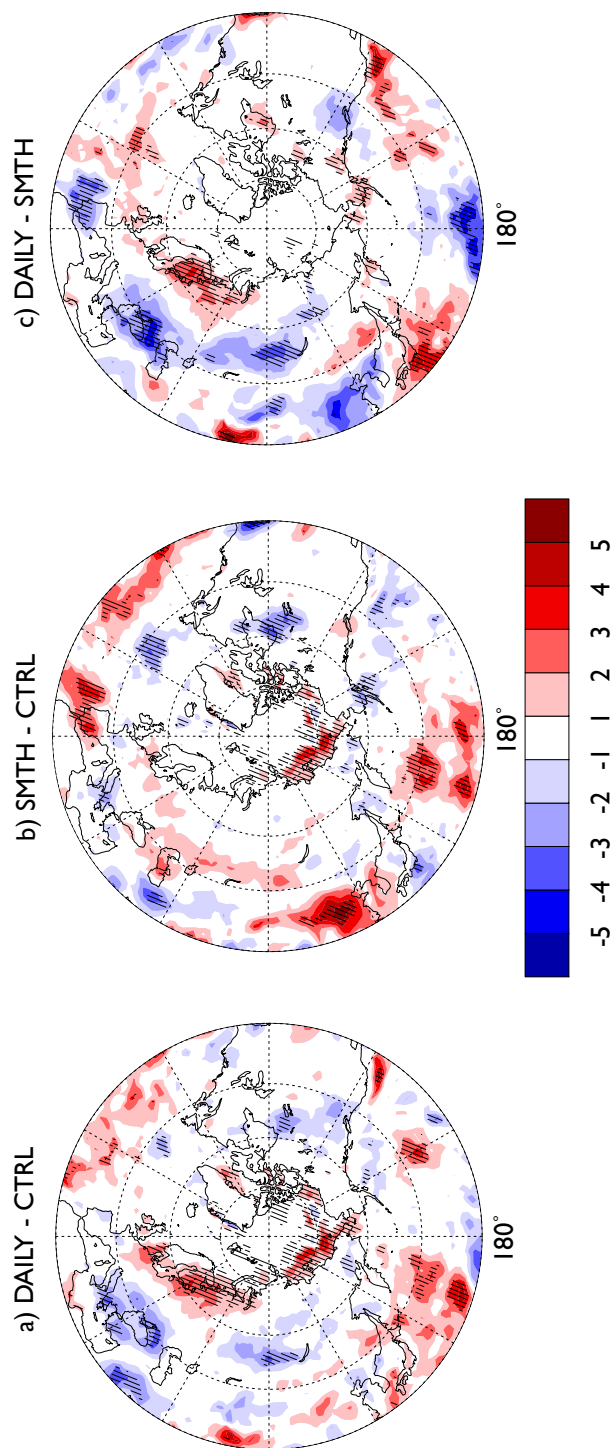


**Figure C.5 Fall Shortwave Radiation Differences**  
Ensemble average (Sep - Oct) short wave radiation anomaly ( $W m^{-2}$ ) a) DAILY-CONTROL, b) SMTH-CONTROL, c) DAILY-SMTH. Crosshatching signifies statistical significance at the 95% or greater level based on Student's t-test.

Positive net downward shortwave radiation anomalies occur for the two experiments (DAILY and SMTH) over the Laptev, East Siberian, Chukchi and Beaufort seas (Figure C.5a and b). Positive anomalies at the ice edge are due to a decrease in reflected shortwave radiation, a consequence of the replacing high albedo sea ice by lower albedo ocean. Positive anomalies are also seen in the western part of North Pacific. There is more shortwave into the surface over Finland, North West Russia, and western and eastern North Pacific in DAILY (Figure C.5c) than SMTH.

Large positive anomalies in total fluxes (sensible heat, latent heat, and longwave radiation) are seen out of the Arctic Ocean over the region of below average 2006 sea ice and large negative anomalies over the central Arctic (Figure C.6a and b). Negative anomalies are present over Chukotka and southwest of Hudson Bay. There are small negative heat flux anomalies in DAILY-SMTH in the Arctic Ocean over reduced sea ice areas, but the largest differences are seen over the midlatitude North Pacific and North Atlantic (Figure C.6c).

## **C.2 Atmospheric Response**

When sea ice is reduced, positive temperature anomalies occur over the Canadian Archipelago and around most of the central Arctic Basin in the two experiments (Figure C.7a and b). There are negative temperature anomalies along the North Atlantic sector of the Arctic (Figure C.7a and b). Between the two experiments (Figure C.7c), less warming occur over the Kara, Laptev and East Siberian seas as well as over parts of Siberia, Alaska and North West Canada in DAILY than SMTH. The high latitude Atlantic Sector is slightly warmer in DAILY than SMTH.

Sea level pressure varies greatly between the two experiments (close to 2 hPa) and only a few features are statistically significant. A negative pressure anomaly over the Mediterranean Sea (Figure C.8a and b) is the only large-scale

feature found in both experiments. A large center of positive pressure anomalies over Northwest Europe in DAILY-SMTH is the most striking difference between the experiments (Figure C.8c). In addition, there is a center of negative SLP anomalies over eastern North Atlantic (Figure C.8c).

The 500 hPa Geopotential height anomalies vary considerably for the response to 2006 ice conditions and is consistent with the SLP response (Figure C.9a and b). There is a large positive height anomaly over Northwest Europe in DAILY-SMTH (Figure C.9c) that overlies the positive SLP anomaly, suggesting the differences in the response is equivalent barotropic.

The two experiments show positive precipitation anomalies in the East Siberian and Beaufort seas, Hudson Bay, and the Mediterranean Sea (Figure C.10a and b). Differences between the experiments (DAILY-SMTH) shows lower precipitation over Northwest Europe and eastern North Pacific (Figure C.10c). Higher precipitation occurs in DAILY-SMTH over eastern North Atlantic, the Black Sea Region and British Columbia. The two ice forcings for 2006 display notably different precipitation anomalies, suggesting that the exact nature of the ice forcing has an impact on the large-scale climate.

The two experiments display reduced low-level cloud amounts over the reduced ice areas along Greenland, across the North Atlantic and along the Eurasian arctic seas. Positive low-level cloud anomalies are seen in Chukotka and over the Canadian Archipelago (Figure C.11a and b). The two experiments differ (DAILY-SMTH) mainly in the Eurasian Arctic with a negative anomalies over the Laptev and Kara seas and Northern Europe in DAILY – SMTH (Figure C.11c). There are positive low-level cloud anomalies in Figure C.11c over western Eurasia at around 50N.

### Net Upward Heat Flux Anomaly ( $W m^{-2}$ ) (Sep - Oct 2006)

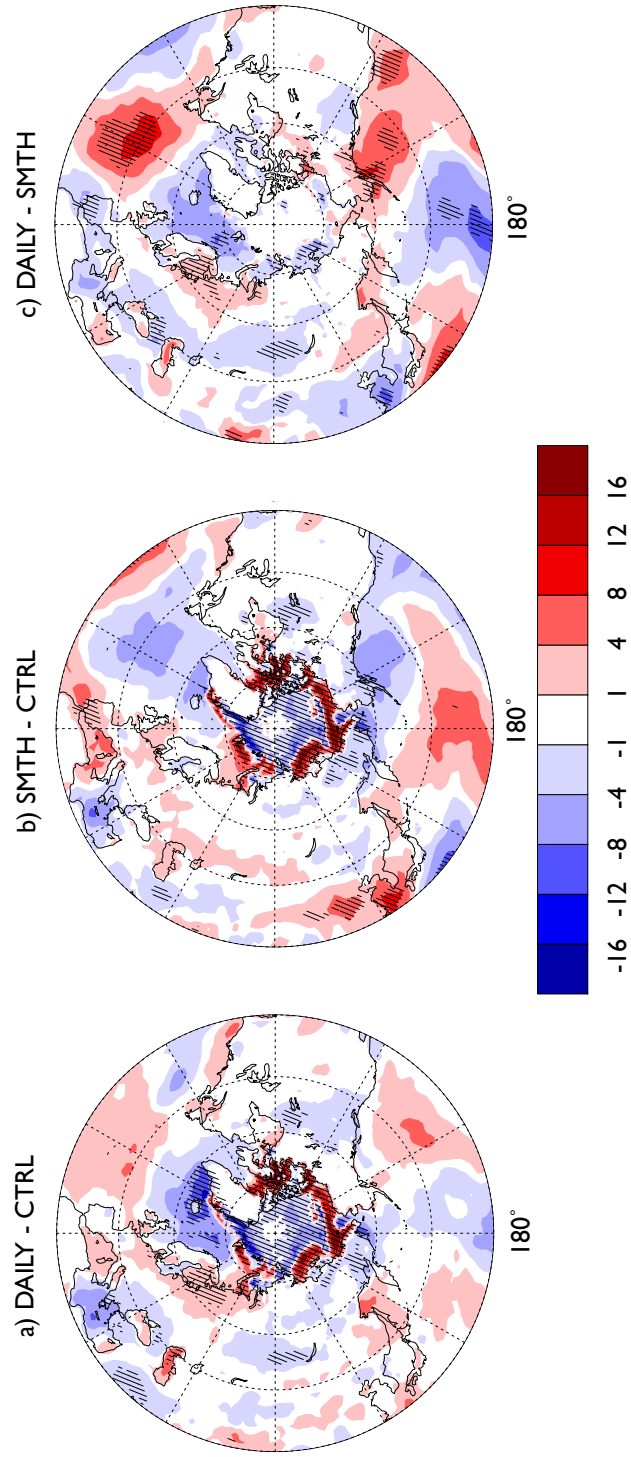


**Figure C.6 Fall Net Upward Heat Flux Differences**  
Ensemble average (Sep - Oct) net upward heat flux anomaly ( $W m^{-2}$ ) a) DAILY-CONTROL, b) SMTH-CONTROL, c) DAILY-SMTH. Crosshatching signifies statistical significance at the 95% or greater level based on Student's t-test.

Surface Air Temperature Anomaly (K) (Sep - Oct 2006)

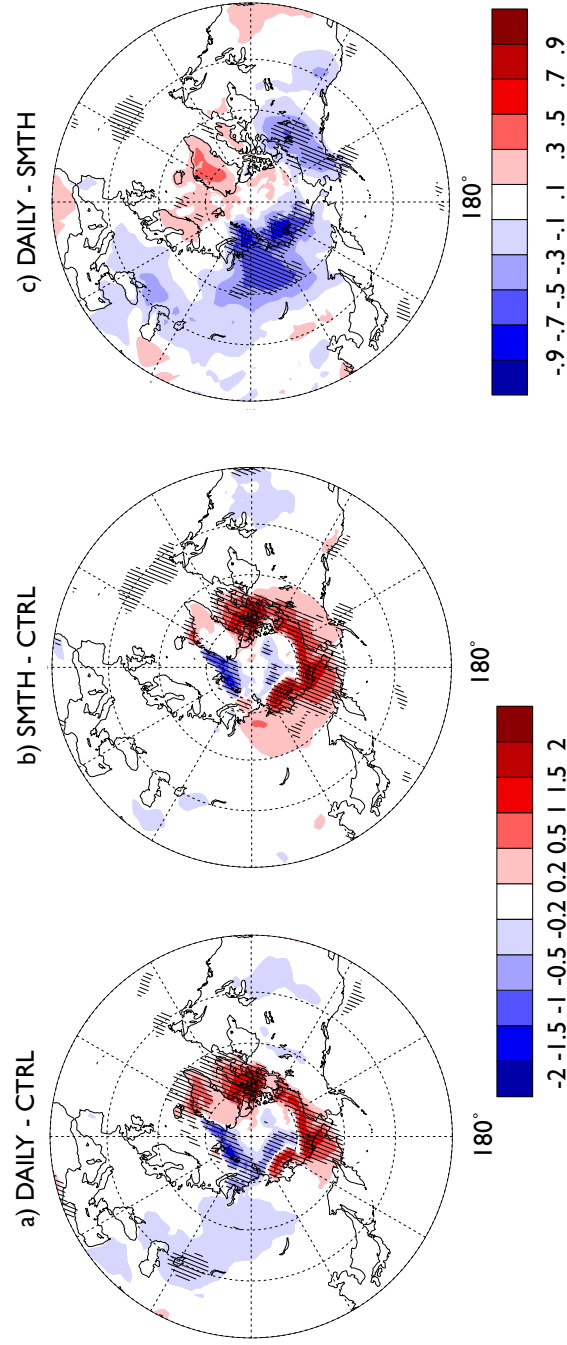


**Figure C.7 Fall Temperature Differences**  
Ensemble average (Sep - Oct) temperature anomaly (K) a) DAILY-CONTROL, b) SMTH-CONTROL, c) DAILY-SMTH. Crosshatching signifies statistical significance at the 95% or greater level based on Student's t-test.

### Sea Level Pressure Anomaly (hPa) (Sep - Oct 2006)

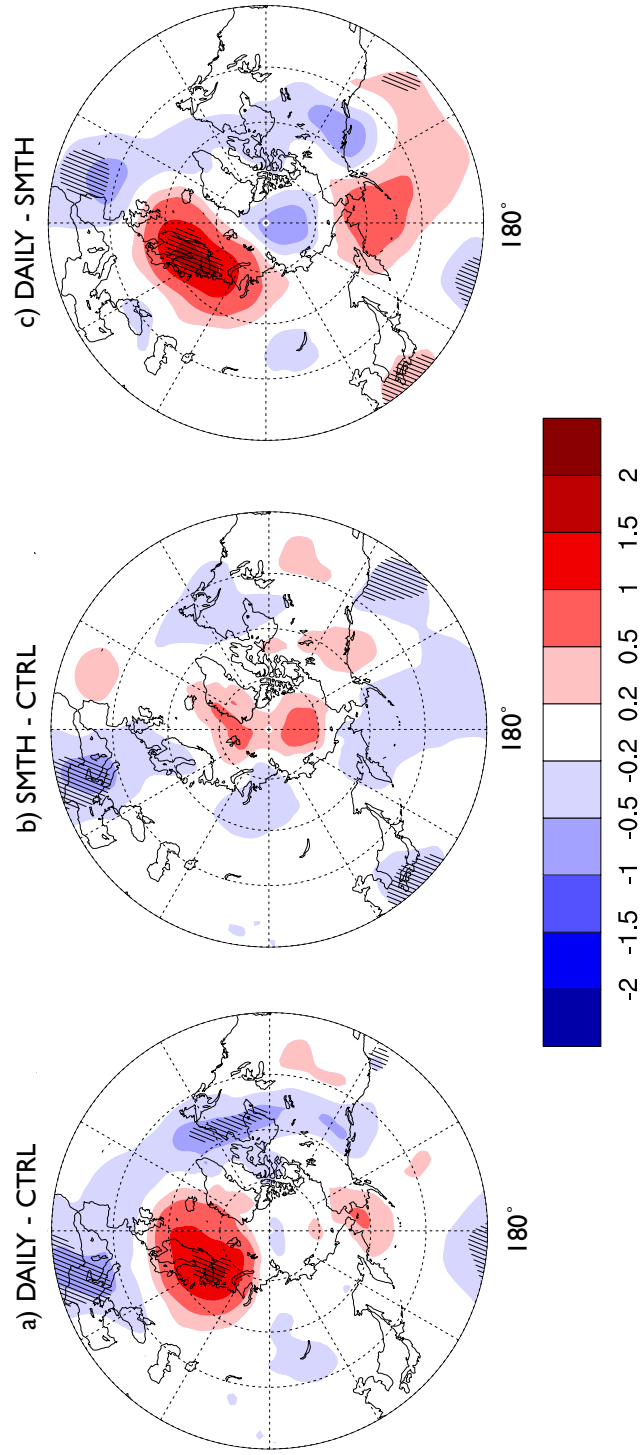


**Figure C.8 Fall Sea Level Pressure Differences**

Ensemble average (Sep - Oct) sea level pressure anomaly (hPa) a) DAILY-CONTROL, b) SMTH-CONTROL, c) DAILY-SMTH. Crosshatching signifies statistical significance at the 95% or greater level based on Student's t-test.



### 500 hPa Geopotential Height Anomaly (m) (Sep - Oct 2006)

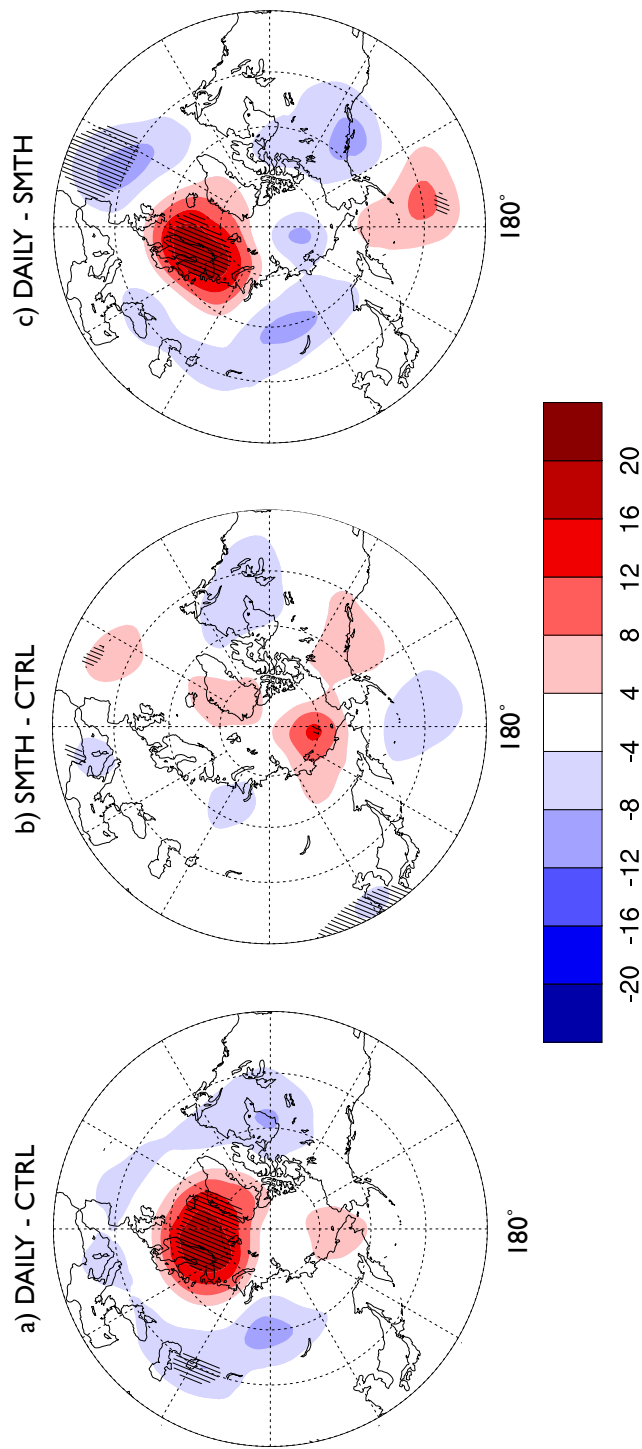


**Figure C.9 Fall 500 hPa Geopotential Height Differences**  
Ensemble average (Sep - Oct) 500 hPa geopotential height anomaly (m) a) DAILY-CONTROL, b) SMTH-CONTROL, c) DAILY-SMTH. Crosshatching signifies statistical significance at the 95% or greater level based on Student's t-test.

Precipitation Anomaly (mm day<sup>-1</sup>) (Sep - Oct 2006)

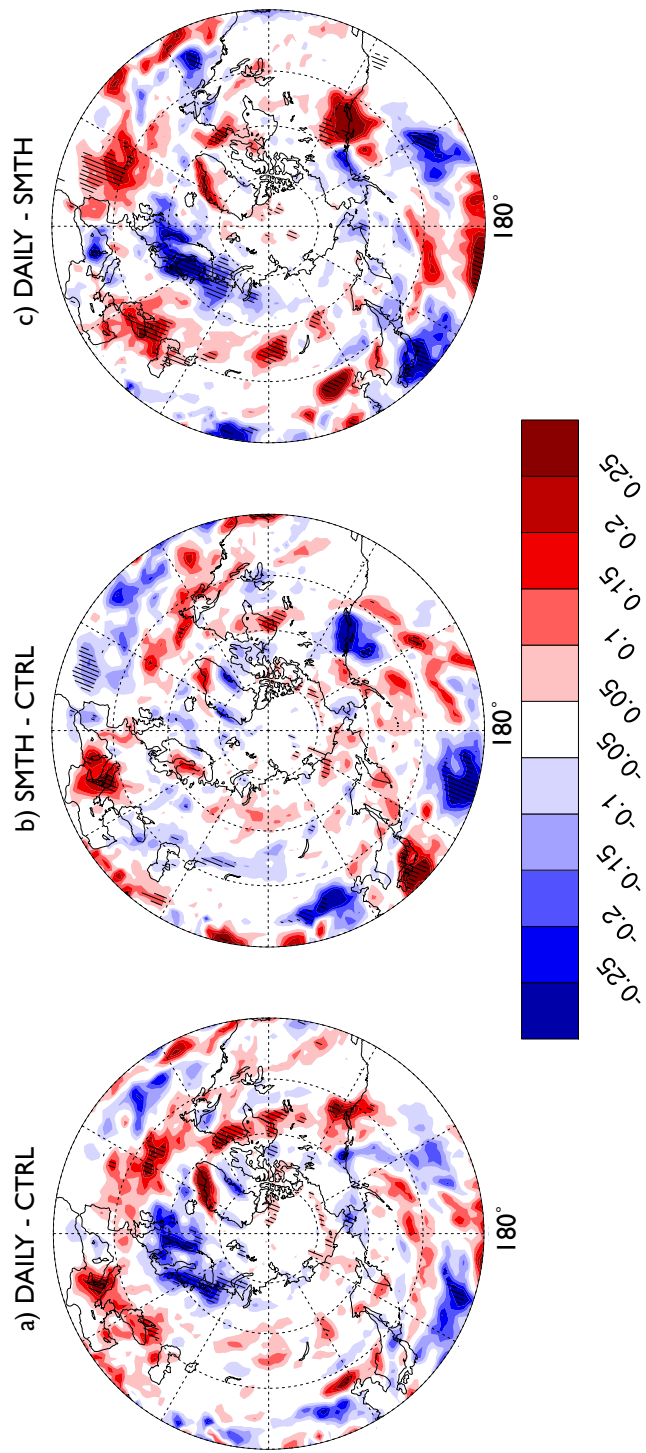


**Figure C.10 Fall Precipitation Differences**

Ensemble average (Sep - Oct) total precipitation anomaly (mm day<sup>-1</sup>) a) DAILY-CONTROL, b) SMTH-CONTROL, c) DAILY-SMTH. Crosshatching signifies statistical significance at the 95% or greater level based on Student's t-test.

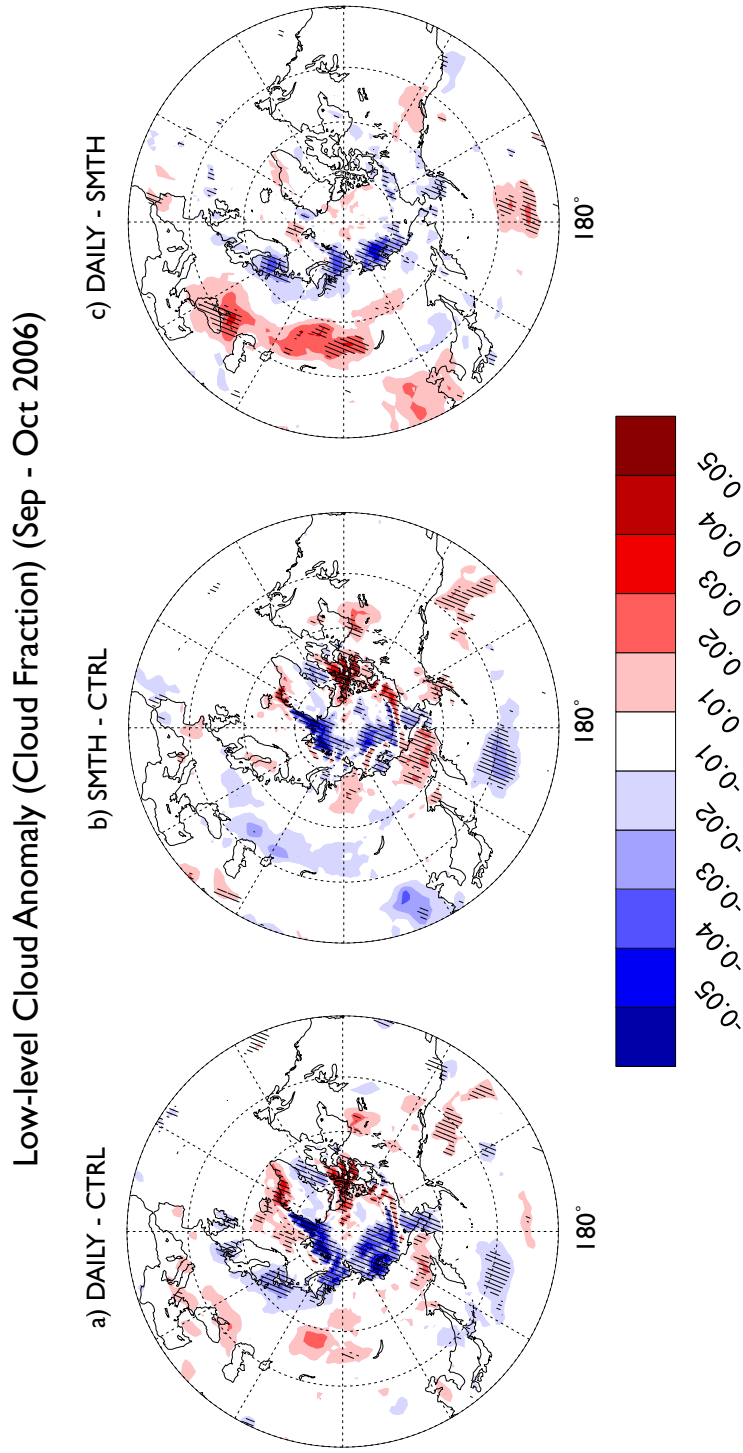


**Figure C.11 Fall Low-level Cloud Differences**  
 Ensemble average (Sep - Oct) low-level cloud anomaly (cloud fraction) a) DAILY-CONTROL, b) SMTH-CONTROL, c) DAILY-SMTH. Crosshatching signifies statistical significance at the 95% or greater level based on Student's t-test.

### Medium-level Cloud Anomaly (Cloud Fraction) (Sep - Oct 2006)

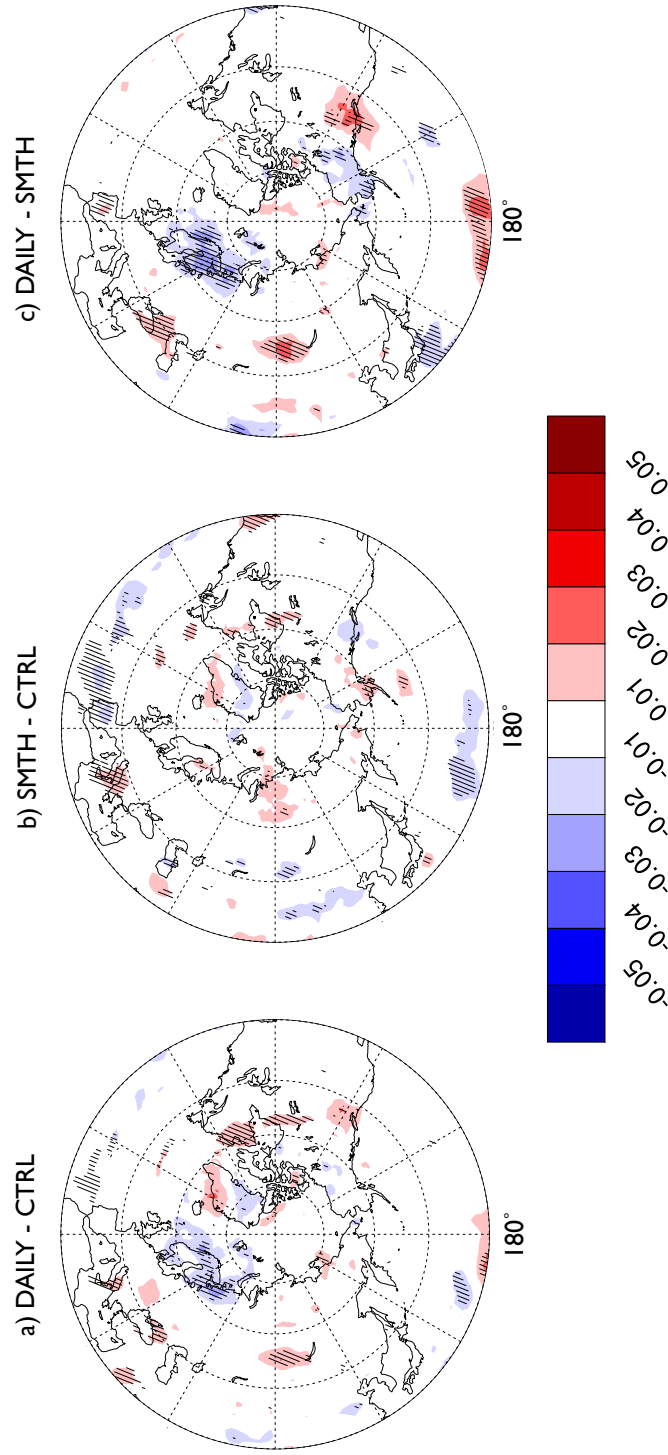


**Figure C.12 Fall Medium-level Cloud Differences**  
Ensemble average (Sep - Oct) medium-level cloud anomaly (cloud fraction) a) DAILY-CONTROL, b) SMTH-CONTROL, c) DAILY-SMTH. Crosshatching signifies statistical significance at the 95% or greater level based on Student's t-test.

The mid-level cloud response is negligible over the Arctic Ocean and generally weak in the midlatitudes (Figure C.12a and b). Similar to the low-level cloud response, mid-level clouds differ most over Northern Europe where DAILY-SMTH displays negative anomalies (Figure C.12c).

The high-level cloud response is generally weak for the entire domain. The largest anomalies in DAILY-SMTH show decreased cloud amounts over Northern Europe and increased cloud amounts over Spain (Figure C.13c).

Positive specific humidity anomalies occur over the Canadian Archipelago and the Beaufort, East Siberian, and Laptev seas, and the central North Atlantic. Negative anomalies occur over the Northern Atlantic (Figure C.14a and b). In DAILY-SMTH there is less moisture over the Kara, and Laptev seas, Alaska and Northwest Territories and the central North Atlantic and more moisture over the Norwegian and Greenland seas (Figure C.14c). The anomaly patterns of low-level humidity corresponds to the 2-m temperature anomalies (Figure C.7).

### High-level Cloud Anomaly (Cloud Fraction) (Sep - Oct 2006)

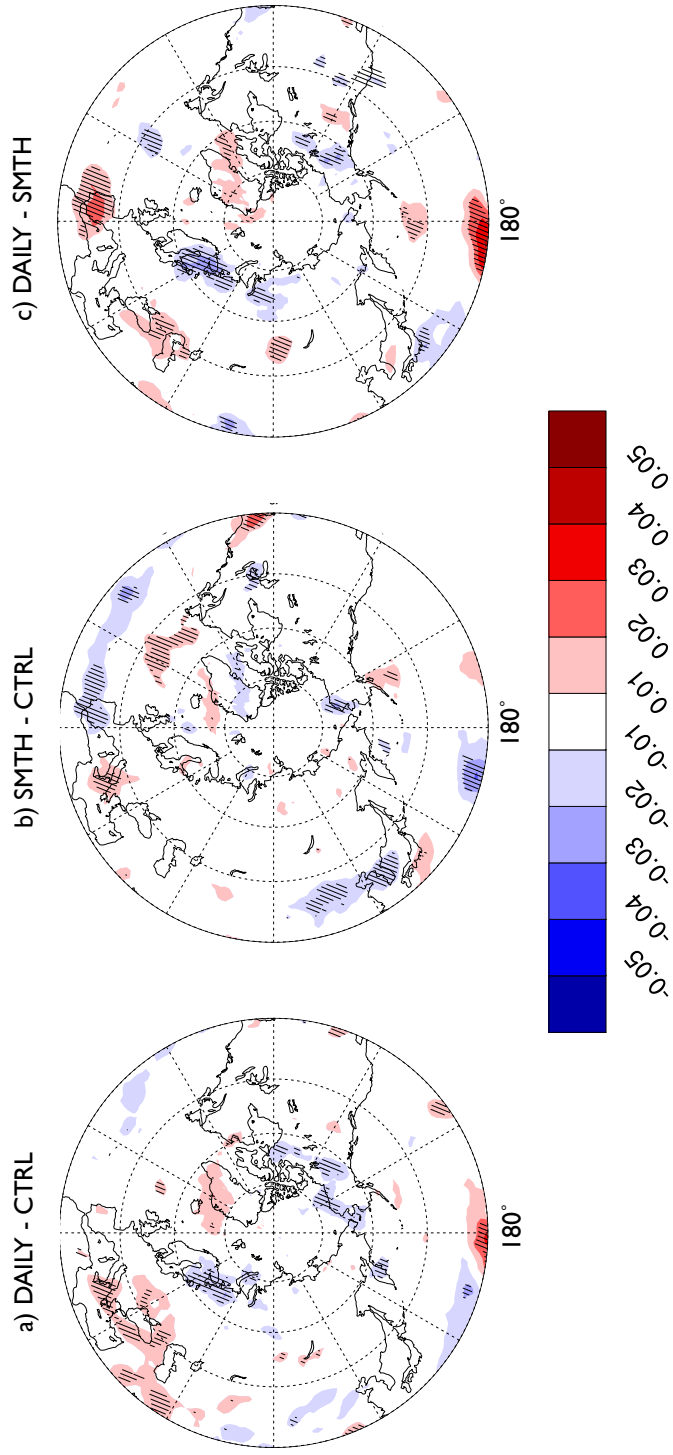


**Figure C.13 Fall High-level Cloud Differences**  
Ensemble average (Sep - Oct) high-level cloud anomaly (cloud fraction) a) DAILY-CONTROL, b) SMTH-CONTROL, c) DAILY-SMTH. Crosshatching signifies statistical significance at the 95% or greater level based on Student's t-test.

1000 hPa Specific Humidity Anomaly ( $\text{g kg}^{-1}$ ) (Sep - Oct 2006)

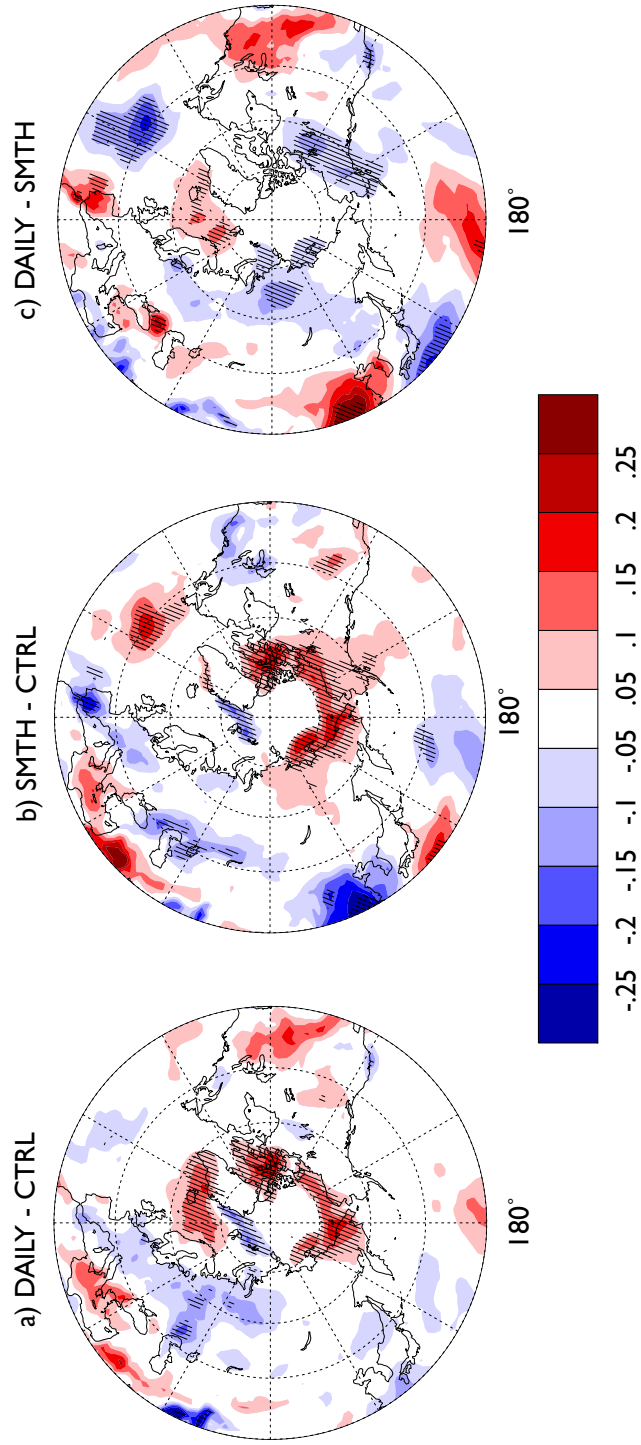


**Figure C.14 Fall Specific Humidity Differences**  
Ensemble average (Sep - Oct) 1000 hPa specific humidity anomaly ( $\text{g kg}^{-1}$ ) a) DAILY-CONTROL, b) SMTH-CONTROL, c) DAILY-SMTH. Crosshatching signifies statistical significance at the 95% or greater level based on Student's t-test.

### C.3 Storm Track Response

Poleward heat transport represented by 2-10 days bandpassed  $v'T'$  at 850 hPa displays a positive anomaly off the coast of Labrador and negative over Alaska (Figure C.15a and b). The bandpassed  $v'T'$  at 850 hPa for DAILY-SMTH displays higher heat transport over Eastern Canada and lower over Northern Europe (Figure C.15c). Higher variability in poleward heat transport indicates higher storm activity (Section 2.3.3).

Poleward momentum transport, represented by 2-10 days bandpassed  $u'v'$  at 200 hPa, does not display many similar anomalies between the experiments (Figure C.16a and b). However, DAILY-SMTH displays lower bandpassed  $u'v'$  at 200 hPa over the Mediterranean Sea and higher in the Kara Sea (Figure C.16c). Higher values of poleward heat transport indicates higher storm activity (Section 2.3.3).

Storm track density is a generally noisy field and DAILY and SMTH display similar features as a response to 2006 sea ice anomalies (Figure C.17a and b). However, DAILY-SMTH (Figure C.17c) does indicate more storms in the Gulf of Alaska, off the coast of Japan and over the Mediterranean Sea.

Figure C.18 displays the mean 200 hPa zonal wind from SMTH in contours and anomalies (DAILY-SMTH) in shading. The figure indicates a weakening and retraction of the polar jet streak over the northern North Atlantic. A strengthening further south indicates a southward shift of the jet. A southward shift in the polar jet is the case for most longitudinal sectors.



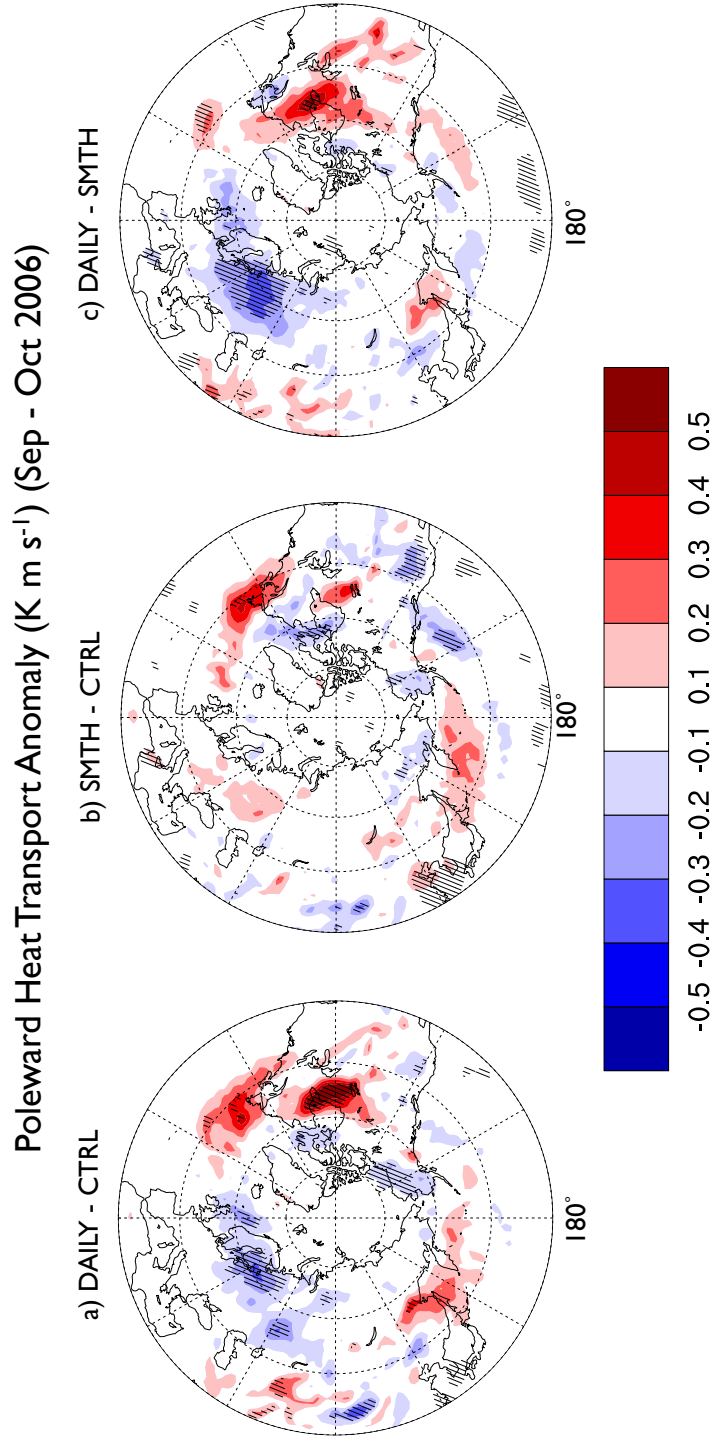


**Figure C.15 Fall Poleward Heat Transport Differences**  
 Ensemble average (Sep - Oct)  $v'T'$  850 hPa 2 - 10 days bandpassed anomaly ( $\text{K m s}^{-1}$ ) a) DAILY-CONTROL, b) SMTH-CONTROL, c) DAILY-SMTH. Crosshatching signifies statistical significance at the 95% or greater level based on Student's t-test.

Poleward Momentum Transport Anomaly ( $\text{m}^2 \text{s}^{-2}$ ) (Sep - Oct 2006)

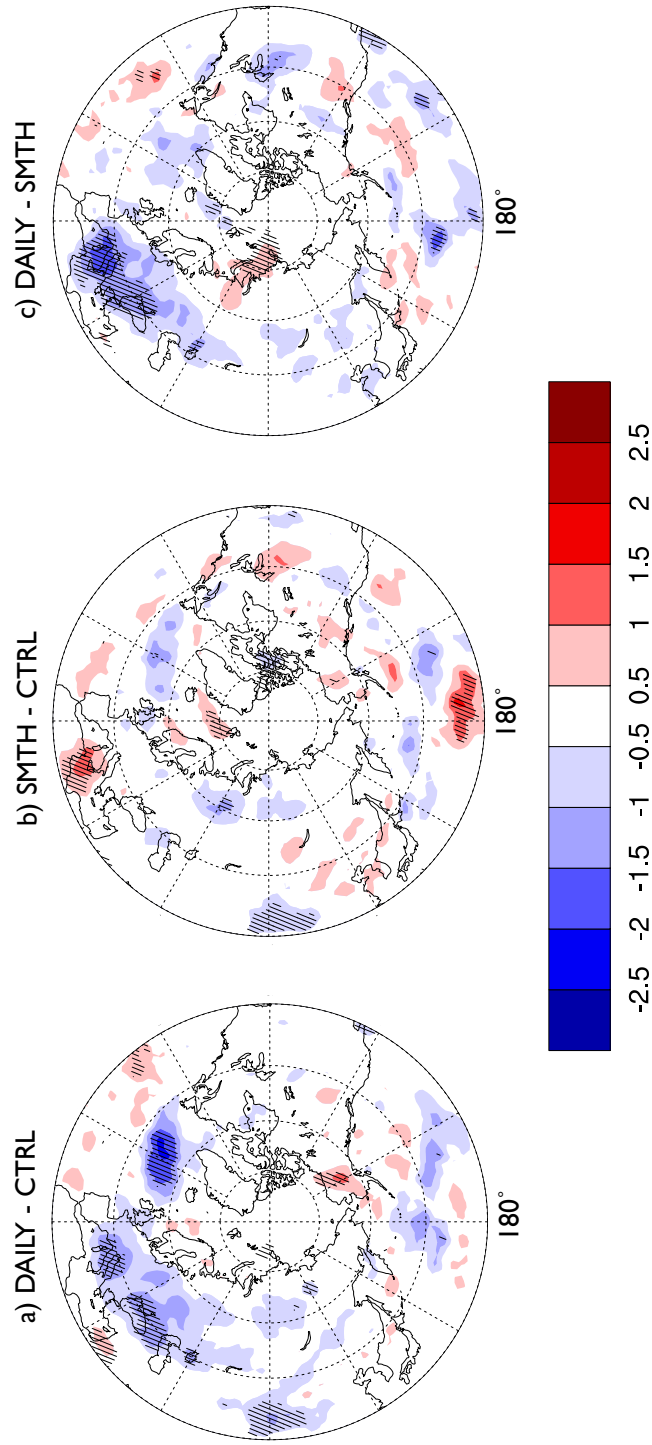


**Figure C.16 Fall Poleward Momentum Transport Differences**  
 Ensemble average (Sep - Oct)  $u'v'$  200 hPa 2-10 days bandpassed anomaly ( $\text{m}^2 \text{s}^{-2}$ ) a) DAILY-CONTROL, b) SMTH-CONTROL, c) DAILY-SMTH. Crosshatching signifies statistical significance at the 95% or greater level based on Student's t-test.

### Fall Smoothed Storm Density Anomaly (Storm Count) (Sep - Oct 2006)

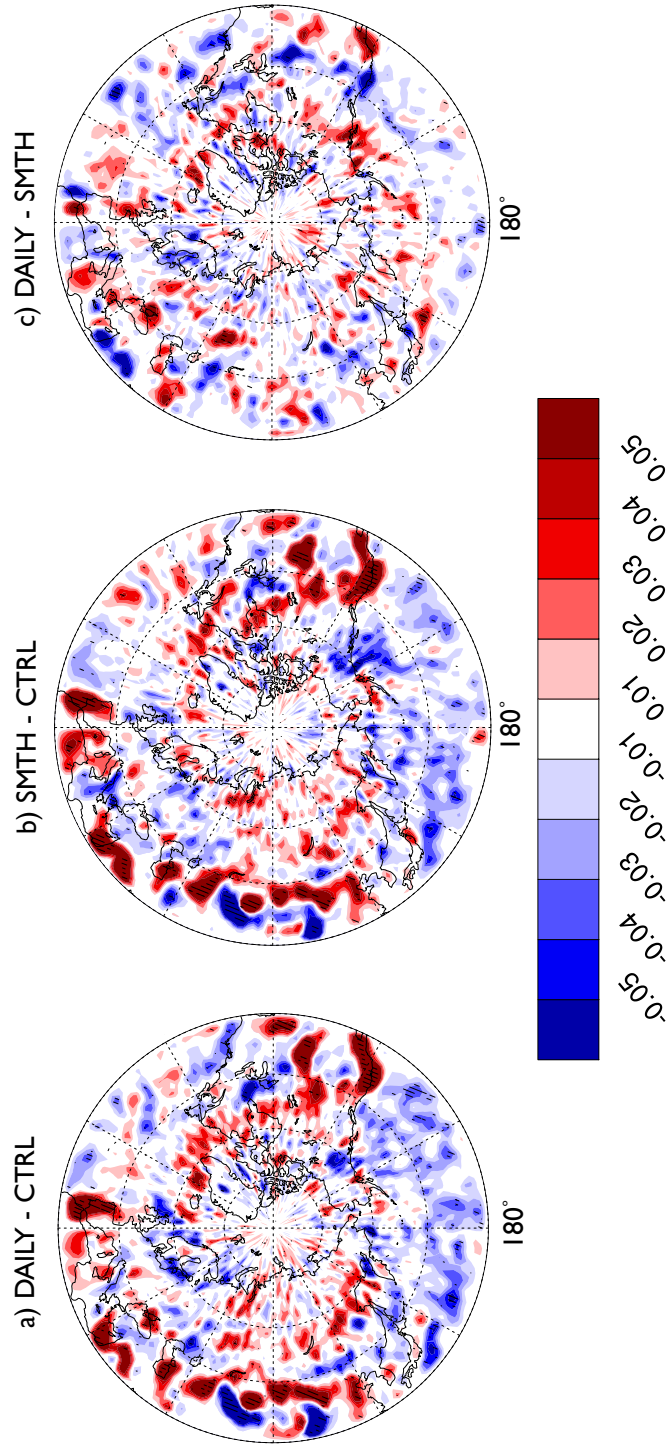


**Figure C.17 Fall Smoothed Storm Density Differences**  
Ensemble average (Sep - Oct) smoothed storm count anomaly (unitless) a) DAILY - CTRL, b) SMTH - CTRL, c) DAILY - SMTH. Crosshatching in c) signifies statistical significance at the 95% or greater level based on Student's t-test.

200hPa Zonal Wind Mean and Anomaly ( $\text{m s}^{-1}$ )  
DAILY - SMTH (Sep - Oct 2006)

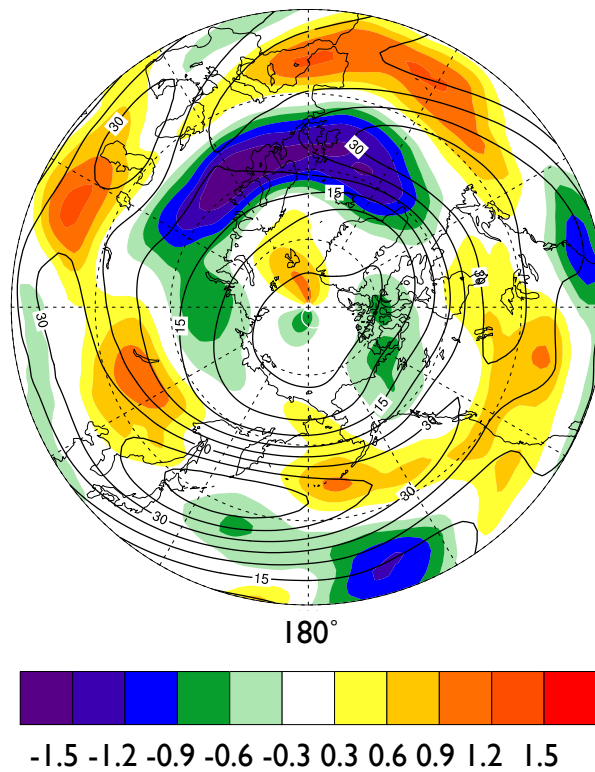


**Figure C.18 Fall Zonal Wind**

Ensemble average ( $\text{m s}^{-1}$ ) Sep - Oct zonal wind speed 200 hPa. Shading indicates anomaly DAILY-SMTH and contours denotes SMTH climatological zonal wind.

## **Appendix D Difference Between DAILY and SMTH Atmospheric Response During Winter**

Interpretation of 2006-07 winter season follows the same layout as for fall in Appendix C. The climatological winter SIC (CTRL) (Figure D.1b) is between 96 and 98% in most of the central Arctic Basin. Lower concentrations extend out to the southern part of the Barents Sea, Newfoundland, northern Bearing Sea and the Sea of Okhotsk. SIC in DAILY (Figure D.1a) resembles CTRL but does not extend as far equatorward in the Atlantic and Pacific sector as well as SIC being higher (over 99%) in most of the central Arctic basin. The 2006-07 winter anomaly (Figure D.1c) is therefore positive in the central Arctic but negative along the equatorward ice edge.

### **D.1 Surface Flux Response**

Figure D.2a and b indicate higher sensible heat fluxes south of the 2006 equatorward sea ice edge and over the central North Pacific. In contrast, the central basin and the high latitude Atlantic Ocean display below average fluxes. DAILY-SMTH displays lower heat fluxes out of the ocean around the Aleutian Islands and higher fluxes off the west coast of the US (Figure D.2c).

The latent heat flux response to 2006 sea ice resembles that of sensible heat, with positive flux anomalies south of the 2006 ice edge and in the central North Pacific. Negative anomalies occur in the central Arctic basin and in the Barents Sea (Figure D.3a and b). DAILY-SMTH displays negative flux anomalies in the Gulf of Alaska and positive along the West Coast of the US (Figure D.3c).

Larger longwave fluxes out of the ocean are present in the Barents Sea, Baffin and Hudson Bay, Davis Strait, and around and south of the Aleutian Islands in response to 2006 ice anomalies. Lower fluxes occur in the central Arctic basin and Northern Europe (Figure D.4a and b). DAILY-SMTH reveals

small differences, with positive anomalies along the West Coast of the US and negative anomalies in the northern Midwest US. There are also positive flux anomalies in the Laptev, Chukchi and Beaufort seas (Figure D.4c).

Shortwave radiation differences between DAILY and SMTH are relatively small in the Arctic since this shortwave radiation is not an important component of the surface energy budget in the winter months (Figure D.5c).

Total upward heat flux anomalies are positive south of the equatorward 2006 ice edge as well as in the central North Pacific and are negative in the central Arctic basin as well as off the coast of Norway (Figure D.6a and b). DAILY-SMTH displays positive anomalies along the West Coast of the US.

## **D.2 Atmospheric Response**

The 2-m temperature response to winter 2006 ice anomalies is characterized by below average temperature over the central Arctic Ocean and anomalously warm temperatures above large parts of Northern Europe, Barents Sea, Chukchi Sea, Shelekhov Gulf, Hudson Bay, Davis Strait, and Labrador Sea (Figure D.7a and b). DAILY-SMTH displays large significant positive anomalies over Beringia and negative anomalies over the continental US (Figure D.7c). The most striking difference in Figure D.7 is the opposite temperature response over the continental US.

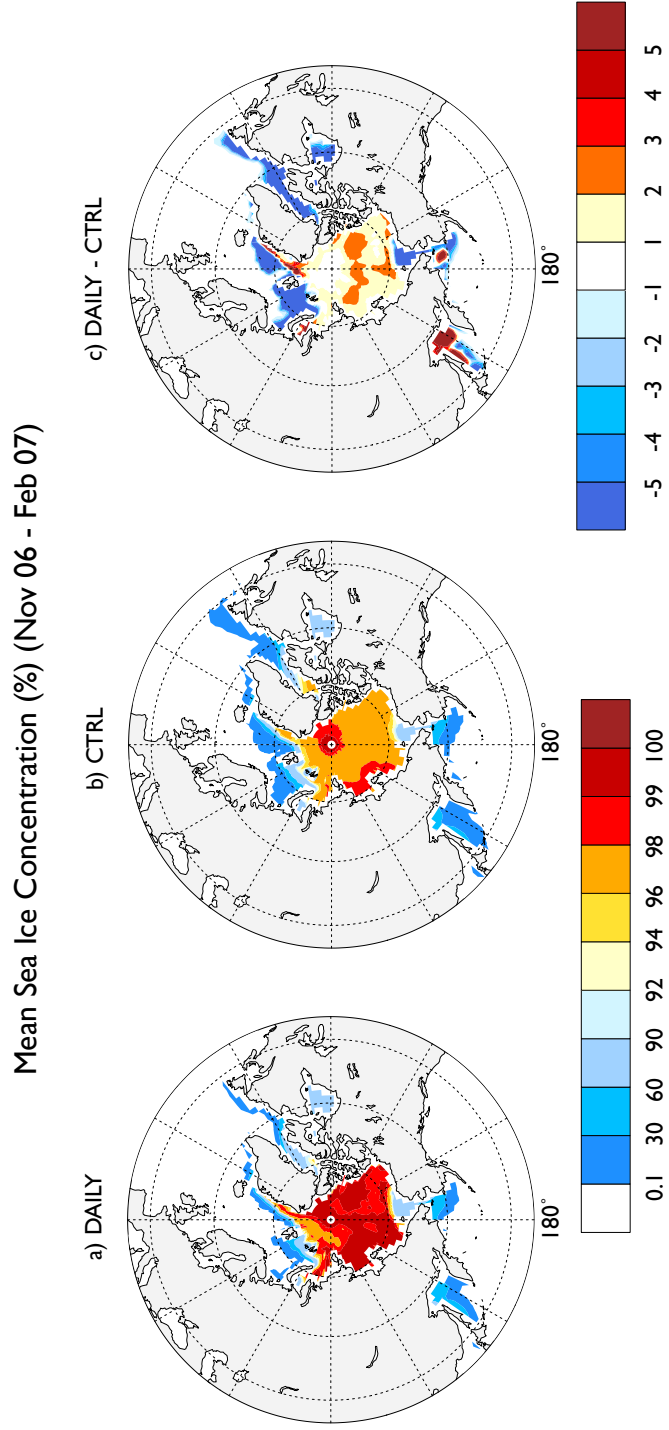


**Figure D.1 Winter Sea Ice Concentration**  
 Average sea ice concentration (%) Nov 06 – Feb 07. a) DAILY, b) CONTROL, c) DAILY-CTRL. Note scale is non-linear in the left panels.

### Sensible Heat Flux Anomaly ( $W m^{-2}$ ) (Nov 06 - Feb 07)

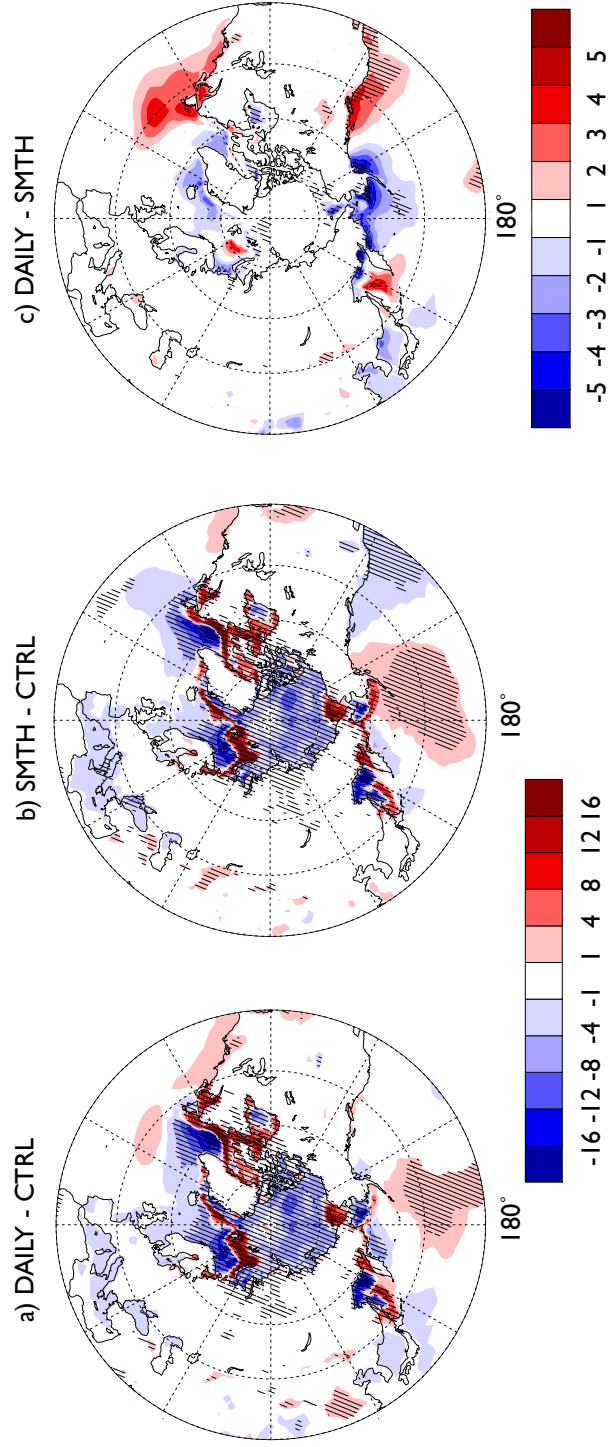


**Figure D.2 Winter Sensible Heat Flux Differences**

Ensemble average (Nov – Feb) sensible heat flux anomaly ( $W m^{-2}$ ) a) DAILY-CTRL, b) SMTH-CTRL, c) DAILY-SMTH. Crosshatching signifies statistical significance at the 95% or greater level based on Student's t-test.



Latent Heat Flux Anomaly ( $W m^{-2}$ ) (Nov 06 - Feb 07)

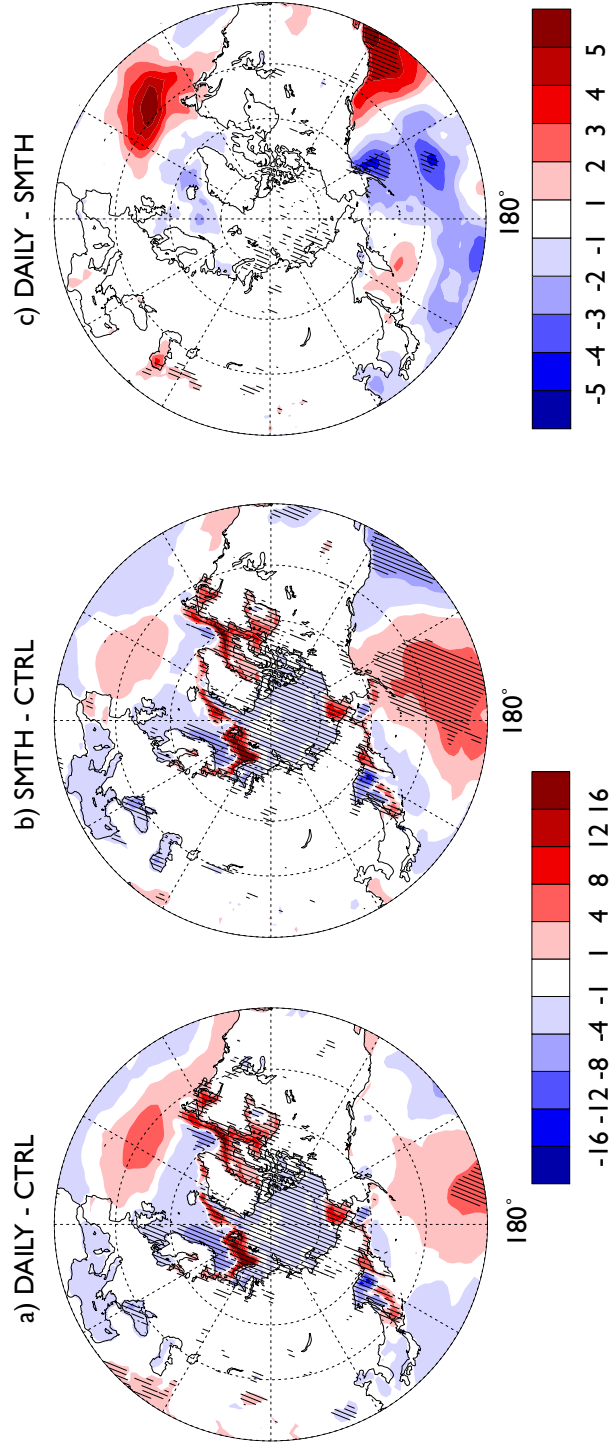


**Figure D.3 Winter Latent Heat Flux Differences**  
Ensemble average (Nov – Feb) latent heat flux anomaly ( $W m^{-2}$ ) a) DAILY-CTRL, b) SMTH-CTRL, c) DAILY-SMTH. Crosshatching signifies statistical significance at the 95% or greater level based on Student's t-test.

### Longwave Radiation Anomaly ( $W m^{-2}$ ) (Nov 06 - Feb 07)

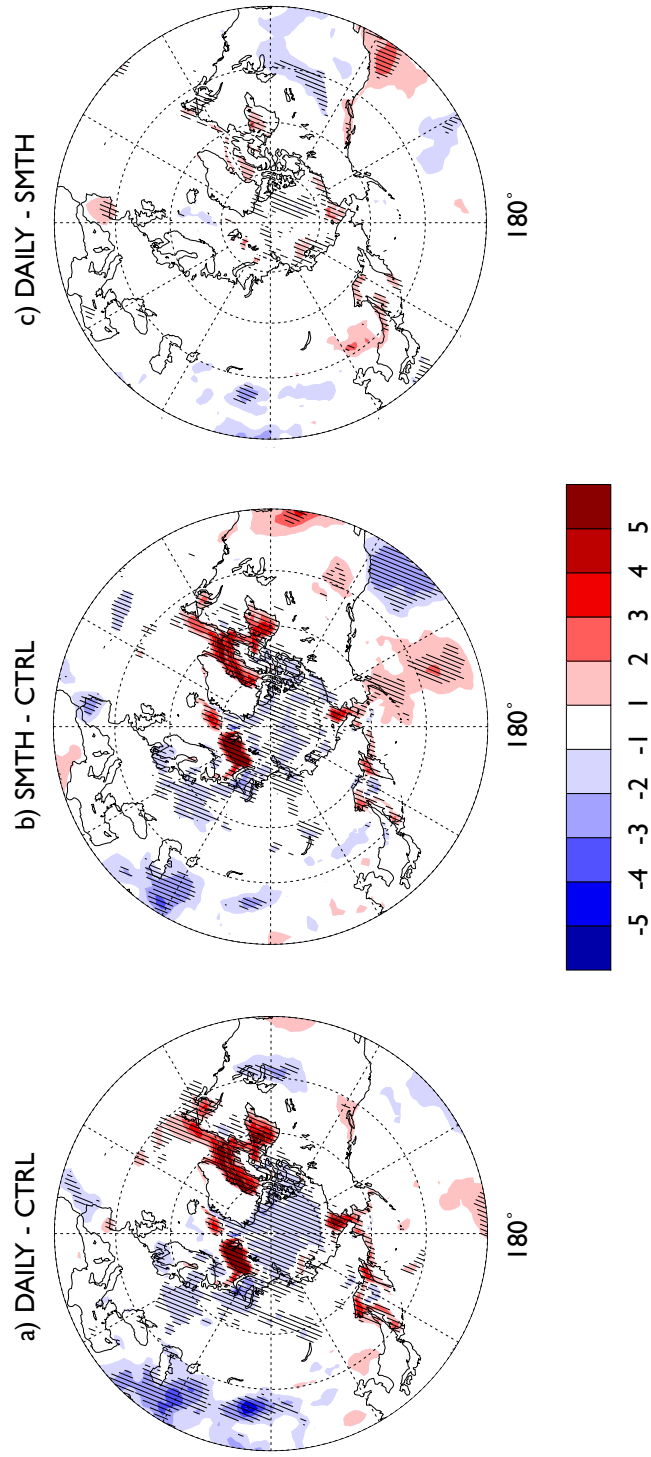


**Figure D.4 Winter Longwave Radiation Differences**  
Ensemble average (Nov – Feb) long wave radiation flux anomaly ( $W m^{-2}$ ) a) DAILY-CTRL, b) SMTH-CTRL, c) DAILY-SMTH. Crosshatching signifies statistical significance at the 95% or greater level based on Student's t-test.

### Shortwave Radiation Anomaly ( $W m^{-2}$ ) (Nov 06 - Feb 07)

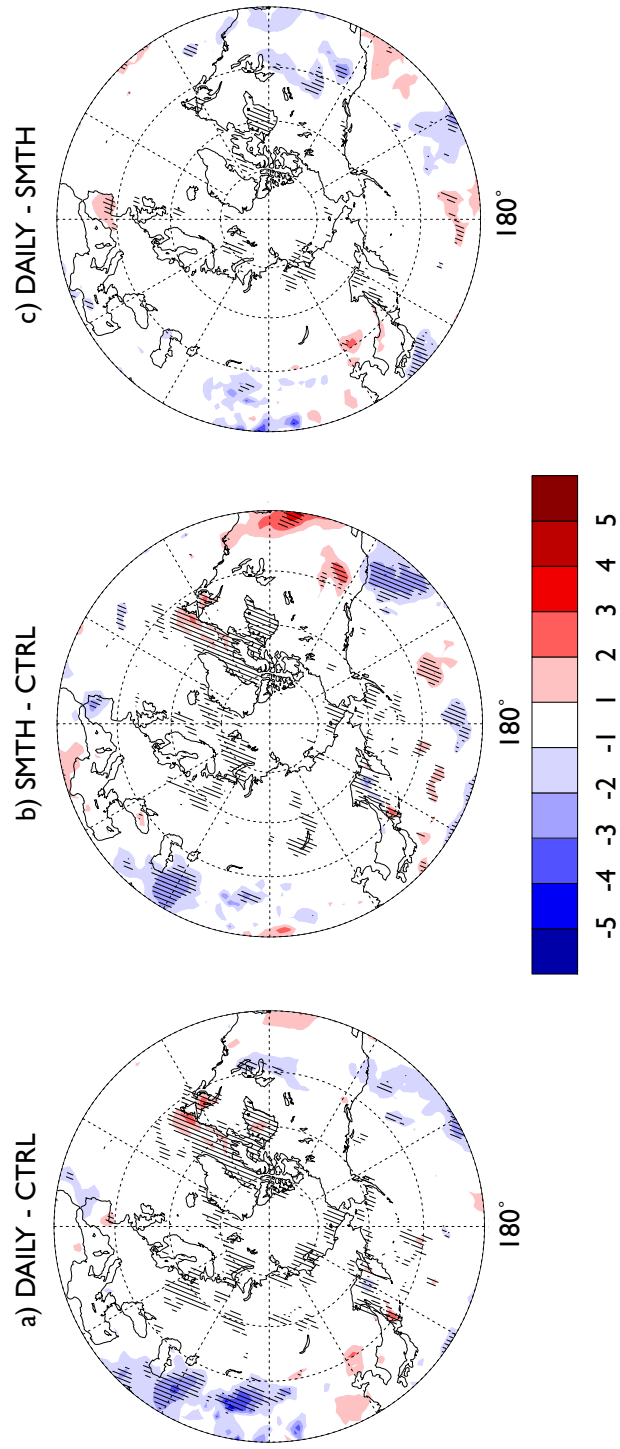


**Figure D.5 Winter Shortwave Radiation Differences**  
Ensemble average (Nov – Feb) short wave radiation flux anomaly ( $W m^{-2}$ ) a) DAILY-CTRL, b) SMTH-CTRL, c) DAILY-SMTH. Crosshatching signifies statistical significance at the 95% or greater level based on Student's t-test.

### Net Upward Heat Flux Anomaly ( $W m^{-2}$ ) (Nov 06 - Feb 07)

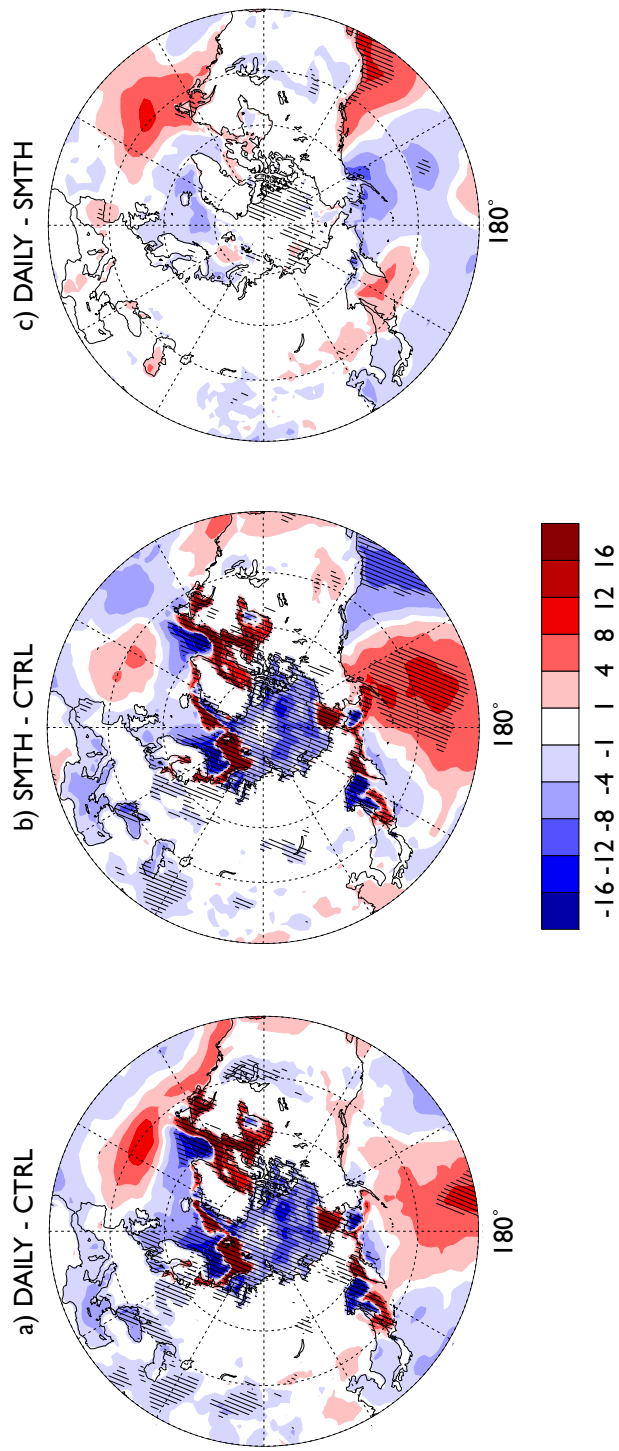


**Figure D.6 Winter Net Upward Heat Flux Differences**  
Ensemble average (Nov – Feb) net upward heat flux anomaly ( $W m^{-2}$ ) a) DAILY-CTRL, b) SMTH-CTRL, c) DAILY-SMTH. Crosshatching signifies statistical significance at the 95% or greater level based on Student's t-test.

Surface Air Temperature Anomaly (K) (Nov 06 - Feb 07)

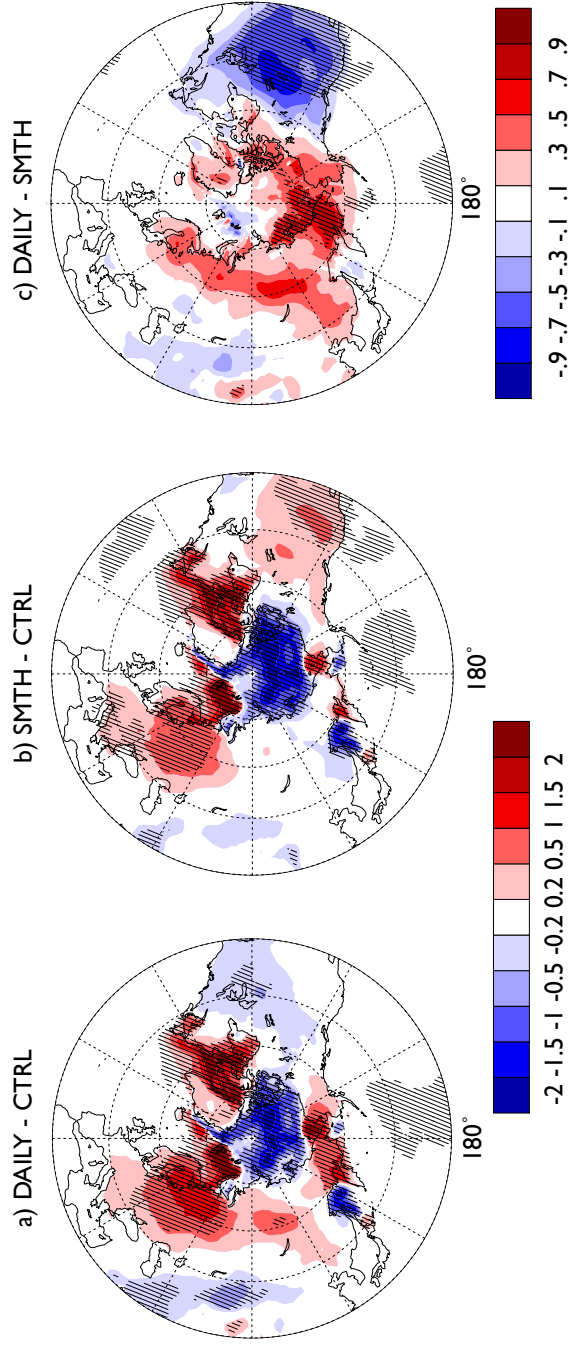


**Figure D.7 Winter Temperature Differences**  
Ensemble average (Nov – Feb) temperature anomaly (K) a) DAILY-CTRL, b) SMTH-CTRL, c) DAILY-SMTH.  
Crosshatching signifies statistical significance at the 95% or greater level based on Student's t-test.

### Sea Level Pressure Anomaly (hPa) (Nov 06 - Feb 07)

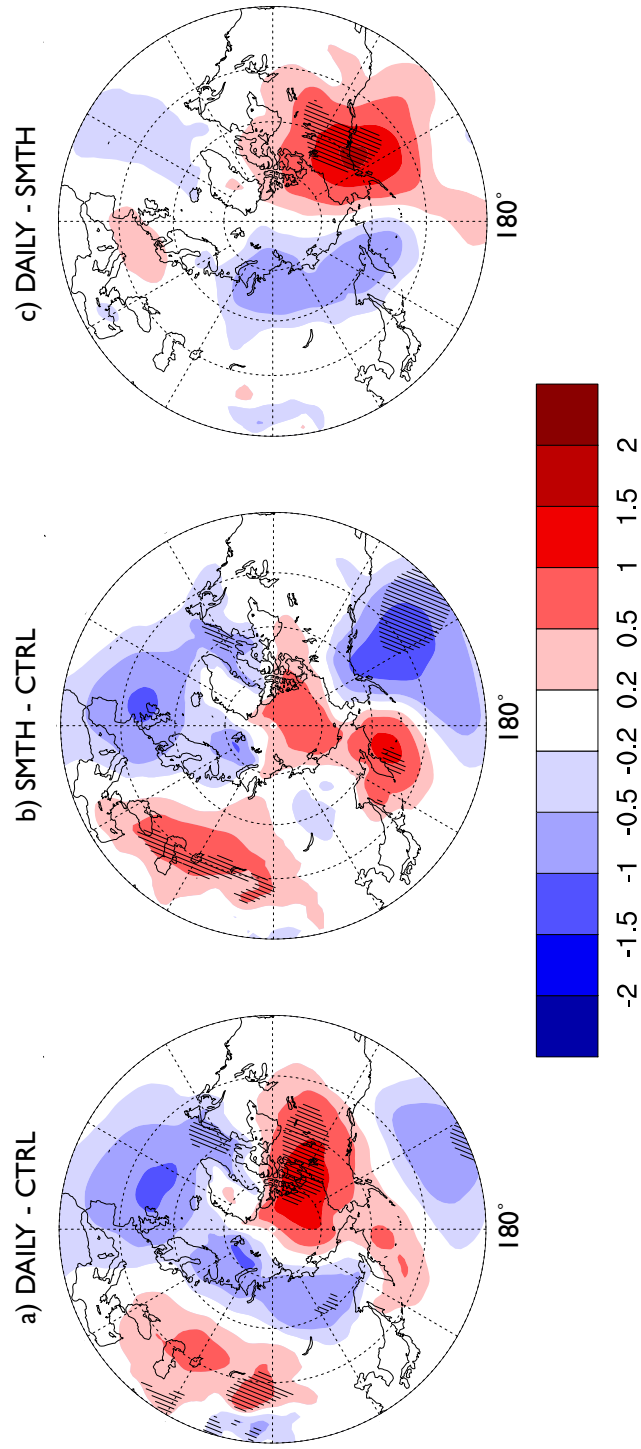


**Figure D.8 Winter Sea Level Pressure Differences**  
Ensemble average (Nov – Feb) sea level pressure anomaly (hPa) a) DAILY-CTRL, b) SMTH-CTRL, c) DAILY-SMTH. Crosshatching signifies statistical significance at the 95% or greater level based on Student's t-test.

Few generalizations can be made between 2006 sea ice and climatology with respect to SLP, but there is lower pressure in the Labrador Sea in both experiments (Figure D.8a and b). DAILY-SMTH displays a center of high pressure stretching inland from the Gulf of Alaska to parts of the Northwest Territories in DAILY (Figure D.8c). The overall patterns in Figure D.8a and b are similar but the slight shifts in the pattern centers and strengths leads to a fairly large-scale difference seen in Figure D.8c.

A center of high 500 hPa geopotential height is found over Ukraine and Kazakhstan in response to 2006-07 ice anomalies (Figure D.9a and b). DAILY-SMTH displays a positive height anomaly (Figure D.9c) co-located with the SLP high (Figure D.8c) DAILY – SMTH. There is also an anomalous low center over the continental US in geopotential height which does not have a counterpart in in the SLP response (Figure D.9c).

There is reduced precipitation over the Arctic Ocean and increased precipitation over the Barents Sea and eastern North Pacific (Figure D.10a and b) in the response to winter 2006-07 ice anomalies. The precipitation anomaly response in the North Pacific to both ice forcings in winter (Figure D.10a and b) can be interpreted as a southward shift in the storm tracks, with the shift somewhat stronger in the SMTH ensemble. There is a larger reduction in precipitation in SMTH than DAILY over the southern US, resulting in significant positive anomalies (Figure D.10c).

### 500 hPa Geopotential Height Anomaly (m) (Nov 06 - Feb 07)

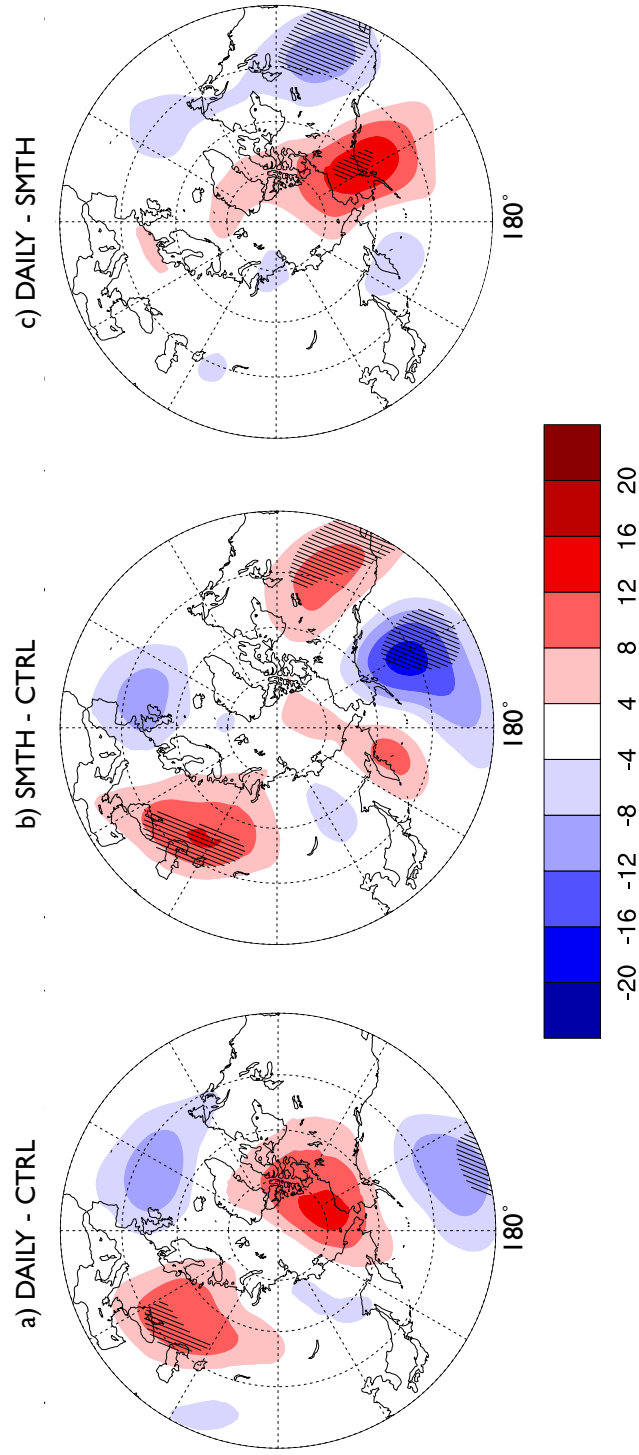


**Figure D.9 Winter 500 hPa Geopotential Height Differences**  
Ensemble average (Nov – Feb) 500 hPa geopotential height anomaly (m) a) DAILY-CTRL, b) SMTH-CTRL, c) DAILY-SMTH. Crosshatching signifies statistical significance at the 95% or greater level based on Student’s t-test.



Precipitation Anomaly (mm day<sup>-1</sup>) (Nov 06 - Feb 07)

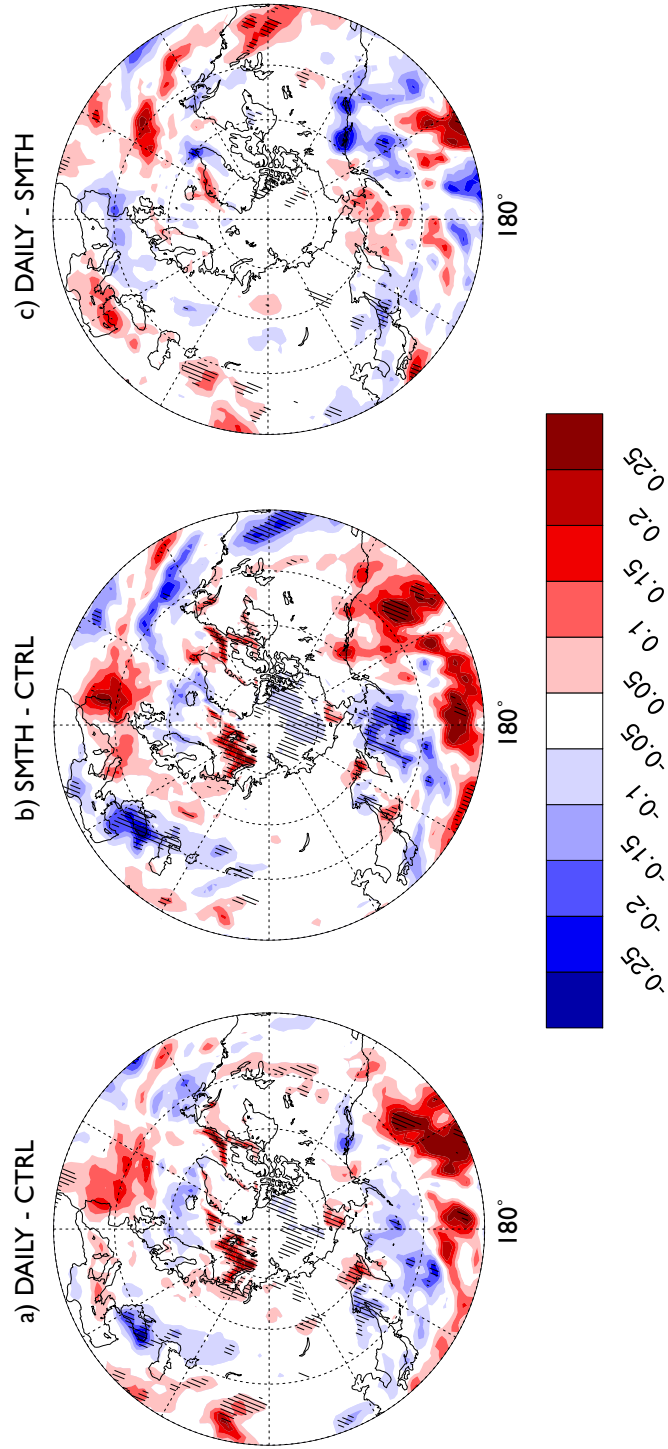


**Figure D.10 Winter Precipitation Differences**

Ensemble average (Nov – Feb) precipitation anomaly (mm day<sup>-1</sup>) a) DAILY-CTRL, b) SMTH-CTRL, c) DAILY-SMTH. Crosshatching signifies statistical significance at the 95% or greater level based on Student's t-test.

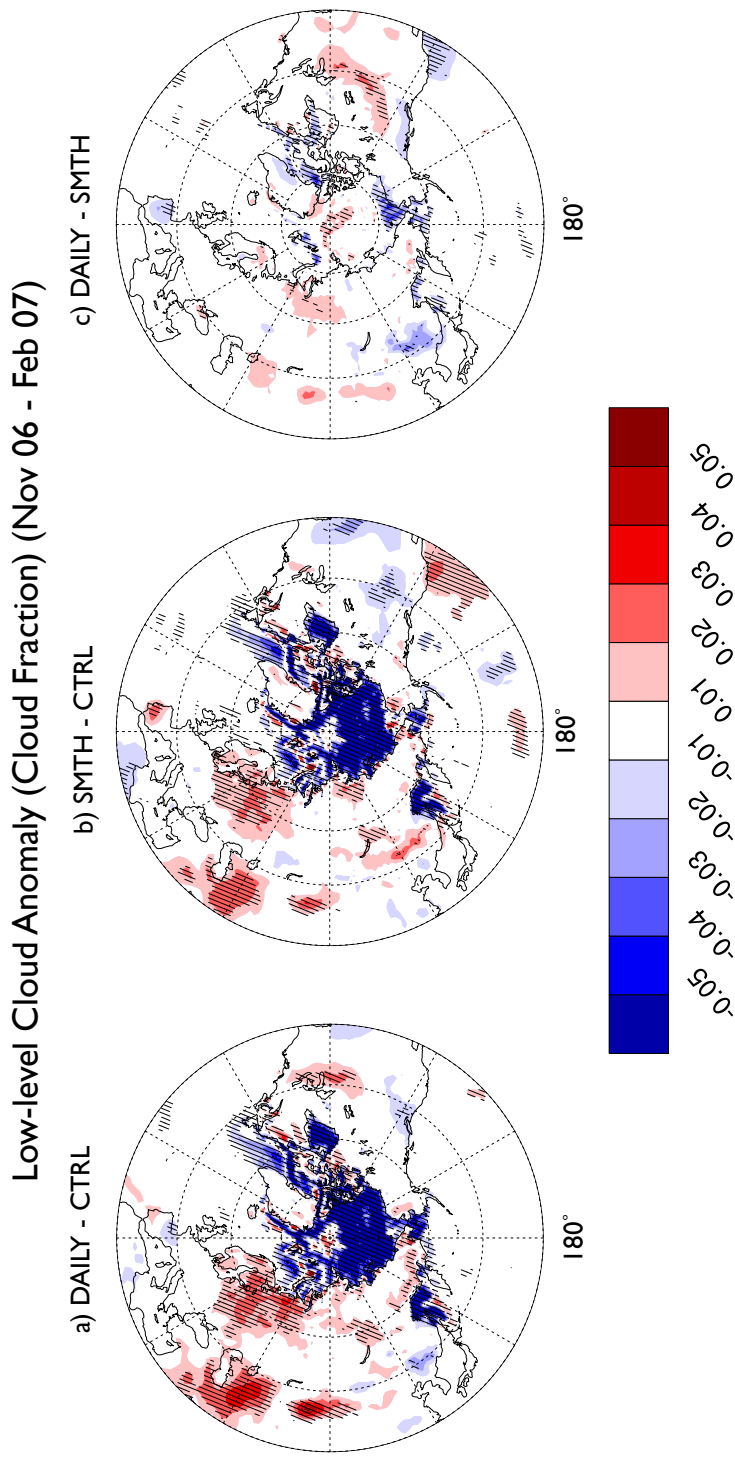


**Figure D.11 Winter Low-level Cloud Differences**  
 Ensemble average (Nov – Feb) low-level cloud anomaly (fraction) a) DAILY-CTRL, b) SMTH-CTRL, c) DAILY-SMTH. Crosshatching signifies statistical significance at the 95% or greater level based on Student’s t-test.

Almost the entire winter ice covered region and surrounding oceans have less low cloud amounts as a response to 2006-07 sea ice. Positive low cloud anomalies occur over Northern Europe and the Middle East (Figure D.11a and b). DAILY-SMTH cloud response is relatively weak but higher cloud amounts are found over the central Arctic basin and the northern US (Figure D.11c). Negative low-cloud anomalies are found over Chukchi Sea, Davis Strait, and Hudson Bay and off the coast of California in DAILY-SMTH.

More mid-level clouds are seen in response to 2006-07 ice in the Barents and Labrador seas and also in regions of the eastern North Pacific (Figure D.12a and b). DAILY-SMTH displays a weak response in mid-level clouds with a slight decrease located over South East Alaska (Figure D.12c).

Positive high-cloud anomalies are found over the Mediterranean Sea and negative anomalies south of the Aleutian Islands in response to 2006-07 winter ice conditions (Figure D.13a and b). In DAILY-SMTH there are more high clouds located over eastern US (Figure D.13c).

There are negative 1000 hPa specific humidity anomalies over the central Arctic basin and the central North Pacific and positive anomalies over Northern Europe in response to winter 2006-07 sea ice conditions (Figure D.14a and b). DAILY-SMTH displays a large significant area of negative humidity over large parts of continental US and off the West Coast of the US in DAILY (Figure D.14 c).

Medium-level Cloud Anomaly (Cloud Fraction) (Nov 06 - Feb 07)

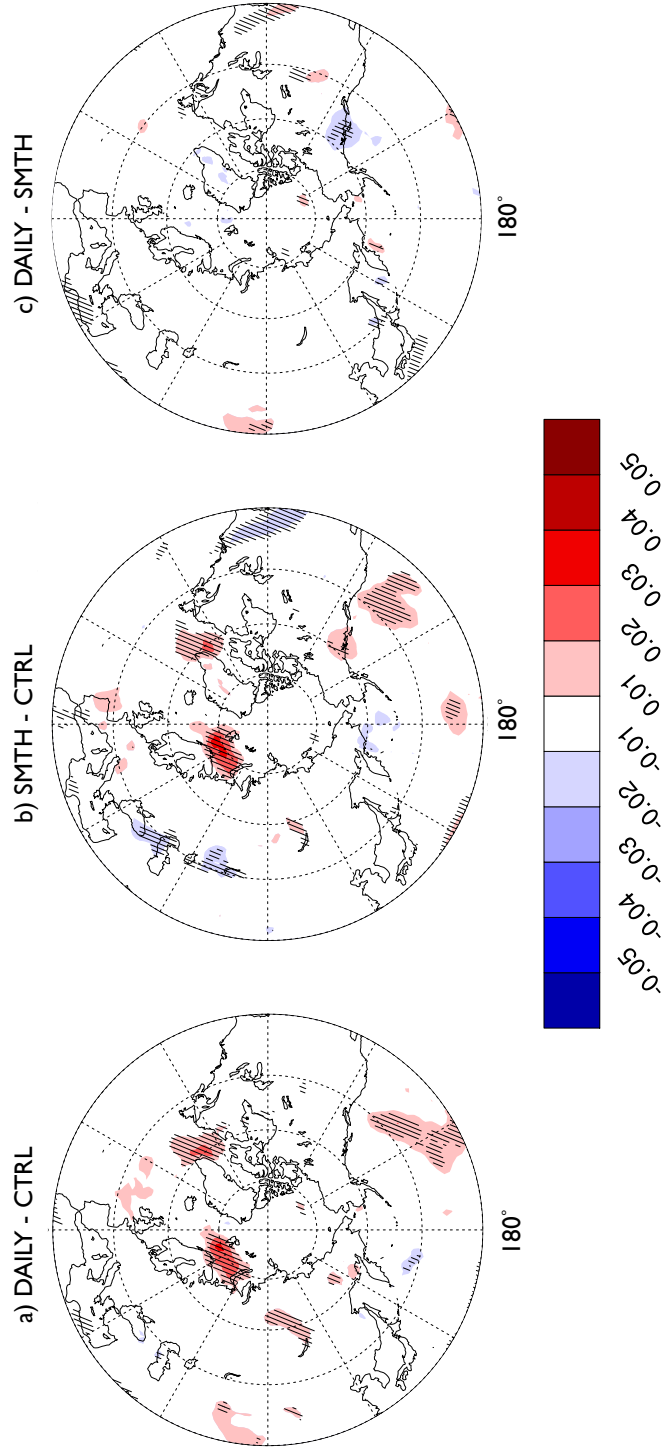


**Figure D.12 Winter Medium-level Cloud Differences**  
Ensemble average (Nov – Feb) medium-level cloud anomaly (cloud fraction) a) DAILY-CTRL, b) SMTH-CTRL, c) DAILY-SMTH. Crosshatching signifies statistical significance at the 95% or greater level based on Student’s t-test.

### High-level Cloud Anomaly (Cloud Fraction) (Nov 06 - Feb 07)

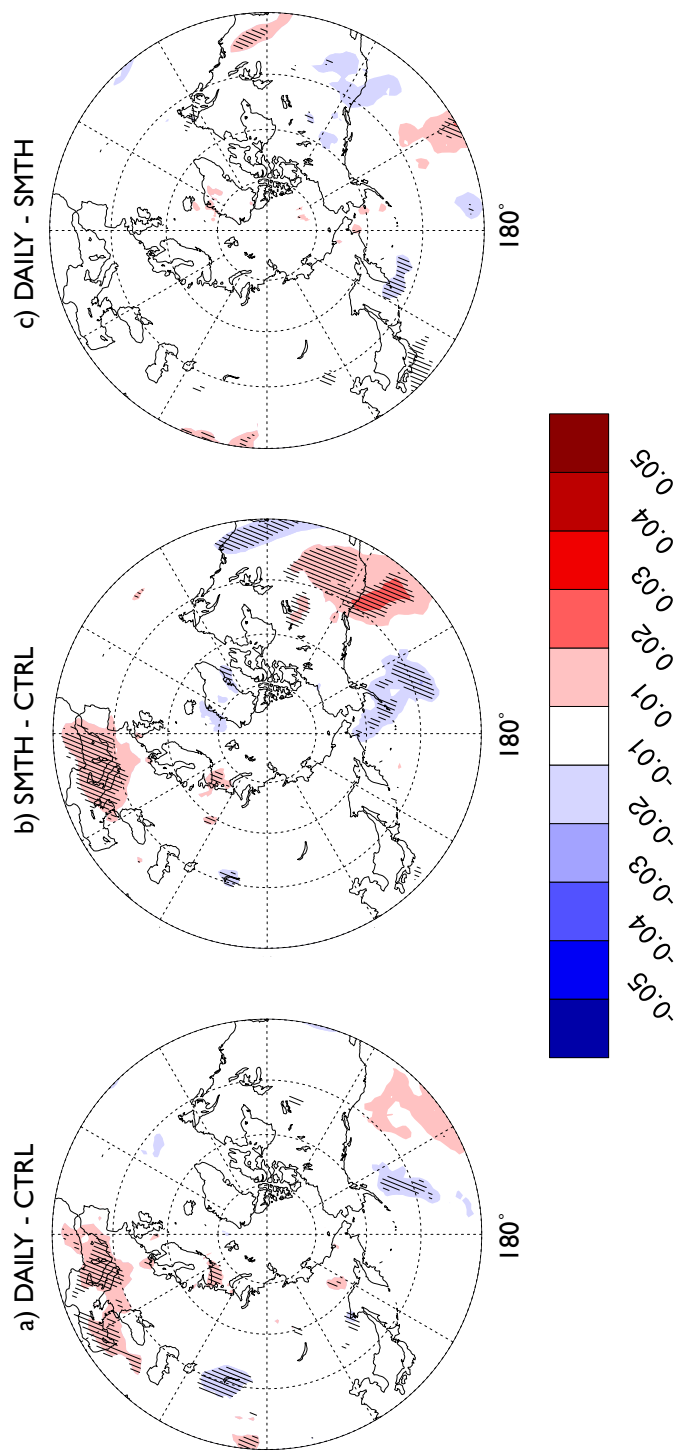


**Figure D.13 Winter High-level Cloud Differences**  
Ensemble average (Nov – Feb) high-level cloud anomaly (cloud fraction) a) DAILY-CTRL, b) SMTH-CTRL, c) DAILY-SMTH. Crosshatching signifies statistical significance at the 95% or greater level based on Student's t-test.

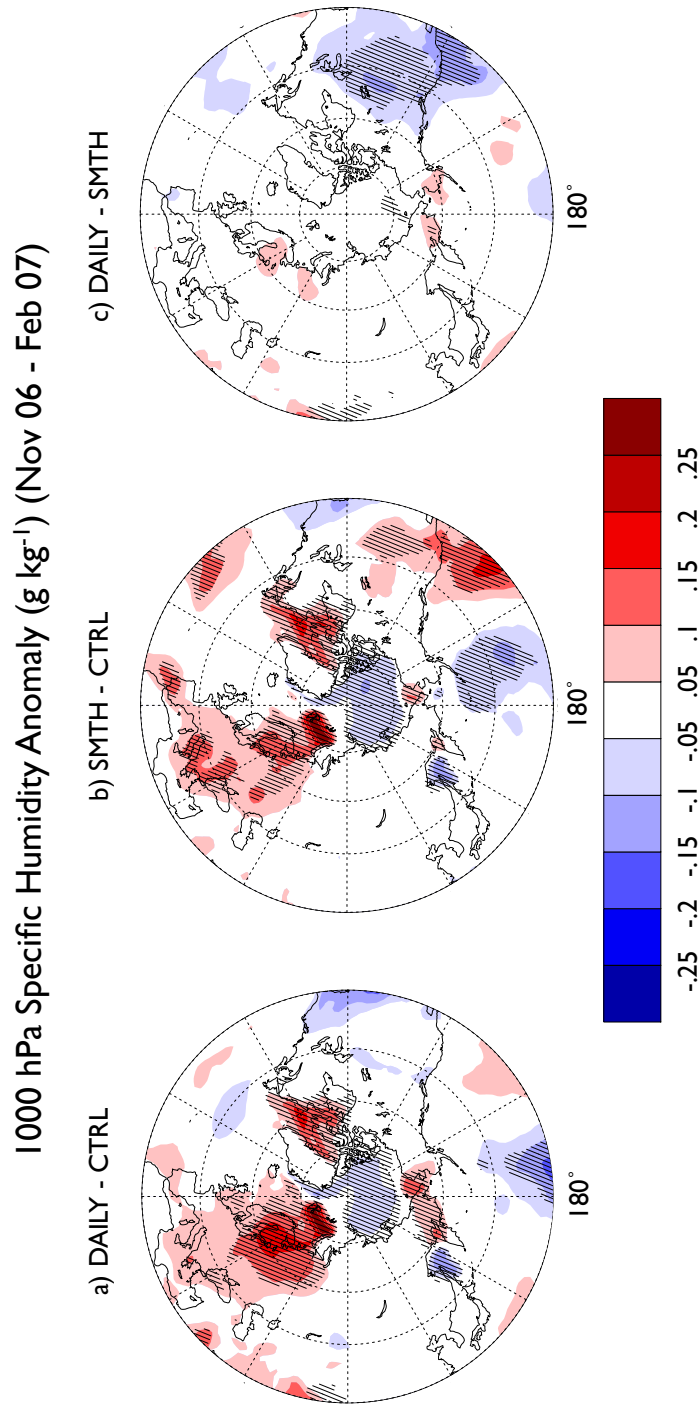


**Figure D.14 Winter Specific Humidity Differences**  
 Ensemble average (Nov – Feb) 1000hPa specific humidity anomaly (g kg<sup>-1</sup>) a) DAILY-CTRL, b) SMTH-CTRL, c) DAILY-SMTH. Crosshatching signifies statistical significance at the 95% or greater level based on Student's t-test.

### D.3 Storm Track Response

The 2 – 10 days bandpassed 850 hPa  $v'T'$  displays a southward shift, though of different magnitudes, in response to 2006-07 winter sea ice in the two experiments (Figure D.15a and b). DAILY-SMTH indicates that SMTH has a stronger southward storm track shift in the North Pacific while DAILY displays a general weakening of the midlatitude storm tracks (Figure D.15c).

The 2 – 10 days bandpassed 200 hPa  $u'v'$  momentum transport anomaly in response to 2006-07 ice is negative over North America and Western Europe (Figure D.16a and b). The decrease across North America is stronger in DAILY than SMTH causing negative anomaly over North America in DAILY – SMTH (Figure D.16c).

Individual storm track fields are noisy and can be difficult to interpret. DAILY-SMTH displays positive storm density in the eastern North Pacific consistent with a southward shifted North Pacific storm track (Figure D.17c).

Figure D.18 displays DAILY-SMTH 200 hPa zonal wind anomalies with shading and mean SMTH with contours. The main feature is a stronger polar jet streak over North America in DAILY than SMTH.

Poleward Heat Transport Anomaly ( $\text{K m s}^{-1}$ ) (Nov 06 - Oct 07)

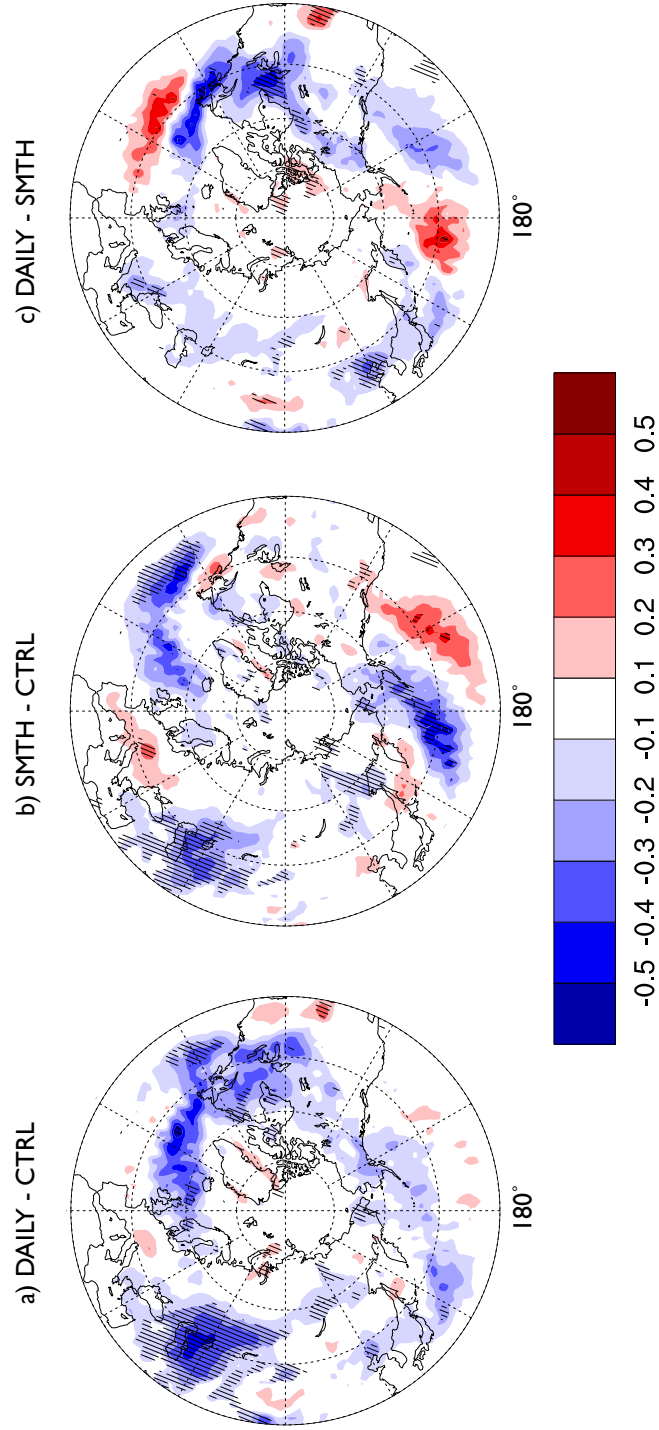


**Figure D.15 Winter Poleward Heat Transport Differences**

Ensemble average (Nov – Feb)  $v'T'$  850 hPa 2 – 10 days bandpassed anomaly ( $\text{K m s}^{-1}$ ) a) DAILY-CTRL, b) SMTH-CTRL, c) DAILY-SMTH. Crosshatching signifies statistical significance at the 95% or greater level based on Student's t-test.



### Poleward Momentum Transport Anomaly ( $\text{m}^2 \text{s}^{-2}$ ) (Nov 06 - Feb 07)

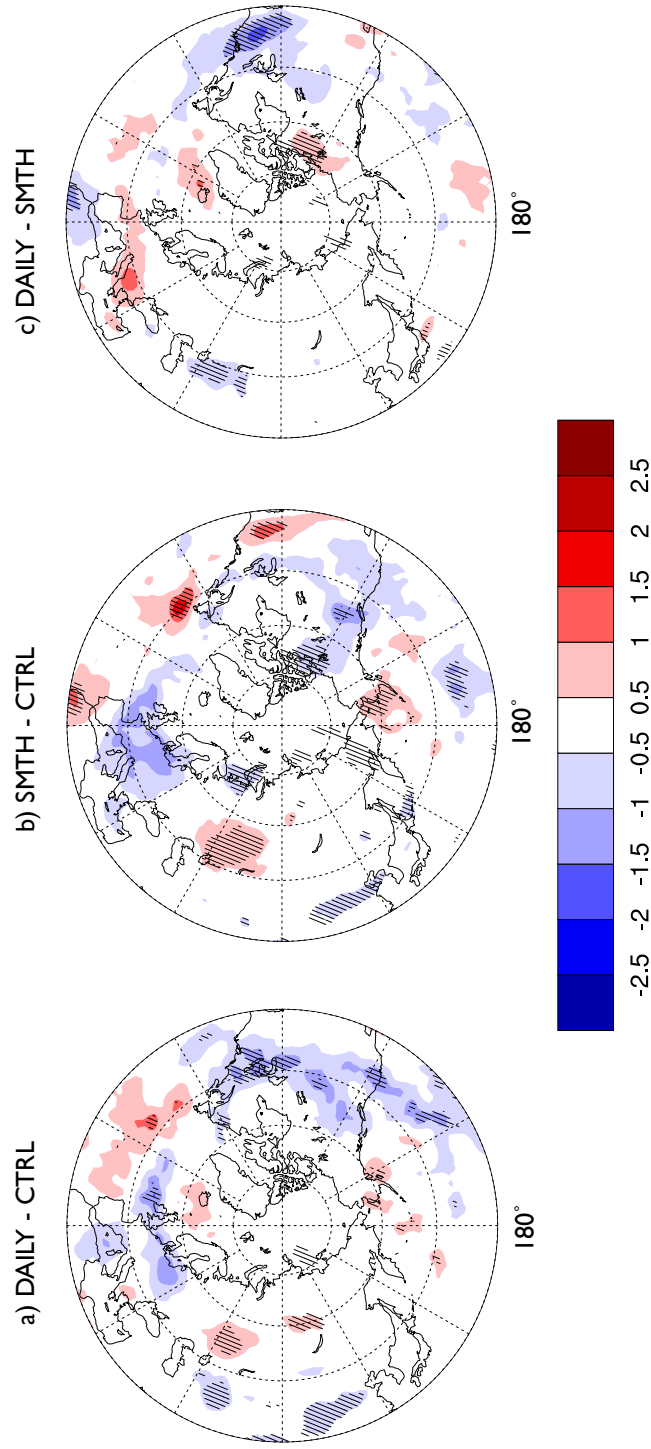


**Figure D.16 Winter Poleward Momentum Transport Differences**  
Ensemble average (Nov – Feb)  $u'v'$  200 hPa 2 – 10 days bandpassed anomaly ( $\text{m}^2 \text{s}^{-2}$ ) a) DAILY-CTRL, b) SMTH-CTRL, c) DAILY-SMTH. Crosshatching signifies statistical significance at the 95% or greater level based on Student's t-test.

Smoothed Storm Density Anomaly (Unitless) (Nov 06 - Feb 07)

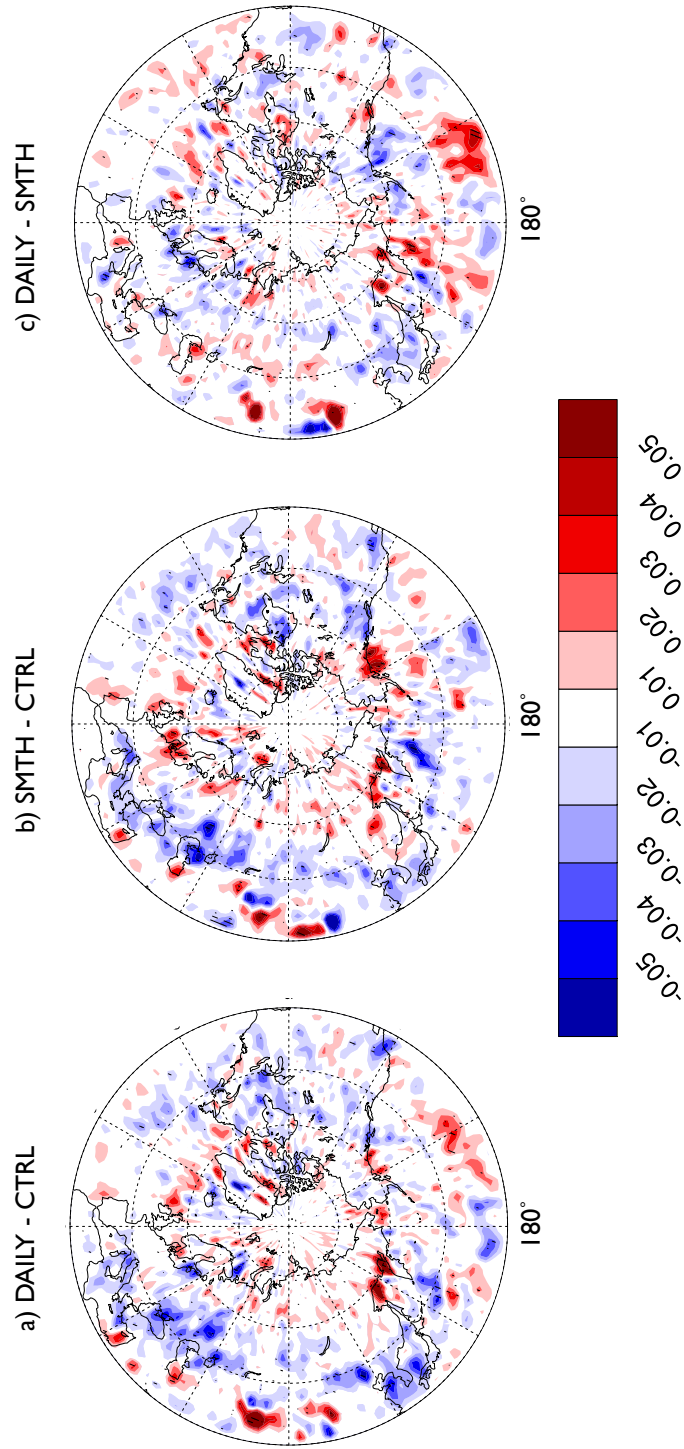


**Figure D.17 Winter Smoothed Storm Density Differences**  
Ensemble average (Nov - Feb) smoothed storm density anomaly a) DAILY, b) SMTH, c) DAILY-SMTH. Crosshatching in c signifies statistical significance at the 95% or greater level based on Student's t-test.

200hPa Zonal Wind Mean and Anomaly ( $\text{m s}^{-1}$ )  
DAILY - SMTH (Nov 06 - Feb 07)

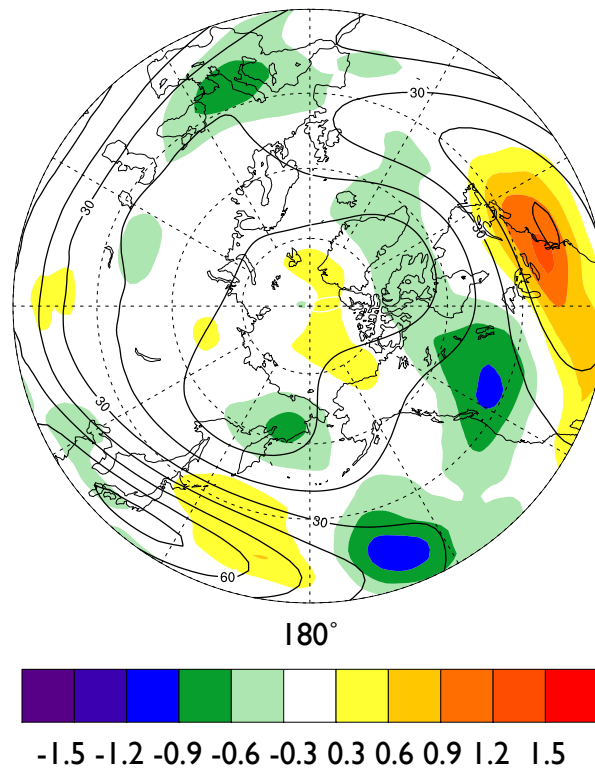


**Figure D.18 Winter Zonal Wind**

Ensemble average (Nov – Feb) zonal wind speed at 200 hPa ( $\text{m s}^{-1}$ ). Shading indicates anomaly DAILY-SMTH and contours denotes SMTH climatological zonal wind.

## Appendix E Synthesis of Atmospheric Response by Region

Several fields display statistically significant differences in the Northern Hemisphere atmospheric response to a daily varying (DAILY) and smoothed (SMTH) sea ice forcing. This section aims to summarize and discuss regional model response by synthesizing the results and putting them in the large-scale climate context. Figure E.1 highlights regions identified to consistently have a significant atmospheric response in multiple fields.

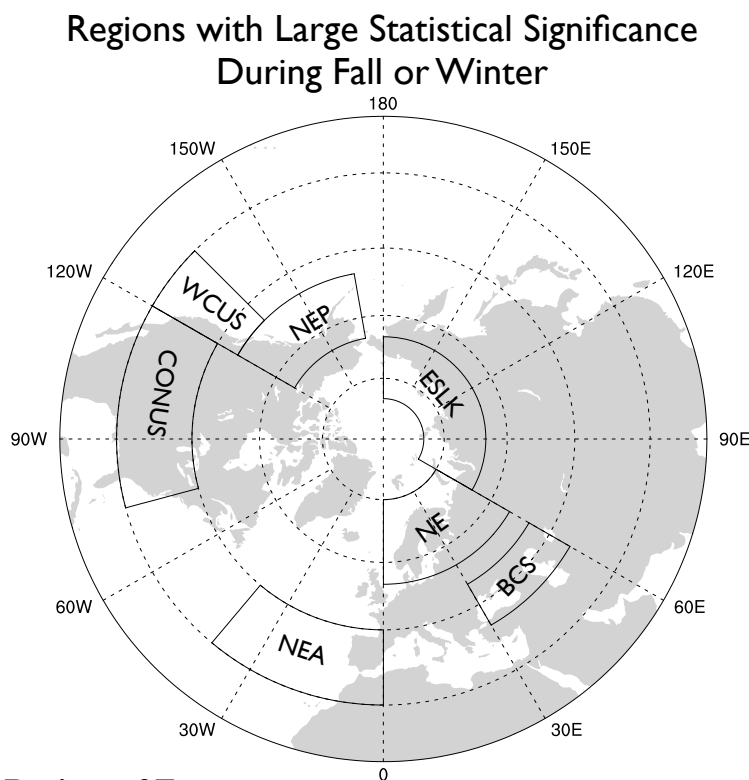


**Figure E.1 Regions of Focus**

Regions with notable differences between DAILY and SMTH during fall and/or winter with significance at the 95% or greater level based on Student's t-test. Regions include Northern Europe (NE), East Siberian, Laptev and Kara seas (ESLK), Black Sea and Caspian Sea (BCS), Continental US (CONUS), northeast Pacific (NEP), northeast Atlantic (NEA), and west coast US (WCUS).

### **E.1 Northern Europe Region (Fall)**

A region with large differences between DAILY and SMTH during fall (Sep – Oct 2006) is Northern Europe (NE) 0 – 60E and 55 – 75N (Figure E.1).

Finland and northern Russia have about 1-2  $\text{W m}^{-2}$  higher sensible heat fluxes out of the surface and the western part of Barents Sea has between 3-4  $\text{W m}^{-2}$  less latent heat flux loss. Finland has between 2-3  $\text{W m}^{-2}$  increased long wave radiation out of the surface. The northern Russia part of NE and Finland receives between 1-4  $\text{W m}^{-2}$  higher incoming solar radiation at the surface. Combining total heat fluxes (latent, sensible, and longwave) out of the surface yield between 1-4  $\text{W m}^{-2}$  increased fluxes out of the surface over Finland and northern Russia and between 4-12  $\text{W m}^{-2}$  decreased fluxes over western Barents Sea.

Two-meter air temperature is similar between DAILY and SMTH, but there are regions with 0.1 to 0.3K higher temperatures in the Norwegian Sea. SLP is generally higher over NE region with a maximum of 1.5 hPa and 500 hPa geopotential height is co-located and has central max of roughly 16 m. Precipitation is lower in most of the NE Region with differences up to over -0.25  $\text{mm day}^{-1}$ . Cloud cover at low, medium, and high levels are all lower by up to 4% over large parts of Scandinavia and the northern Russia.

Relative humidity is not much different over land between DAILY and SMTH, but differences between 0.1 and 0.15  $\text{g kg}^{-1}$  occur in the Norwegian Sea. Bandpassed 850 hPa  $v'T'$  displays negative anomalies in most of the Russian part of NE with up to over 0.3  $\text{K m s}^{-1}$  and also in the North Sea.

In sum, this response suggests that a difference in sea ice variability can impact the atmospheric response. Sea ice extends into the East Siberian, Laptev and Kara seas during fall. The daily sea ice (DAILY) the ice edge progresses rapidly equatorward and grid points in this region can experience a shift from zero to hundred percent SIC in as little as a week. With smoothed sea ice based on a

thirty day running average (SMTH) the same process might take as much as a month. During fall ice in East Siberian, Laptev and Kara seas will therefore close up with sea ice faster in DAILY leading to lower fluxes out of the warmer ocean water (Figure C.6c) thus providing less energy to the atmosphere. This causes circulation patterns to change and through large-scale dynamical changes impacts the Northern Hemisphere.

Storm track characteristics have been analyzed using several measures. 2 – 10 days bandpassed 850 hPa  $v'T'$ , a measure of poleward heat transport (Figure C.15), is reduced over much of the NE region indicating reduced cyclone activity. 2 – 10 days bandpassed 200 hPa  $v'T'$ , a measure of poleward momentum transport (Figure C.16), shows fewer differences in the NE region but indicates reduced momentum transport into the region from the south. Due to the noisiness of the storm track algorithm, the anomalies do not attain much significance, however this field also indicates fewer (Figure C.17) and also weaker storms in NE. Figure E.2 confirms that DAILY has fewer (4%) and weaker storms (more storms with higher SLP and fewer with low SLP) compared to SMTH. The anomalies form a consistent picture. There is likely reduced storm activity in NE, which result in higher pressure (Figure C.8) and higher geopotential height (Figure C.9). Fewer storms also result in reduced convection, cloud cover (Figure C.11 – C.13) and precipitation (Figure C.10). With decreased cloud cover, solar radiation received at the surface increases (Figure C.5), warming the surface and net long wave radiation to space increases (Figure C.4) as a result of warmer surface. Reduced storminess in the Norwegian Sea leads to less atmosphere – ocean interaction limiting sensible and latent heat flux (Figure C.2 – C.3) into the atmosphere.

Ensemble Average Storm Count for NE Region  
(Sep - Oct 2006)

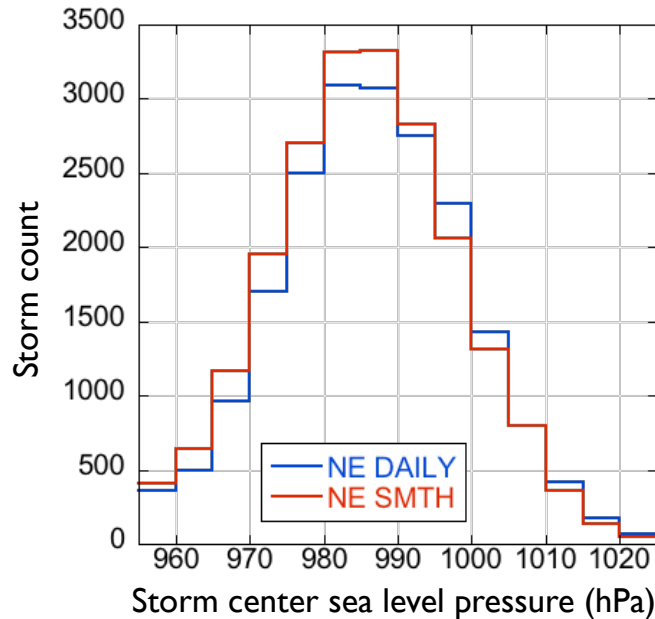


**Figure E.2 Storm Count NE Region**

Storm center sea level pressure (hPa) and number of storm centers in the NE region (Sep – Oct 2006).

### E.2 West Coast US (Fall)

The west coast of the continental US (WCUS) 120 – 135W and 30 – 50N (Figure E.1) experiences significant differences in DAILY – SMTH during fall (Sep – Oct 2006).

Sensible heat fluxes are similar between DAILY and SMTH (Figure C.2). Latent heat fluxes over ocean are more positive in DAILY in large parts of this region with maximum anomalies of over  $3 \text{ W m}^{-2}$  occurring off the coast of northern California (Figure C.3). Net longwave radiation out of the ocean off the coast of Southern California is higher in DAILY than SMTH with a maximum value of  $3 \text{ W m}^{-2}$  (Figure C.4). Similarly net solar radiation into the lower atmosphere is higher in DAILY in this area with a maximum over  $5 \text{ W m}^{-2}$  (Figure C.5). The total flux anomaly out of the ocean off the coast of California is therefore mostly positive and between  $1\text{-}2 \text{ W m}^{-2}$  (Figure C.6). Only a slight 2-

m air temperature increase is found in the location of the flux anomalies (Figure C.7).

Sea level pressure remains mostly unchanged on the coast, but further off the coast (upwind) there is a high pressure anomaly between 0.2-0.5 hPa DAILY – SMTH (Figure C.8). This pressure feature does not have a counterpart in 500 hPa geopotential height (Figure C.9). Precipitation changes are small, though there is a slight decrease in low clouds (Figure C.11). Specific Humidity is reduced off the coast of northern California with more than  $0.15 \text{ g kg}^{-1}$  in DAILY (Figure C.14).

Little change can be seen in change in storm track characteristics on the West Coast of the US. Little or no change occurs in the bandpassed poleward heat transport and only small changes are present in bandpassed poleward momentum transport off the coast of northern Baja California where DAILY has between 0.5 and  $1 \text{ m}^2 \text{ s}^{-2}$  lower values than SMTH (Figure C.16). The storm track algorithm used reveals a decrease in storms on the Pacific North West (PNW - Washington and Oregon) coast, but an increase of storms over southern California (Figure C.17).

Circulation anomalies may provide the best explanation for the differences between DAILY and SMTH over the US West Coast. Higher SIC in DAILY in East Siberia, Kara and Laptev seas leads to a cooler Arctic ( $-0.1\text{K}$  in average between  $70$  and  $90^\circ\text{N}$ ) DAILY – SMTH (Figure C.7). A cooler Arctic leads to an equatorward shift in the maximum temperature gradient and the polar jet (Figure C.18). A southward shifted jet is consistent with a southward shift in storms. Bandpassed poleward heat transport is not much different between DAILY and SMTH, but bandpassed poleward momentum transport is lower in DAILY off the coast of Baja California (Figure C.16).

Storm track analysis indicates a decrease (Figure E.3) and southward shift in storms across this section of the North Pacific. More storms occur by the



coast of Southern California and fewer storms reach the northern Californian and the PNW coast (Figure C.17).

Fewer storms over the northern and central Californian and PNW coast leads to reduced cloud amounts at low and high level (Figure C.11 and C.13) as well as reduced humidity (Figure C.14). This increases solar radiation reaching the lower atmosphere as well as increases longwave radiation out of the ocean off the central California coast (Figure C.5 and C.4). The lower specific humidity is consistent with the increased latent heat fluxes that occur over the central California coast (Figure C.3). Weak temperature anomalies are consistent with small sensible heat flux anomalies (Figure C.2).

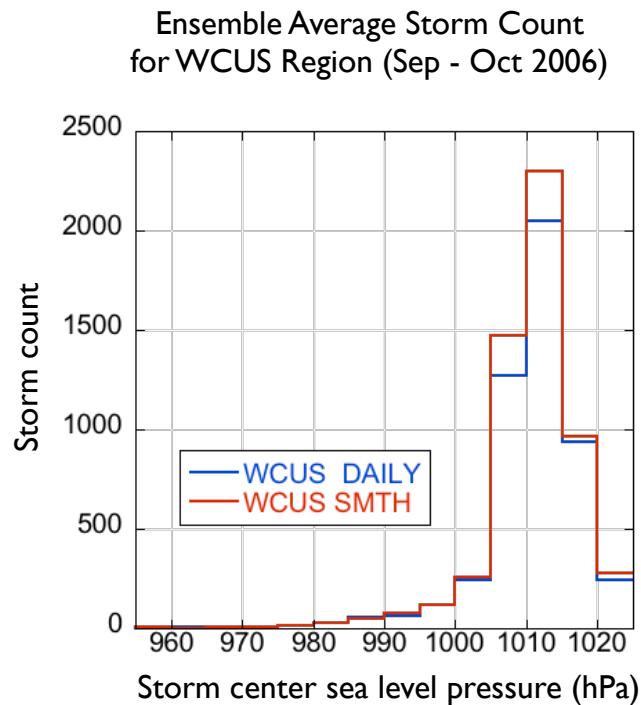


**Figure E.3 Storm Count WCUS Region**

Storm center sea level pressure (hPa) and number of storm centers in the WCUS region (Sep – Oct 2006)

### **E.3 Gulf of Alaska and Northeast Pacific (Fall)**

Northeast Pacific (NEP) 120 – 170W and 50 – 65N (Figure E.1) shows significant differences in the atmospheric response during fall to DAILY and SMTH sea ice conditions.

Sensible heat flux anomalies are positive in DAILY in the central to northern part of the Gulf of Alaska with maximum fluxes over  $4 \text{ W m}^{-2}$  (Figure C.2). Latent heat flux anomalies are large in the northern and southern part of the Gulf with maximum flux differences over  $5 \text{ W m}^{-2}$  (Figure C.3). Solar radiation fluxes at the surface are higher in DAILY over South West and South East Alaska with maximums between  $1\text{-}2 \text{ W m}^{-2}$ . The same is the case for long wave radiation out of the surface in Southwest Alaska (Figure C.5 and C.4).

There are colder temperatures over large parts of Alaska and Yukon in DAILY with anomaly maximums around  $-0.5\text{K}$  (Figure C.7). Higher precipitation occurs in DAILY between Yukon and British Columbia (Figure C.10). Cloud cover is consistently lower over southern Alaska and higher over eastern British Columbia (Figure C.11 - C.13). The northern parts of the Gulf as well as most of Alaska and Yukon have about  $0.1 \text{ g kg}^{-1}$  less moisture (Figure D.6). Only weak changes are evident in storm activity based on storm tracking and 2-10 days bandpassed measures (Figure C.15 - C.17).

Storm activity does not likely play a key role in the Gulf of Alaska anomalies. The cooling of East Siberian, Laptev, Kara, and Beaufort seas and large parts of Siberia is upwind from Alaska and is likely able to advect eastward to Alaska (Figure C.7). Cooling of the Siberian sector therefore favors descending air temperature resulting in lower moisture (Figure C.14) and lower cloud amount (Figure C.11 - C.13) in NEP. The low cloud amount in DAILY allows more longwave radiation to escape as well as more solar radiation to reach the surface (Figure C.4 and C.5). The larger sensible heat flux out of the ocean in the

northwest part of the Gulf is likely driven by the colder SAT's in the same area (Figure C.2 and C.3). The large latent heat anomaly south of the Gulf off the coast of British Columbia is likely due to increased storm activity (Figure C.3).

#### **E.4 Northeast Atlantic and Caspian-Black Sea (Fall)**

A region in the northeast Atlantic (NEA) 30 – 45N and 0 – 40W (Figure E.1) and a region containing both the Black Sea and the Caspian Sea (BCS) 40 – 50N and 30 – 60E (Figure E.1) both display notably different responses between DAILY and SMTH. The differences in the eastern part of NEA strongly co-vary with the differences in BCS and the two regions will therefore be described together.

Sensible heat flux is between 1-2  $W m^{-2}$  higher west in the NEA region in DAILY and up to over 3  $W m^{-2}$  lower around Gibraltar and the BCS region (Figure C.2). Latent Heat is higher in DAILY west in NEA with anomalies of over 5  $W m^{-2}$  (Figure C.3). Positive anomalies over 4  $W m^{-2}$  are also located over Morocco and BCS. Longwave and shortwave radiation are each over 2  $W m^{-2}$  higher in west NEA and over 2  $W m^{-2}$  lower around Gibraltar and over 4  $W m^{-2}$  lower over BCS (Figure C.4 and C.5).

There are negative SLP anomalies between 0.5-1 hPa over NEA in DAILY (Figure C.8) that are co-located with geopotential height anomalies of up to -12 m (Figure C.9). DAILY shows increased precipitation in NEA and BCS between 2 and 2.5  $mm day^{-1}$  (Figure C.10). Increased cloud cover in DAILY occurs at all levels in BCS and NEA with maximum of 4% (Figure C.11 - Figure C.13). Moisture is decreased in the western part of NEA but increased in eastern NEA and in BCS with around 2  $g kg^{-1}$  increase in DAILY (Figure C.14). The 2 – 10 days bandpassed 200 hPa  $u'v'$  poleward momentum flux is lower over BCS and in large areas between BCS and NEA. The storm track algorithm indicates increased cyclone activity in both regions (Figure C.17).

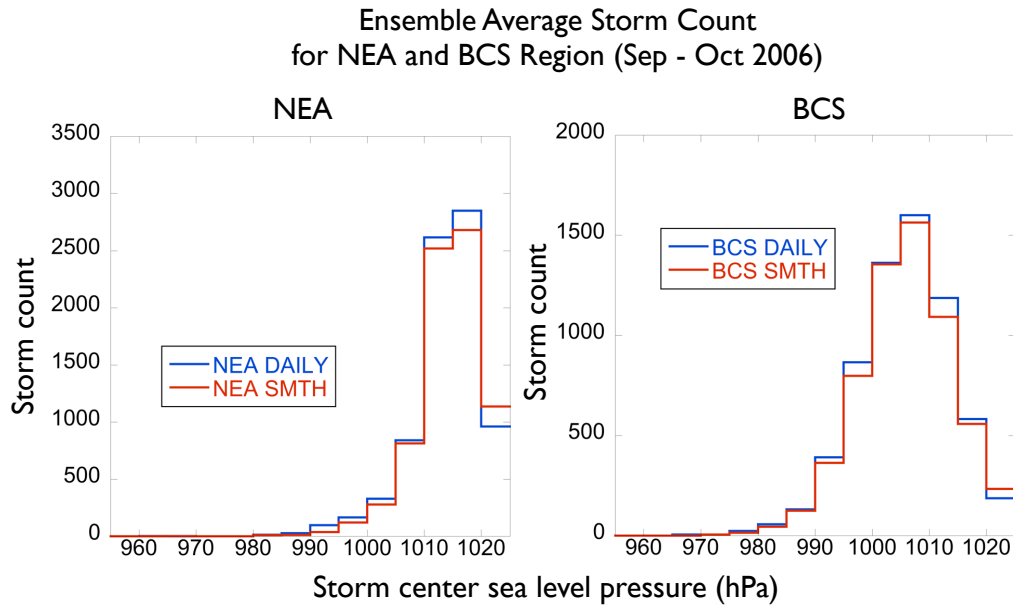


**Figure E.4 Storm Count NEA and BCS Region**

Strength (hPa) and number of storm centers in the NEA (left) and BCS (right) region (Sep – Oct 2006).

Figure C.18 indicates a shift in the general circulation causing the polar jet to shift south towards the NEA region favoring storm development in the region. Signs of increased cyclone activity can be seen in storm tracks (Figure E.4) and increased latent heat release from both regions. Higher storm activity leads to negative SLP anomalies with a displaced negative 500 hPa geopotential height response in NEA near Gibraltar. This feature does not show up as clearly in BCS, but the same mechanism is suggested. Lower pressure in both regions is associated with ascending air and increased clouds at all levels leading to increased precipitation and specific humidity. Increased clouds reduce net solar radiation at the surface and is consistent with decreased sensible and longwave fluxes out of the surface.

### **E.5 East Siberian, Laptev and Kara Seas (Fall)**

The region of the three arctic seas East Siberian, Laptev, and Kara (ESLK) 65 – 80N and 60 – 180E (Figure E.1) is more directly driven by the ice

than more equatorward locations since the area of highest difference between DAILY and SMTH forcing is in this region (Appendix B.1).

Sensible heat fluxes are smaller in DAILY in most of the region with a maximum over  $3 \text{ W m}^{-2}$  negative anomalies (Figure C.2). Latent heat anomalies are also smaller with a maximum of over  $1 \text{ W m}^{-2}$  (Figure C.3). Longwave radiation out of the ocean is increased in parts of the ocean with a maximum of about  $2 \text{ W m}^{-2}$  (Figure C.4). Solar radiation reaching through the lower atmosphere does not change much (less than  $1 \text{ W m}^{-2}$ ) (Figure C.5) as would be expected at high latitudes during fall.

Temperature is lower in the whole region with maximum negative anomalies reaching close to 1K in DAILY (Figure C.7). Precipitation remains unchanged, likely due to small moisture amounts, but low cloud amounts are reduced over most of the region with anomalies reaching more than 4% (Figure C.11). High and medium level clouds do not notably change. Specific humidity is reduced by between  $0.05\text{-}0.1 \text{ g kg}^{-1}$  in DAILY over the Laptev, Kara, and parts of East Siberian seas. Bandpassed poleward heat transport at 850 hPa is similar between DAILY and SMTH, but bandpassed momentum transport at 200 hPa is higher over the Kara Sea in DAILY (Figure C.16).

DAILY has a larger amount of high SIC in most of this domain (Appendix B.1). This leads to reduced sensible and latent heat fluxes out of the ocean in DAILY. This contributes to lower air temperatures, reduced ascending air and lower amount of clouds. This increases the net longwave radiation out of the surface. For high latitudes during fall the difference in solar radiation through the lower atmosphere will not be reduced notably in magnitude due to mean radiation fluxes being low. Similarly low precipitation changes occur which is to be expected with initially low precipitation in the region.

## **E.6 Continental United States (Winter)**

Fall shows more significant response in difference between DAILY and SMTH in most regions though this is not the case for the continental US (CONUS) 30 – 45N, 75 – 120W (Figure E.1) where the differences are larger in winter.

Sensible heat is not much different over the region, but the west coast displays large positive anomalies in DAILY (Figure D.2). The same is true for latent heat (Figure D.3). Solar radiation at the surface is reduced in parts of Washington and Montana (Figure D.5) and longwave radiation from surface is reduced across the northern Midwest (Figure D.4) and increased off the west coast.

The temperatures are colder in most of CONUS with negative anomalies reaching a maximum almost 1K (Figure D.7), which result in negative geopotential height anomalies over large parts of CONUS (Figure D.9). Precipitation is increased in North Dakota and in the eastern midwest with up to over 0.2 mm day<sup>-1</sup> (Figure D.10). There are more low-(high)level clouds over the northern (eastern) CONUS (Figure D.11 and D.13). Specific humidity is decreased in large parts of the northern and western states (Figure D.14). Bandpassed poleward heat transport is larger in DAILY over Texas, lower in Oregon and largely negative north of CONUS (Figure D.15). Bandpassed poleward momentum transport is lower in DAILY over the eastern Mid-west and the East Coast US (Figure D.16).

Much of the differences between DAILY and SMTH are likely due to the high-pressure anomaly over southern Alaska and the co-located geopotential height anomaly. The associated anticyclonic circulation around this high results in more air being advected into CONUS from the north versus from the west (Figure D.18). This leads to a general cooling of CONUS. The anomalous high has the

opposite effect on western Alaska and eastern Russia when warmer Pacific air is advected from the south. The cooling of the continent causes the increased latent and sensible heat fluxes out of the ocean on the West Coast US. The cold air advecting from the north is consistent with negative bandpassed poleward heat transport anomalies along the northern states. The southward advection leads to increased convective activity south of the bandpassed poleward heat transport anomalies, producing low clouds and some increased precipitation.

A negative geopotential height anomaly forms due to colder temperatures over CONUS. This leads to anticyclonic anomalous circulation advecting air from the Gulf of Mexico and Texas into the eastern Midwest resulting in a more cloud formation and more precipitation.